Regulation of Topoisomerase I–Induced Mutagenesis and Its Impact on Aging in Yeast

Dissertation

Zur Erlangung des Grades

Doktor der Naturwissenschaften

Am Fachbereich Biologie

Der Johannes Gutenberg-Universität Mainz

Kristi Lyn Jensen

geb. am 28.12.1988 in Kansas, United States of America

Mainz, 2025

Dekan: Prof. Dr. Eckhard Thines

1.Berichterstatter:

2.Berichterstatter:

Tag der mündlichen Prüfung: 27. November, 2025

Table Of Contents

Summary

Aging is characterized by several molecular hallmarks, including accumulation of mutations in the genome. Given the interconnected nature of these hallmarks of aging, it is challenging to distinguish causative factors from their consequences. However, genomic instability is a strong candidate as a driver of aging due to its role in accumulating cellular damage over time, ultimately compromising genome integrity and cellular function. One of the most frequent forms of DNA damage is the incorporation of ribonucleotides (rNMPs) into the genome, which can lead to mutations and genome instability, making rNMP processing an intriguing candidate for influencing aging.

Here, we investigate the role of Topoisomerase I (Top1) in rNMP repair and its impact on genomic integrity and aging. We find that Top1-mediated DNA damage is elevated in aged yeast cells compared to their younger counterparts, suggesting an age-associated increase in Top1 activity or its mutagenic consequences. Furthermore, processes known to extend lifespan, such as caloric restriction, reduce Top1-dependent mutation accumulation, reinforcing the link between genome stability and aging. While rNMP processing does not appear to influence yeast lifespan under normal conditions, we demonstrate that loss of RNase H2 activity shortens lifespan in worms, and that subsequent degradation of Top1 in adult worms rescues lifespan to wildtype levels. These findings support a model in which Top1 activity at rNMPs contributes to genomic instability and may act as a pro-aging factor, especially under conditions where rNMP removal is impaired.

Together, this work highlights a mechanistic connection between genome maintenance pathways and aging, advancing our understanding of how genomic instability shapes lifespan.

Zusammenfassung

Das Altern ist durch mehrere molekulare Kennzeichen geprägt, darunter insbesondere die Anhäufung von Mutationen im Genom. Aufgrund der engen Verknüpfung dieser Kennzeichen ist es jedoch schwierig, ursächliche Faktoren von ihren Folgen klar zu unterscheiden. Genomische Instabilität gilt dabei als aussichtsreicher Kandidat für einen treibenden Faktor des Alterns, da sie im Laufe der Zeit zur Akkumulation zellulärer Schäden beiträgt und damit sowohl die Integrität des Genoms als auch die Zellfunktion beeinträchtigt. Eine besonders häufige Form von DNA-Schädigung stellt die Inkorporation von Ribonukleotiden (rNMPs) in das Genom dar, die zu Mutationen und Instabilität führen kann. Dadurch wird die Verarbeitung von rNMPs zu einem zentralen Ansatzpunkt in der Alternsforschung.

In dieser Arbeit untersuchen wir die Rolle der Topoisomerase I (Top1) bei der rNMP-Verarbeitung und deren Einfluss auf die Genomstabilität und den Alterungsprozess. Wir konnten zeigen, dass Top1-vermittelter DNA-Schaden in gealterten Hefezellen im Vergleich zu jüngeren Zellen erhöht ist, was auf eine altersabhängige Zunahme der Top1-Aktivität oder ihrer mutagenen Konsequenzen hinweist. Zudem konnten wir nachweisen, dass Lebensspanne-verlängernde Prozesse wie kalorische Restriktion die Anhäufung Top1-abhängiger Mutationen reduzieren und damit den Zusammenhang zwischen Genomstabilität und Altern unterstreichen. Während die rNMP-Verarbeitung unter Standardbedingungen offenbar keinen Einfluss auf die Lebensspanne von Hefe ausübt, konnten wir zeigen, dass der Verlust der RNase-H2-Aktivität die Lebensspanne bei *C. elegans* deutlich verkürzt und dass der gezielte Abbau von Top1 in adulten Würmern diesen Effekt auf Wildtyp-Niveau zurückführt. Diese Ergebnisse stützen ein Modell, in dem Top1-Aktivität an rNMPs wesentlich zur genomischen Instabilität beiträgt und insbesondere unter Bedingungen gestörter rNMP-Entfernung als pro-aging-Faktor wirkt.

Insgesamt verdeutlicht diese Arbeit eine mechanistische Verbindung zwischen DNA-Stoffwechsel, Genomstabilität und Altern und leistet damit einen Beitrag zum Verständnis der Frage, wie genomische Instabilität die Lebensspanne von Organismen beeinflusst.

Abbreviations

Abbreviation	Meaning
AGS	Aicardi-Goutières Syndrome
AID*	Auxin-inducible Degron
BER	Base Excision Repair
CI	Confidence Interval
CLS	Chronological Lifespan
CPT	Camptothesin
CR	Caloric Restriction
DMSO	Dimethyl Sulfoxide
DNA	Deoxyribonucleic Acid
dNTP(s)	Deoxyribonucleoside Triphosphate(s)
dsDNA	Double stranded DNA
DPC(s)	DNA-Protein Crosslink(s)
DSB(s)	Double-Strand Break(s)
ERC	Extrachromosomal rDNA circle(s)
EV	Empty Vector
FOA (5-FOA)	5-Fluoroorotic Acid
FRB	FKBP12-rapamycin binding domain
HR	Homologous Recombination
HU	Hydroxyurea
ID4	Indel Signature 4 (COSMIC mutational signature)
IMB	Institute of Moleuclar Biology
MBF	MluI Cell Cycle Box Binding Factor (transcription factor complex)
MLE	Maximum Likelihood Estimate
MMR	Mismatch Repair
NER	Nucleotide Excision Repair
NHEJ	Non-Homologous End Joining
OD	Optical Density; typically 600nm
OE	Overexpression
PEG	Polyethylene Glycol
Pol	DNA Polymerase (α, δ, or ε depending on context)
PPCF	Protein Production Core Facility
PBS	Phosphate-buffered saline
RED	Ribonucleotide Excision-Deficient (allele of RNase H2)
RER	Ribonucleotide Excision Repair
RLS	Replicative Lifespan

RNA	Ribonucleic Acid
rNMP(s)	Ribonucleoside Monophosphate(s)
rNTP(s)	Ribonucleoside Triphosphate(s)
SC	Synthetic Complete Medium
SBF	Swi4/Swi6 Cell Cycle Box Binding Factor
seDSB	Single-Ended Double-Strand Break
SEM	Standard error of the mean
SOC	Super Optimal broth with Catabolite repression
SPO	Sporulation Medium
SSTR	Short Simple Tandem Repeat
TAM	Transcription-Associated Mutagenesis
Top1	DNA Topoisomerase I
Top1-DPC	Top1-DNA Protein Crosslink
Top1-cc	Topoisomerase I Cleavage Complex
TOR	Target of Rapamycin
WT	Wildtype
YPD	Yeast extract Peptone Dextrose

1. Introduction

1.1. Aging and Genomic Instability

Aging is a complex biological process defined by the progressive decline of physiological functions and an increased susceptibility to disease and mortality (López-Otín *et al.*, 2013, 2023). It affects multiple organ systems simultaneously and occurs across all levels of biological organization, from molecular and cellular dysfunction to tissue and systemic failure. This complexity makes it challenging to distinguish causal factors from correlated changes that may not directly contribute to biological decline. Lifespan is shaped by both genetic and environmental factors, with several conserved molecular mechanisms contributing to aging across species. Among these, genomic instability plays a central role, linking molecular damage to functional decline over time. These mechanisms, collectively referred to as the molecular hallmarks of aging, provide a unifying framework for understanding the processes that drive age-related decline.

1.1.1. The Molecular Hallmarks of Aging

Nine key hallmarks of aging have been proposed: genomic instability, telomere attrition, epigenetic alterations, loss of proteostasis, deregulated nutrient sensing, mitochondrial dysfunction, cellular senescence, stem cell exhaustion, and altered intercellular communication (López-Otín *et al.*, 2013). More recently, three additional hallmarks, which predominantly affect multicellular organisms, have been included: impaired macroautophagy, chronic inflammation, and dysbiosis, defined as alterations in the microbiome (López-Otín *et al.*, 2023). A defining feature of these hallmarks is that they must fulfill three criteria: (1) they manifest progressively as organisms age, (2) their experimental exacerbation accelerates aging, and (3) their modulation can slow, halt, or even reverse aspects of the aging process (López-Otín *et al.*, 2013, 2023).

The hallmarks of aging are highly interconnected, with dysfunction in one process often amplifying deficits in others. For example, DNA damage causes stochastic epigenetic changes (Soto-Palma *et al.*, 2022; Yang *et al.*, 2023). These changes alter gene expression patterns, disrupt proteostasis, and increase the incidence of further DNA damage, creating a vicious cycle in which genomic instability reinforces epigenetic and proteostatic dysfunction. This interplay illustrates the difficulty of distinguishing primary drivers from secondary consequences and helps

explain why aging research is often dominated by correlative findings. Nevertheless, genomic instability remains a strong candidate for a foundational driver of aging, initiating a cascade of cellular dysfunction that ultimately manifests in diverse aging phenotypes (Schumacher *et al.*, 2021).

1.1.2. Genomic Instability as a Driver of Aging

The somatic mutation theory of aging, one of the earliest hypotheses to propose a link between DNA damage accumulation and age-related decline in tissue function, suggests that the progressive accumulation of mutations in somatic cells leads to functional deterioration and organismal aging (Szilard, 1959). While this theory provides a useful framework, evidence suggests that mutation accumulation alone does not fully explain the aging process (Schumacher *et al.*, 2021). Instead, genomic instability may act as a broader destabilizing force, contributing to aging through multiple mechanisms: (1) mutations in essential genes can cause cellular dysfunction, reducing tissue integrity and organ function over time, especially if mutations occur in progenitor cells, and (2) DNA damage and its subsequent repair disrupt cellular maintenance systems, such as DNA methylation, chromatin organization and transcriptional regulation, thereby accelerating physiological decline (Yang *et al.*, 2023). Both mechanisms demonstrate how genomic instability serves as a multifaceted driver of the aging process.

Genomic instability is widely regarded as a central hallmark of aging, yet the mechanisms by which it contributes to age-related decline are complex and variable between individuals. Evidence from human and model organism based studies demonstrates that both exogenous and endogenous DNA damage can accelerate aging, whereas defects in DNA repair pathways often drive premature aging syndromes. At the same time, counterarguments caution against viewing genomic instability as the sole determinant of lifespan. The following sections explore these perspectives.

1.1.2.1. Accelerated Aging Caused by Exogenous DNA Damage

Exposure to high doses of exogenous genotoxins is strongly associated with early signs of aging. For example, individuals who have undergone DNA-damaging chemotherapeutic or radiation-based treatments for childhood cancer frequently exhibit premature aging phenotypes relative to their siblings, including early-onset frailty, cardiovascular disease, and cognitive decline (Armstrong *et al.*, 2014). A similar set of phenotypes has also been observed among

testicular cancer survivors who underwent radiation therapy or chemotherapy as adults (Lubberts *et al.*, 2020). Other well-known examples of DNA damage that drives premature aging in various tissues include exposure to high doses of radiation (Richardson, 2009), cigarette smoke (Bernhard *et al.*, 2007), and UV exposure (Gonzaga, 2009). These observations suggest that excessive genomic damage from exogenous sources accelerates aging-related decline in humans.

1.1.2.2. Accelerated Aging Caused by Intrinsic Sources of DNA Damage

Though exogenous sources of DNA damage undoubtedly contribute to aging, intrinsic sources of genomic instability are far more pervasive, affecting all cells throughout the body. Several lines of evidence support the hypothesis that DNA damage and defects in DNA repair processes are the underlying cause of aging, with functional DNA repair systems promoting longevity while defects in these pathways drive premature aging syndromes.

Enhanced DNA repair efficiency slows the aging process. Across species with varying life expectancies, mutation frequency and lifespan show an inverse correlation (Cagan *et al.*, 2022). Long-lived species, such as the naked mole rat, accumulate fewer mutations per year than their shorter-lived counterparts, such as mice. One explanation for this trend is the greater efficiency of DNA repair pathways in long-lived organisms. Supporting this hypothesis, studies have shown that nucleotide excision repair (NER) and base excision repair (BER) are significantly more effective at repairing DNA damage in naked mole rat cell lines compared to those from mice (Evdokimov *et al.*, 2018). Similar patterns are evident across other species: the "immortal jellyfish," *Turritopsis dohrnii*, displays distinct differences in genes related to DNA replication and repair relative to its mortal relative, *Turritopsis rubra* (Pascual-Torner *et al.*, 2022).

Conversely, defects in DNA repair accelerate the aging process (Niedernhofer *et al.*, 2018). Human progeroid syndromes, characterized by premature aging in one or more organs, are linked to mutations that decrease the activity of DNA repair genes. One such syndrome, Ruijs-Aalfs syndrome, is caused by mutations in the SPRTN gene, which encodes a metalloprotease essential for the degradation of proteins crosslinked to DNA, including stalled topoisomerases (Lessel *et al.*, 2014; Stingele *et al.*, 2014, 2016). Defects in SPRTN lead to the accumulation of DNA-protein crosslinks, causing replication stress and genomic instability, all of which contribute to premature aging phenotypes. This pattern is consistent with other progeroid syndromes, such as Werner syndrome and Hutchinson-Gilford progeria, where defects in DNA repair pathways result in genomic instability and accelerated aging (Niedernhofer *et al.*, 2018). Together, these

disorders underscore the essential role of DNA maintenance in preserving cellular function and delaying the onset of age-related decline.

1.1.2.3. Counterarguments to Genomic Instability as a Driver of Aging

Despite the strong correlation between DNA repair efficiency and lifespan, the role of genomic instability in aging is not without contention (Schumacher *et al.*, 2021; Chatsirisupachai and De Magalhães, 2024). One counterargument is that enhancing a single DNA repair pathway does not consistently extend lifespan in the laboratory context (Mangerich *et al.*, 2010; Shaposhnikov *et al.*, 2015). Another counterargument arises from genomic studies, which indicate that genomic maintenance pathways are not strongly linked to age-related diseases or extreme longevity (Schumacher *et al.*, 2021). A further challenge to this hypothesis is the observation that while aged cells exhibit a higher mutational burden than young cells, the increase does not appear substantial enough to account for the full spectrum of aging-related pathologies (Smith, 1962).

These observations are not necessarily surprising. Given the redundancy among repair mechanisms and the tissue-specific relevance of different types of DNA damage and repair pathways, overexpressing a single DNA repair process is unlikely to have a significant impact on lifespan and may even be detrimental in cell types with low levels of DNA damage. Associative studies on aging-related diseases and longevity also fail to account for this complexity. Moreover, accurately tracking faithful DNA repair is challenging, and may obscure additional effects, such as reshaping the epigenetic landscape and influencing other hallmarks of aging. Notably, mutation events themselves may not be necessary for DNA damage to drive aging (Yang *et al.*, 2023).

A final counterargument is drawn from humans carrying mutator alleles of the major replicative DNA polymerases (Robinson *et al.*, 2021). Although these individuals exhibit high rates of early-onset colorectal and endometrial tumors, the authors report a lack of progeroid-like symptoms. However, mutations causing similar defects in yeast produce shorter replicative lifespan, especially in the context of faulty mismatch repair pathways (Lee *et al.*, 2019). This raises the possibility that the early onset of cancer in patients with mutator phenotypes masks an early aging phenotype. While genomic instability may initiate and exacerbate age-related decline, the counterarguments postulated here illustrate the multifaceted nature of aging. However, they fail to eliminate genomic instability as a driver of aging, merely suggesting that multiple, interacting factors shape the aging process.

These counterarguments acknowledge the complexity of aging but do not refute the central role of genomic instability in driving the process. Understanding how DNA damage accelerates aging and how repair mitigates its effects remains a critical avenue for research, with important implications for interventions that promote healthy aging. To set the stage, the following sections examine the molecular processes that preserve genome integrity, with a particular focus on how ribonucleotide contamination of the genome may contribute to aging.

1.2. DNA and RNA as the Information Storage and Messaging Molecules

Given the importance of genome stability for the central argument of this thesis, a detailed understanding of the mechanisms by which cells safeguard their DNA is essential. At the most fundamental level, both the chemical composition and the three-dimensional architecture of DNA contribute to its stability and the accuracy of its duplication (Alberts *et al.*, 2007). The deoxyribose-phosphate backbone and complementary base-pairing properties ensure fidelity by maintaining a stable structure and preventing mispairing. Meanwhile, the double-stranded, anti-parallel, helical conformation provides a robust framework that facilitates error detection, repair processes, and the recruitment of DNA-binding proteins essential for replication and genome maintenance.

A critical feature of nucleic acid chains is their directional polarity, which arises from the asymmetry of the sugar-phosphate backbone (Alberts *et al.*, 2007). Each nucleic acid strand has a 5′ end, where a phosphate group is attached to the fifth carbon of the sugar, and a 3′ end, where a hydroxyl (-OH) group is attached to the third carbon (Figure 1A). DNA usually exists as a duplex with the two strands being reverse complements. The antiparallel nature of double-stranded DNA (dsDNA) results from the geometric constraints of proper base pairing, which ensures stable hydrogen bonding and provides the structural foundation for essential processes such as DNA replication and repair.

Beyond its chemical composition and directional constraints, DNA possesses additional structural features that enhance genome stability. The negative supercoiling of DNA, maintained by topoisomerases, relieves torsional strain and prevents spontaneous strand breaks, reducing the likelihood of genomic instability (Champoux, 2001). In eukaryotic cells, DNA is further stabilized by its organization into chromatin, where it is wrapped around histone proteins to form nucleosomes. This packaging not only protects DNA from physical and chemical damage but

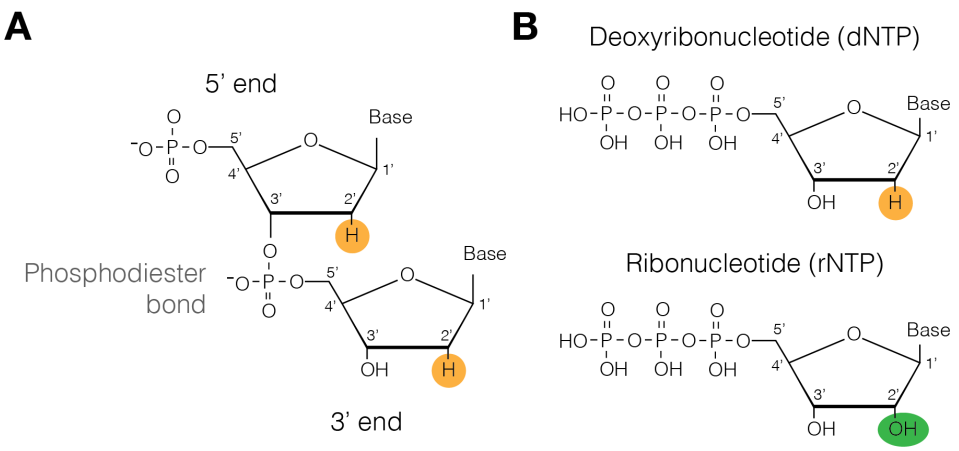

Figure 1 Structural features of DNA and RNA nucleotides and the phosphodiester backbone

(A) DNA strands have inherent polarity, defined by the orientation of the sugar-phosphate backbone. The 5′ end contains a terminal phosphate group, while the 3′ end terminates in a free hydroxyl group. Nucleotides are joined via phosphodiester bonds between the 3′ hydroxyl of one sugar and the 5′ phosphate of the next, establishing directionality. (B) Comparison of deoxyribonucleotides (dNTPs) and ribonucleotides (rNTPs). Both contain a nitrogenous base, a triphosphate group, and a five-carbon sugar, but rNTPs have a hydroxyl group at the 2′ position (green), which contributes to the chemical instability of RNA.

also regulates access to genetic material, ensuring that processes such as transcription and replication occur accurately and at the appropriate time. Collectively, these structural and biochemical features of DNA contribute to the preservation of genetic information, ensuring that cells maintain genome integrity across generations.

While DNA serves as the permanent repository of genetic information, RNA acts as an intermediary in gene expression, facilitating the transfer of genetic instructions from DNA to protein. Ribonucleotides, the basic building blocks of RNA, are distinguished from deoxyribonucleotides at the 2' position of the sugar moiety: the ribose in RNA contains a hydroxyl group, whereas the deoxyribose in DNA has a hydrogen atom at this position (Figure 1B). This 2' hydroxyl renders RNA considerably more susceptible to hydrolytic degradation (Figure 2; Li and Breaker, 1999). Thus while RNA is well-suited for transient amplification and transmission of genetic information, it is not an ideal substrate for long-term information storage. A growing body of evidence underscores the necessity of maintaining the distinct roles of DNA and RNA, as disruptions to this division can have severe consequences (Kellner and Luke, 2020).

1.3. DNA Replication: An Overview

The process of DNA replication goes beyond simply copying the genome to allow for cellular division; replication enzymes must navigate structural impediments such as torsional stress, nucleosomes, and damaged molecules while ensuring fidelity through the precise selection of dNTPs and the exonucleolytic proofreading of misincorporations (Alberts *et al.*, 2007). DNA repair pathways complete the process by facilitating the faithful correction of misincorporated bases and repair at damaged sites. Through coordinated action, the genome is replicated with remarkable accuracy despite challenging conditions.

A fundamental challenge in DNA replication arises from the inherent limitations of DNA polymerases: they cannot initiate strand synthesis *de novo*. Therefore, replication initiation relies on an RNA polymerase, which *can* initiate RNA synthesis *de novo* (Frick and Richardson, 2001). The primase subunit of the Pol-α-Primase complex catalyzes the synthesis of short RNA primers, approximately 10 nucleotides in length, to initiate DNA replication at the replication origin. The DNA polymerase α subunit then extends the RNA primer to initiate DNA strand synthesis. These RNA primers, while necessary for replication initiation, also introduce a significant source of rNMP incorporation into the genome (Williams, Lujan and Kunkel, 2016).

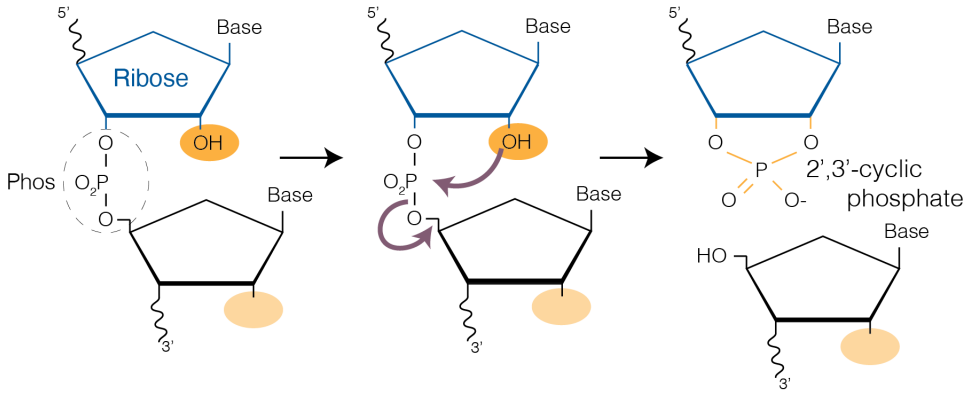

Figure 2 Mechanism of spontaneous RNA backbone cleavage via 2′-OH-mediated hydrolysis.

Ribonucleotides within RNA are inherently unstable due to the presence of a 2′ hydroxyl group on the ribose sugar. This 2′-OH can act as a nucleophile, attacking the adjacent phosphodiester bond in a base-catalyzed reaction. The result is cleavage of the RNA backbone and formation of a 2′,3′-cyclic phosphate on the upstream nucleotide and a 5′ hydroxyl group on the downstream fragment. This spontaneous hydrolysis contributes to RNA instability and distinguishes RNA from the more chemically stable DNA, which lacks the 2′ hydroxyl group.

To fully appreciate the extent of rNMP incorporation during priming requires a foundational understanding of DNA replication, particularly the different mechanisms of DNA synthesis carried out on the leading strand compared to the lagging strand. DNA polymerases catalyze the formation of a covalent bond between the growing strand and an incoming nucleoside triphosphate only when the nascent strand possesses a free 3'-hydroxyl (-OH) group (Alberts *et al.*, 2007). Yet, dsDNA has opposite polarity, therefore, DNA synthesis must occur in opposite directions on the two template strands. At each replication origin, two replication forks are established and move in opposite directions away from the replication origin. Consequently, one strand—the leading strand—is synthesized continuously in the direction of the replication fork's movement, mostly by DNA polymerase ε, while the lagging strand must be synthesized discontinuously through repeated cycles of priming and extension by coordinated action between Pol-α-Primase and DNA polymerase δ. Lagging strand synthesis generates fragments containing the RNA primer and about 200 nucleotides of DNA called Okazaki fragments. Therefore, priming incorporates approximately 600,000 rNMPs into the yeast genome and approximately 150 million rNMPs into the human genome (Williams and Kunkel, 2014; Williams, Lujan and Kunkel, 2016).

The completion of DNA replication produces two exact, continuous copies of the genome (Sun *et al.*, 2023). To achieve this, RNA primers must be removed and all DNA fragments ligated to form continuous strands of DNA. The mechanism of lagging strand synthesis necessitates frequent RNA primer removal and ligation of the Okazaki fragments as the fork proceeds. To this end, DNA polymerase δ catalyzes strand-displacement of the RNA primer and a short stretch of DNA when it encounters the previously synthesized Okazaki fragment. This generates an RNA-DNA flap structure, which is cleaved off by 5’ DNA flap endonuclease, exemplified by human FEN1. The resulting DNA nick is sealed by DNA ligase 1. Through this highly coordinated maturation process, the vast majority of ribonucleotides incorporated during DNA replication are efficiently removed and replaced with deoxyribonucleotides, ensuring the proper composition of the DNA strands and the ligation of thousands to millions of Okazaki fragments in the process.

1.4. Fidelity of DNA Polymerases

Faithful replication of the genome relies on three key mechanisms: (I) high-fidelity nucleotide selection by DNA polymerases, (II) exonuclease-based proofreading activity, and (III) downstream repair pathways that correct misincorporated bases (Kunkel and Bebenek, 2000).

While DNA polymerases efficiently prevent the incorporation of mispaired dNTPs via mechanisms I and II, these mechanisms are less effective at discriminating against and proofreading the incorporation of correctly base-paired ribonucleotides (Nick McElhinny, Watts, *et al.*, 2010). In this context, genome integrity becomes more dependent on mechanism III—post-replicative excision of incorporated ribonucleotides. Mutations affecting any of the three mechanisms result in mutator phenotypes and genomic instability, contributing to aging (Schumacher *et al.*, 2021), cancer (Barbari and Shcherbakova, 2017), and autoimmune diseases (Aditi *et al.*, 2021).

1.4.1. Base-Pairing Fidelity: Nucleotide Selection by DNA Polymerases

High-fidelity nucleotide selection is driven by the shape complementarity of correctly paired bases (Kunkel and Bebenek, 2000). When an incorrect nucleotide enters the active site, it disrupts proper Watson-Crick base-pairing geometry, creating a steric clash that hinders the conformational changes required for catalysis. If a mispaired nucleotide is added, DNA polymerases with 3' to 5' exonuclease activity can remove the mispaired base via proofreading. The presence of a mismatch within a few bases of the DNA terminus results in the nascent strand being translocated to the exonuclease site of the DNA polymerase to remove the incorrect base(s). Together, these mechanisms ensure an exceptionally low base substitution frequency of approximately 1 nucleotide change for every 10 billion bases replicated.

1.4.2. Sugar Discrimination: Preventing rNMP Incorporation

DNA polymerases face yet another challenge when replicating DNA within the nuclear milieu: distinguishing between rNTPs and dNTPs. This presents a significant challenge due to the vastly higher intracellular concentrations of rNTPs during S-phase, which are 30- to 200-fold greater than those of the corresponding dNTPs (Brown and Suo, 2011). Though DNA polymerases can partially discriminate against rNTPs, DNA replication nevertheless results in widespread incorporation of single ribonucleoside monophosphates (rNMPs) into the genome. Estimates suggest that in yeast, 13,000 rNMPs are incorporated per replication cycle, while in mice, the number is more than 1 million (Reijns *et al.*, 2012; Williams and Kunkel, 2014). This number exceeds the combined load of all other non-canonical bases encountered by the cell (Kellner and Luke, 2020).

DNA polymerases achieve sugar selectivity primarily through the steric gate residue located in the active site, which prevents incorporation of rNTPs by creating steric hindrance

against the ribose 2'-hydroxyl group (Brown and Suo, 2011). The specific amino acid responsible for this function varies by polymerase family; replicative polymerases α, δ, and ε utilize a tyrosine residue as the steric gate. Mutations in this residue abrogate sugar selectivity, leading to severe replication defects and inviability (Pavlov, Shcherbakova and Kunkel, 2001). Beyond the steric gate, additional residues influence rNTP discrimination. Recent studies have identified a sensor residue on the polymerase finger domain that enhances sugar selectivity (Parkash *et al.*, 2023). This discovery aligns with observations that rNMP incorporation rates differ among polymerases, suggesting that multiple residues contribute to sugar selectivity (Figure 3; (Nick McElhinny, Kumar, *et al.*, 2010; Parkash *et al.*, 2023). Alleles of DNA polymerase with steric gate mutations have become valuable tools for dissecting rNMP removal pathways, and facilitating the identification of the distinct roles of DNA polymerases α, δ, and ε in replication (Lujan, Williams and Kunkel, 2016). Despite the robust exonuclease activity of replicative DNA polymerases in correcting base mispairing, their ability to recognize and remove misincorporated ribonucleotides is far inferior (Göksenin *et al.*, 2012; Williams *et al.*, 2012; Clausen *et al.*, 2013).

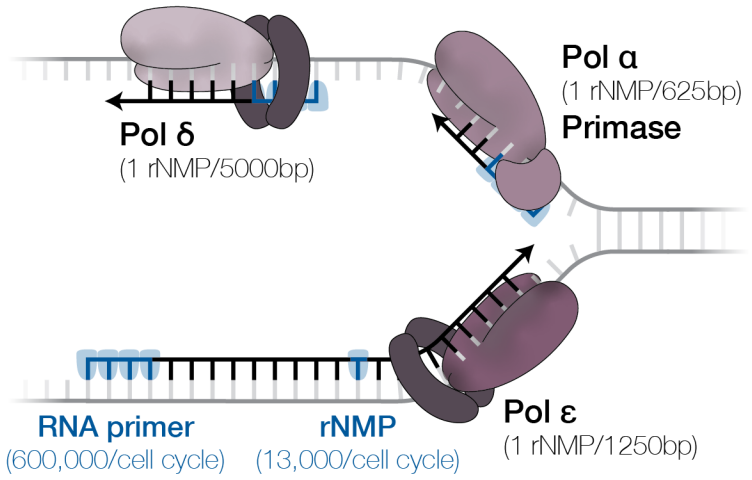

Figure 3 Ribonucleotide incorporation during eukaryotic DNA replication

At the replication fork, three replicative DNA polymerases contribute to DNA synthesis: DNA polymerase ε (Pol ε) synthesizes the leading strand, while DNA polymerase δ (Pol δ) and DNA polymerase α-primase (Pol α-primase) alternate in synthesizing the lagging strand. Pol α-primase initiates each Okazaki fragment with an RNA primer (blue), which is extended by Pol α before handoff to Pol δ. All three polymerases incorporate ribonucleotides (rNMPs, light blue) into DNA at distinct frequencies. Pol α has the highest rNMP incorporation rate (~1 rNMP per 625 bp), followed by Pol ε (~1 rNMP per 1250 bp) and Pol δ (~1 rNMP per 5000 bp). RNA primers are a major source of ribonucleotides in the genome, with ~600,000 RNA primer-derived rNMPs and ~13,000 rNMPs from polymerase misincorporation per cell cycle in yeast.

This reveals a fundamental difference between base-pair fidelity and sugar discrimination, wherein rNMPs evade proofreading mechanisms and must instead be removed by specialized post-replicative repair pathways. Given the high frequency of rNMP incorporation, their removal is crucial to alleviating the substantial burden they impose on the cell in the context of preserving genome stability.

1.5. Consequences of Genomic Ribonucleotides

The unintended incorporation of rNMPs into DNA during replication and repair undermines genome stability (Williams and Kunkel, 2014). Retention of rNMPs in the genome can lead to altered DNA structure, changes in chromatin state, replication stress, and imperfect DNA repair. These effects cause genomic instability, increasing the risk of mutations or chromosome breaks. This underscores the fundamental principle that long-term genetic information is best preserved in DNA rather than RNA and introduces the possibility that genomic rNMPs—drivers of genomic instability—may also drive aging processes.

1.5.1. Structural Changes in DNA Caused by Embedded rNMPs

The presence of rNMPs in the DNA helix leads to structural perturbations, though the extent of these changes remains debated in the literature. Early crystallography studies indicated that rNMP incorporation caused a global shift from the more extended B-form DNA to the more compact A-form (Egli, Usman and Rich, 1993). However, more recent studies indicate that these structural alterations are more localized, with the rNMP site adopting A-form characteristics while adjacent dNMPs retain the C2'-endo form characteristic of B-form (DeRose *et al.*, 2012). This conformational preference arises due to steric hindrance introduced by the 2’ hydroxyl group on the rNMP. Thus, the overall impact on the DNA helix is probably limited.

Despite the limited long-range structural changes, localized changes in DNA structure still have the possibility to perturb chromatin structure. In eukaryotic cells, DNA is wrapped around histone octamers to form nucleosomes, a process that requires specific interactions with B-form DNA (Dunn and Griffith, 1980). Changes to DNA structure can inhibit DNA-histone interactions. Indeed, early biochemical data indicated that an RNA-DNA hybrid composed of one strand of RNA and one strand of DNA failed to form nucleosomes. In fact, nucleosome assembly fails on a DNA duplex with 5% or more rNMPs (Hovatter and Martinson, 1987). Even a single ribonucleotide was found to reduce nucleosome formation *in vitro* by 20%. To date, no studies have addressed the effect of high rNMP load on chromatin architecture *in vivo*. In light of the

biochemical data, one may expect drastic effects on nucleosome position and deposition. Loss of nucleosomes from the genome can result in defects in various cellular processes, as DNA accessibility is crucial for proper gene regulation and chromatin organization. Given the importance of DNA structure in mediating DNA-protein interactions, it is likely that other DNA-binding proteins, such as transcription factors or telomere-binding proteins, may also be affected by rNMP-induced distortions in DNA.

1.5.2. Defects in DNA Replication and Repair Caused by rNMPs

DNA replication is carried out by DNA-dependent DNA polymerases meaning that they only synthesize new DNA using DNA as a template. This selectivity for DNA template appears to be strict *in vitro*, as progression of DNA replication can be stalled by the presence of even a single ribonucleotide in the template strand of DNA (Nick McElhinny, Kumar, *et al.*, 2010). In yeast, replication bypass efficiency depends on the polymerase as well as the base identity of the ribonucleotide in the template (Watt *et al.*, 2011). Lagging strand DNA polymerase δ is the most sensitive to rNMPs in the template strand with bypass probability ranging from 7.4% on templates containing rA or rU to 63% on templates containing rC. The bypass probability of rG varied between two different sequence contexts, indicating that the surrounding sequence plays a crucial role in determining bypass efficiency. The leading strand DNA polymerase ε bypass efficiency ranges from 32-85%. If these data hold true in the *in vivo* condition, the replication of the rNMP containing genome will encounter many impediments to fork progress. Indeed, yeast strains harboring high numbers of rNMPs in the genome progress slowly through S-phase and have elevated dNTP levels, indicators of replication stress (Nick McElhinny, Kumar, *et al.*, 2010).

Another significant source of replication stress arises due to the presence of the 2’ hydroxyl group on the ribose sugar: as mentioned in section 1.2, ribonucleotides are prone to spontaneous hydrolysis. When the hydrolyzed rNMP is embedded in DNA, it produces a nick in the DNA backbone, which terminates in a 2’ 3’ cyclic phosphate and a 5’ hydroxyl group making it a so-called “dirty” break that cannot be simply religated without first converting the ends into ligatable 3’ hydroxyl termini and 5’ phosphate termini. If a replication fork encounters such a nick, it is converted into a single-ended DNA double-strand break (seDSB), which presents a severe threat to genomic integrity (Schindler *et al.*, 2023). Unlike canonical double-strand breaks that have two DNA ends available for repair, seDSBs are particularly hazardous because they lack a second DNA end, preventing direct repair via non-homologous end joining (NHEJ). Instead, the cell must rely on homologous recombination (HR) or fork restart pathways to resolve

the lesion. If the seDSB occurs in a region lacking homologous sequences, repair can be inefficient, increasing the likelihood of chromosomal rearrangements or replication fork collapse.

A recent study (Schindler *et al.*, 2023) delineated the genetic network required for repairing seDSBs that arise from rNMP incorporation, introducing the nick-lesion synthesis (NLS) pathway as a key mechanism involved in addressing these lesions. Key genetic links of NLS include homologous recombination-based DNA repair, and the replication-coupled nucleosome assembly pathway which facilitates the deposition of newly synthesized histones onto the two daughter strands produced by DNA replication. The mechanism by which faulty histone deposition leads to lethality in the context of seDSBs has not yet been elucidated, but the connection is particularly intriguing in the context of the aging, where nucleosome occupancy is reduced. These findings provide crucial insight into how cells mitigate the consequences of rNMP-induced breaks and suggest that defects in these pathways could contribute to genome instability in higher eukaryotes.

1.5.3. Defects in Transcription Caused by rNMPs

Genomic rNMPs have the potential to disrupt transcription elongation by DNA-dependent RNA polymerases as well. However, only one study has been conducted on the topic to date (Agapov, Olina and Kulbachinskiy, 2022). This study utilized human mitochondrial RNA polymerases to assay *in vitro* transcription rates on templates containing rNMPs, a particularly relevant model given that mitochondrial genomes retain higher numbers of rNMPs compared to the nuclear genome due to lack of post-replicative repair processes (Wanrooij and Chabes, 2019). The study found an increased incidence of early transcription termination *in vitro* when RNA polymerase encountered a single rNMP embedded in the transcribed strand (Singh *et al.*, 2022). This effect was exacerbated when multiple consecutive rNMPs were embedded. The effect of rNMPs on transcription *in vivo* has yet to be explored, but based on *in vitro* data, one can speculate that there will be a dose dependent defect, with increased pre-mature termination rates as rNMP content rises. Given that yeast cells are able to survive an rNMP load of approximately 1 rNMP per every 100bp of DNA, it leads to the possibility that RNA polymerases are better able to bypass rNMPs *in vivo* than *in vitro*, or perhaps there are undiscovered mechanisms that ensure removal of rNMPs from essential genes.

1.6. Ribonucleotide Excision Repair (RER)

The removal of misincorporated rNMPs is critical for maintaining genome integrity, particularly given their high frequency of incorporation during DNA replication. The ribonucleotide excision repair (RER) pathway is dedicated to this process, with RNase H2 serving as the key enzyme responsible for initiating repair (Williams and Kunkel, 2014; Kellner and Luke, 2020). RNase H2 is a heterotrimeric complex that recognizes rNMPs embedded in DNA and cleaves the DNA backbone at the site of incorporation, facilitating their faithful removal from the genome. The important role of RNase H2 in genome maintenance is underscored by the fact that its deletion is embryonic lethal in mice (Reijns *et al.*, 2022). However, RNase H2 activity is not essential in cultured mouse or human cell lines, nor is it essential in yeast, providing viable model systems to study its mechanism and regulation in greater detail.

1.6.1. Mechanism of RNase H2 Activity

RNase H2 specifically targets RNA-DNA junctions (Rychlik *et al.*, 2010). Structural studies have revealed how RNase H2 recognizes this unique substrate. A tyrosine residue within the enzyme plays a key role by interacting with both the rNMP and the adjacent DNA. The tyrosine's ring structure stacks on top of the deoxyribose sugar at the 3' side of the rNMP, a conformation that would be sterically hindered if a ribose were present. Additionally, its hydroxyl group forms a hydrogen bond with the 2' hydroxyl group of the ribose in the rNMP, reinforcing substrate specificity. A GRG motif within the RNase H2 enzyme further stabilizes substrate recognition by interacting with the 2' hydroxyl group of the ribose and protruding into the minor groove of the RNA-DNA junction. Importantly, this minor groove adopts an altered conformation compared to a standard DNA-DNA helix due to the presence of the rNMP (see section 1.1.3). Together, these interactions allow RNase H2 to distinguish rNMP embedded DNA from other species of nucleic acids

RNase H2 also induces a structural shift in the substrate, forcing a conformational change in the helix that positions it for cleavage (Rychlik *et al.*, 2010). Catalysis occurs at the RNase H2 active site, which coordinates two divalent metal ions and a nucleophilic water molecule to hydrolyze the phosphodiester bond. This reaction leaves a DNA backbone nick with a 3' hydroxyl and 5' phosphate terminus, enabling downstream repair by extension of the 3' hydroxyl group. The remaining rNMP-containing fragment is processed similarly to Okazaki fragment maturation during lagging-strand DNA synthesis (see section 1.2), meaning that DNA strand displacement

creates a flap with the rNMP and a few bases of DNA. Thus, the rNMP is excised from the genome as part of a short oligo cleaved by flap endonucleases (Figure 4).

Notably, RNase H2's recognition of rNMPs is sequence-independent, relying solely on structural features of the RNA-DNA junction for detection, rather than specific nucleotide sequences. This broad specificity allows the enzyme to scan the genome and efficiently remove misincorporated rNMPs, preventing genomic instability regardless of the sequence context.

1.6.2. Cell-Cycle Regulation of RNase H2 Activity

RNase H2 expression levels vary throughout the cell cycle. RNase H2 is encoded by three genes: *RNASEH2A*, *RNASEH2B*, and *RNASEH2C* in human cells, which correspond to the *RNH201, RNH202*, and *RNH203* genes in yeast. The *RNASEH2A*/*RNH201* subunit encodes the catalytic component, while *RNASEH2B*/*RNH202* and *RNASEH2C*/*RNH203* serve as accessory proteins essential for enzymatic activity.

In human cells, *RNASEH2A* expression is induced by the binding of transcription factors E2F1 and E2F3 to its promoter (Sugawara *et al.*, 2022). Accumulation of E2F transcription factor activity, including E2F1 and E2F3, is critical for cell cycle progression from G1 to S-phase, driving the expression of genes required for DNA synthesis and replication (DeGregori *et al.*, 1997). Similar cell-cycle regulation has been described from early studies in yeast; *RNH201* RNA expression and enzymatic activity in protein extracts follows a diphasic pattern, peaking during S-phase and again in G2/M-phase (Arudchandran *et al.*, 2000). Later studies utilized alleles of *RNH202* in which the expression of the protein was limited to either the S phase or the G2/M

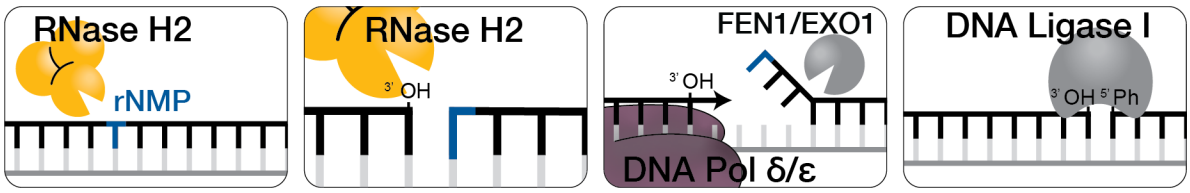

Figure 4 Ribonucleotide excision repair (RER) pathway initiated by RNase H2.

Misincorporated ribonucleotides (rNMPs) in DNA are recognized and processed by the RER pathway to restore DNA integrity.
(Left to right)
Panel 1: RNase H2 incises the DNA backbone at the 5′ side of the embedded rNMP. **Panel 2:** This cleavage generates a nick with a 3′ hydroxyl group, which primes DNA synthesis. **Panel 3:** DNA polymerase δ or ε extends the 3′ end, displacing the downstream strand containing the rNMP. The displaced flap is removed by the endonuclease FEN1 or exonuclease EXO1.
Panel 4: DNA ligase I seals the nick to complete repair.

phase of the cell cycle (Lockhart *et al.*, 2019). These studies indicated that expression of RNase H2 during G2/M-phase of the cell cycle was sufficient to support RER activity, while restricting expression to S-phase resulted in defects in rNMP processing. In fact, S-phase-specific expression of RNase H2 led to rNMP processing in front of the replication fork, resulting in toxic seDSBs (Lockhart *et al.*, 2019; Schindler *et al.*, 2023). Proper timing of expression ensures that RNase H2 activity is synchronized with DNA replication and repair demands.

Although the specific transcriptional regulators of *RNH201* in yeast remain unclear, its cell cycle-dependent expression suggests the involvement of general cell cycle-regulated transcription factors such as Swi4/Swi6 (SBF complex) and Mbp1/Swi6 (MBF complex)**,** which are known to control genes involved in the G1/S transition (Hendler *et al.*, 2018). The promoter of *RNH201* contains a potential binding site for the MBF complex, CRCGAAA (personal observation). Understanding the conservation of regulatory mechanisms between yeast and human cells may provide further insights into how RNase H2 expression is fine-tuned to ensure genomic stability.

1.6.3. RNase H2 Activity at R-Loops

In addition to its role in RER, RNase H2 is involved in the removal of R-loops, three-stranded nucleic acid structures formed when RNA hybridizes to a DNA strand, generating an RNA:DNA hybrid and a displaced single-stranded DNA loop (Petermann, Lan and Zou, 2022). R-loops are natural intermediates of cellular processes such as transcription, DNA replication, and DNA repair, where they often play a regulatory role. However, their unscheduled formation can lead to transcription-replication conflicts (TRCs) that prevent progression of the replication fork and compromise genome stability. Eukaryotic cells encode for two RNase H enzymes, the second being RNase H1. RNase H1 does not have enzymatic activity against single rNMPs embedded in the genome, the main focus of this thesis, but it does play a role in R-loop metabolism, especially when R-loops become toxic during DNA replication. These dual roles of R-loops in DNA metabolism suggest a need for tight regulation to maintain their beneficial functions while preventing harmful accumulation. RNase H2 aids in R-loop resolution by degrading the RNA moiety of these structures, thereby preventing their persistence.

Notably, RNase H2's function in RER is distinct from its role in R-loop degradation (Cerritelli and Crouch, 2019). This distinction is particularly relevant given the use of a separation-of-function allele, referred to as the ribonucleotide excision-deficient (RED) allele. The RED allele serves as a crucial tool in the experiments described in this thesis, allowing differentiation

between phenotypes arising from defective RER and those caused by unregulated R-loop accumulation.

1.6.4. RNase H2 in Human Disease

Given the pivotal role of RNase H2 in essential nucleic acid processing pathways, it is not surprising that its deficiency is associated with human disease (Cerritelli and El Hage, 2020). RNase H2 safeguards genome integrity by removing misincorporated ribonucleotides, preventing replication stress, and mitigating aberrant nucleic acid structures. When RNase H2 function is compromised, cells accumulate these errors, leading to increased mutagenesis and activation of DNA damage responses. Over time, this genomic instability can contribute to the development of severe pathological conditions. While the most well-characterized disorder linked to RNase H2 mutations is Aicardi-Goutières Syndrome (AGS), emerging evidence suggests broader implications for cancer, aging, and other diseases.

1.6.4.1. Congenital Disease - Aicardi-Goutières Syndrome (AGS)

Aicardi-Goutières Syndrome (AGS) is a severe, early-onset autoinflammatory disorder caused by monogenic mutations in genes involved in nucleic acid metabolism and immune signaling, including, but not limited to, *RNASEH2A, RNASEH2B*, and *RNASEH2C* (Crow, Hayward, *et al.*, 2006; Crow, Leitch, *et al.*, 2006). AGS is characterized by neuroinflammation, microcephaly, cerebral atrophy, and an upregulation of type I interferon-stimulated genes, resembling a chronic viral infection (Aicardi and Goutières, 1984; Goutières, 2005). Molecular studies have shed light on the mechanisms by which RNase H2 deficiencies drive immune activation (Crossley *et al.*, 2023); however, recent findings in a mouse model of AGS suggest that it is the underlying genomic instability, rather than interferon signaling alone, that drives disease progression (Aditi *et al.*, 2021). This raises a key question: is the primary pathogenic factor the accumulation of genomic rNMPs, or is defective R-loop processing the predominant driver of inflammation and neurodegeneration?

During a viral infection, viral genomic material—double stranded RNA, RNA:DNA hybrids, and dsDNA—accumulates in the cytoplasm as a byproduct of viral replication (Crow and Stetson, 2022). These nucleic acid structures are not typically found in the cytosol of uninfected cells thus their presence triggers the host immune systems antiviral response. This response restricts viral replication, enhances antigen presentation, and, in cases of sustained activation, induces programmed cell death to eliminate infected cells. In RNase H2 deficient cells, proper

cellular compartmentalization of DNA is disrupted. Faulty processing of R-loops in the nucleus results in the accumulation of fragmented RNA:DNA hybrids, which are subsequently exported to the cytosol and presented to the host immune system, a situation that mimics viral infection (Günther *et al.*, 2015; Crossley *et al.*, 2023). Consequently, faulty R-loop processing due to RNase H2 deficiency leads to chronic activation of the immune response, resulting in sustained autoimmunity with potentially severe consequences.

Despite the evidence that defective R-loop processing contributes to inflammatory responses, the precise molecular pathology of AGS remains unclear. Findings from a mouse model for AGS suggest that genomic instability arising from accumulated rNMPs, rather than R-loops alone, may be a key driver of disease progression (Aditi *et al.*, 2021). This observation suggests the possibility that rNMP incorporation exacerbates genomic instability, indirectly fueling the immune response. Thus, AGS pathogenesis appears to be driven by a combination of ribonucleotide accumulation and persistent RNA:DNA hybrids, both of which disrupt genome integrity and contribute to sustained immune activation.

AGS in human patients is caused by a biallelic mutations in a single gene. The parents of AGS patients are therefore obligate heterozygous mutation carriers, and present an opportunity to understand the effect of a monoallelic RNase H2 mutation. Interestingly, the parents of AGS patients exhibit increased, yet subclinical levels of autoantibodies, correlating with an increased risk of developing autoimmune diseases (Günther *et al.*, 2015). This observation suggests a potential dosage sensitivity of the RNase H2 complex, implying that full RNase H2 activity is required to mitigate the cumulative genomic stress imposed by rNMPs and R-loops.

1.6.4.2. Cancer

While AGS is the most well-characterized disease associated with RNase H2 deficiency, defects in rNMP removal could contribute to tumorigenesis as well (Hiller *et al.*, 2018; Reijns *et al.*, 2022). The accumulation of rNMPs in DNA can result in replication stress, increased mutagenesis, and genome instability (Kellner and Luke, 2020)—hallmarks of cancer development. However, direct links between RNase H2 mutations and specific cancers remain limited.

One example of a specific type of cancer associated with defective RER is Chronic lymphocytic leukemia (CLL; (Kipps *et al.*, 2017). CLL tumors frequently harbor deletions encompassing the *RNASEH2B* locus. However, *RNASEH2B* deletion is not suspected to be the oncogenic driver in these tumors. *RNASEH2B* lies in close proximity to a microRNA (miRNA)

cluster, which plays a dual role in suppressing tumorigenesis by inhibiting apoptosis and promoting cellular proliferation. RNase H2 loss may contribute to genomic instability, yet the selective advantage conferred by *RNASEH2B* deletion in CLL is more likely due to deregulated miRNA expression rather than direct effects of impaired RER. Nevertheless, the frequent co-deletion of *RNASEH2B* raises questions about whether reduced RNase H2 activity could exacerbate CLL progression by increasing genomic instability or altering DNA repair pathways.

Regardless of the role of RNase H2 inactivation in tumorigenesis, it could provide a potential target for chemotherapeutics (Zimmermann *et al.*, 2018). Mutations in *RNASEH2A, RNASEH2B*, and *RNASEH2C* have been identified in screens for genes whose loss sensitizes cancer cells to the PARP inhibitor olaparib. This discovery provided the first evidence that genomic rNMPs are a source of endogenous DNA damage that renders cells vulnerable to replication stress-targeting therapies. The underlying mechanism was later elucidated: in the absence of RNase H2, rNMPs embedded in DNA persist and are processed by DNA topoisomerase 1 (Top1), leading to the formation of cytotoxic Top1 cleavage complexes. These complexes induce replication-associated DNA breaks**,** promoting synthetic lethality in cells treated with PARP inhibitors. This finding not only demonstrated a functional consequence of impaired rNMP removal in cancer cells but also positioned RNase H2 as a potential target for combination therapies exploiting replication stress pathways.

Building on this observation, RNase H2 deficient cancer cells exhibit significantly higher levels of a distinct class of mutations referred to as ID4 (Reijns *et al.*, 2022). The ID4 cancer signature, as classified by COSMIC, consists of deletions ranging from 2 to 5bp, frequently involving the loss of a single repeat unit within short tandem repeats. These deletions arise due to the interplay between embedded ribonucleotides and the imperfect alternative removal pathway initiated Top1. Interestingly, the ID4 mutation signature is frequently observed in highly expressed genes, even in RNase H2 proficient tumors. For example, prostate cancer samples, despite being RNase H2 proficient, exhibit an increased ID4 signature in highly expressed, prostate-specific genes, indicating that mis-regulated Top1 activity may contribute to genomic instability even in RNase H2 proficient tumors. This suggests that other factors influencing rNMP incorporation or repair, such as replication stress, transcriptional activity, or alternative ribonucleotide processing pathways, could shape the mutational landscape of cancer and provide potential drug targets for treatment.

The above studies show an increase in mutation signature associated with high transcription rates and RER deficiency in tumors, yet they provide no evidence that genomic

instability caused by RER deficiency drives cancer development. To this end, a study in mice provided direct evidence of its oncogenic potential (Hiller *et al.*, 2018). The epidermis-specific inactivity of RNase H2 resulted in 100% penetrance of squamous cell carcinoma, providing evidence for the role of RER deficiency in tumorigenesis. Given this observation, it would be interesting to assess whether monoallelic RNase H2 inactivation, as seen in the parents of AGS patients—which is sufficient to promote a degree of genomic instability that sensitizes them to autoantibody development—also confers an increased cancer risk. If so, this would further underscore the essential role of RNase H2 in suppressing malignant transformation of tissues.

Together, these findings illustrate a direct link between RNase H2 deficiency, rNMP-induced DNA damage, and cancer-associated mutational signatures. The increased reliance of RNase H2-deficient cells on alternative DNA repair pathways reveals a potential vulnerability that could be exploited for therapeutic interventions. Further research is needed to determine whether RNase H2 mutations play a role in human cancer susceptibility and to assess the clinical relevance of targeting Top1-mediated rNMP processing in cancer treatment.

1.6.4.3. Aging

Cancer is widely recognized as an age-associated disease, driven in part by the accumulation of genomic instability, epigenetic alterations, and chronic inflammation—features that also characterize the aging process itself (Berben *et al.*, 2021). Many of the hallmarks of cancer, including genome instability, telomere attrition, and epigenetic dysregulation, overlap with the hallmarks of aging, underscoring the shared molecular pathways that drive both phenomena (López-Otín *et al.*, 2013).

RNase H2 has been implicated in an aging-related phenomenon called inflammaging (Storici *et al.*, 2019). This persistent inflammatory state arises from multiple sources, including the accumulation of DNA in the cytoplasm, which triggers immune activation (Li *et al.*, 2023). Inflammaging and Aicardi-Goutières syndrome (AGS) share key features, including chronic immune activation, persistent inflammation, and aberrant interferon signaling (Goutières, 2005; Li *et al.*, 2023). This similarity suggests a mechanistic link between RNase H2 function, immune dysregulation, and the aging process.

One study aimed to identify molecular markers in cells from long-lived centenarians to uncover mechanisms that contribute to extended lifespan (Storici *et al.*, 2019). A key finding was the upregulation of RNase H2 in centenarian cells. These cells exhibited high RNase H2 protein levels and, coincidentally, very low levels of RNA:DNA hybrids in the cytoplasm compared to

cells from elderly individuals. However, these experiments were conducted using the S9.6 antibody, which is known to recognize multiple nucleic acid species beyond RNA:DNA hybrids, including double-stranded RNA and short DNA duplexes (Smolka *et al.*, 2021). No controls confirming the identity of this cytoplasmic S9.6 signal were reported. The impact of genomic rNMP levels was not addressed in this study.

Another study linked genomic rNMPs to RNase H2 dysfunction, cellular senescence, and the progeroid disorder Werner syndrome (WS; (Sugawara *et al.*, 2022). The authors found that RNase H2 expression is reduced not only in senescent cells but also in quiescent cells, both of which exhibit lower levels of E2F transcription factors. Based on this observation, they proposed that genomic rNMP accumulation increases in senescent cells, potentially contributing to their genomic instability. However, the data supporting this conclusion remain inconclusive. While alkaline gel electrophoresis revealed progressive DNA fragment shortening in late-passage senescent cells compared to early-passage cells, this reduction could result from other forms of DNA damage, such as abasic sites and oxidative lesions (Luke *et al.*, 2010), rather than solely from rNMP incorporation. This technical limitation could also explain the difference in DNA fragmentation between senescent and quiescent cells, both of which have decreased RNase H2 expression levels. Interestingly, the study also reported an increased presence of short double-stranded DNA (dsDNA) species in the cytosol of senescent cells by microfluidics capillary electrophoresis of the cytosolic fraction, lending support to the previous study's findings. Finally, RNA sequencing data from WS patients indicated decreased RNase H2 expression levels, and *in vitro* activity assays confirmed reduced RNase H2 enzymatic activity from WS patient derived fibroblast cell lines. It remains unclear whether genomic rNMP-induced damage or R-loop-associated instability is the primary source of these cytosolic DNA fragments, or whether both mechanisms contribute. In the context of Werner syndrome, where genome instability is a defining feature, the loss of RNase H2 activity may further exacerbate DNA damage accumulation and promote inflammatory signaling, potentially accelerating aging-related phenotypes.

These findings suggest that RNase H2 plays a crucial role in suppressing inflammation and maintaining genomic stability, potentially contributing to healthy aging. By preventing the accumulation of nucleic acid species that trigger immune activation, RNase H2 may act as a protective factor against inflammaging, thereby slowing age-associated functional decline and reducing the risk of inflammatory diseases.

1.7. Topoisomerase I and the Processing of rNMPs

When RNase H2 activity is compromised, rNMPs persist in the genome, leading to downstream consequences on genome integrity (Kellner and Luke, 2020). Persistent rNMPs pose a challenge for DNA metabolic processes and become the substrate for mutagenic, Top1-mediated removal, as they are not recognized by mismatch repair (MMR) and there is limited evidence supporting their processing by base excision repair (BER). Top1 is a critical enzyme for relieving supercoiling during DNA replication and transcription (Pommier *et al.*, 2022). However, rather than simply removing embedded rNMPs, Top1's activity at these sites introduces an unexpected mutagenic risk, revealing its dual role in both maintaining and destabilizing the genome.

1.7.1. Essential Roles of Topoisomerase I in the Cell

The canonical role of Top1 lies in the maintenance of DNA topology during essential genetic processes that require the two strands of DNA to be separated: replication, transcription, and repair (Pommier *et al.*, 2016). The separation of DNA strands results in both over- and underwinding, referred to as positive and negative supercoiling, respectively. During DNA replication, helicases unwind the DNA in front of the fork, generating positive supercoiling, which can create topological barriers that impede fork progression if not properly resolved. Meanwhile, negatively supercoiled DNA is left in the wake of the fork. If left unresolved, supercoiling can stall replication fork progression, resulting in fork collapse, DNA breaks, polymerase slippage, and increased mutation rates. Similar topological effects occur in front of and behind the RNA polymerase during transcription, where it can cause premature transcription termination or excessive R-loop formation behind the RNA polymerase. R-loops contribute to genome instability by exposing single-stranded DNA, which in turn increases the risk of strand breaks, interferes with replication fork progression, and triggers aberrant DNA repair responses. Proper regulation of Top1 activity is therefore essential for preventing topological stress and maintaining genome stability. Disruptions in this regulation can have far-reaching consequences.

The mechanism by which Top1 alleviates torsional strain on the DNA helix proceeds via a transient single-stranded break in the DNA backbone (Pommier *et al.*, 2016). A catalytic tyrosine residue in Top1 performs a nucleophilic attack, generating a covalent intermediate on the 3' side of the nick while leaving a 5' hydroxyl group free. This allows for controlled rotation of the DNA helix to alleviate supercoiling. Once the torsional stress is relieved, the 5'-hydroxyl group realigns

with the Top1 covalent complex (Top1-cc), facilitating reversal of the Top1-DNA adduct and restoring DNA integrity.

While Top1 is essential for maintaining DNA topology and enabling efficient cellular processes, its activity also carries inherent risks (Wojtaszek and Williams, 2024). Failures in the religation step can trap Top1 in a covalent complex with DNA, forming Top1-DNA protein crosslinks (Top1-DPCs). Top1-DPCs are especially problematic when they occur in front of replication forks, where they can impede fork progression and compromise genome stability. This vulnerability is exploited by chemotherapeutic agents that target Top1. By stabilizing the covalent Top1-DNA intermediate and preventing religation, Top1 inhibitors, such as camptothecin, induce persistent DNA lesions that are particularly toxic to rapidly dividing cancer cells. This dual nature of Top1—ensuring genome integrity while also contributing to genomic instability—underlies both its physiological importance and its relevance as a therapeutic target.

1.7.2. Ribonucleotide-Dependent Mutagenesis by Top1

In the absence of RER activity, a mutagenic processing pathway carried out by Top1 results in short deletions, typically 2-5bp in length, at the site of genomic rNMPs (Nick McElhinny, Kumar, *et al.*, 2010; Kim *et al.*, 2011). This phenotype was first described in yeast, where neither RER nor Top1 activity is essential for cellular survival. These seminal studies in yeast laid the foundation for the later discoveries linking similar mutation signatures to tumor genomes and identifying them as the most frequently occurring *de novo* insertion or deletion in the human germline (Reijns *et al.*, 2022).

The enzymatic activity of Top1 at an rNMP follows the same fundamental mechanism as its activity on supercoiled DNA (Sekiguchi and Shuman, 1997). The presence of a ribose sugar introduces structural distortions in the DNA helix (discussed in Section 1.5.1; (Egli, Usman and Rich, 1993; DeRose *et al.*, 2012). Notably, both supercoiled DNA and DNA with embedded rNMPs serve as substrates for Top1, suggesting shared structural features that make these regions particularly susceptible to Top1 cleavage.

Insights into the sugar selectivity of type 1B topoisomerases were initially derived from studies on vaccinia virus Top1 (Sekiguchi and Shuman, 1997). Vaccinia Top1 exhibits strict sequence specificity, cleaving at 5'-(C/T)CCTT↓-3' sequences, where the "↓" denotes the cleavage site (Shuman and Prescott, 1990). While sequence context downstream of the cleavage site does not affect efficiency, the presence of a ribose sugar at the cleavage junction impairs

religation, leading to the accumulation of covalently trapped Top1-DNA intermediates (Shuman and Prescott, 1990; Sekiguchi and Shuman, 1997).

Vaccinia Top1 also exhibits activity on substrates containing ribonucleotides within its recognition sequence (Sekiguchi and Shuman, 1997). When a thymine at the scissile site was substituted with uracil (5'-CCCTrU↓-3'), cleavage proceeded efficiently, generating a novel product corresponding to the distance from the uracil to the end of the duplex DNA. This suggested an intrinsic endoribonuclease activity, yielding fragments with 2',3'-cyclic phosphate and 5'-hydroxyl ends (Figure 5).

These findings were later extended to eukaryotic Top1. Biochemical assays with recombinant yeast Top1 confirmed that it shares ribonuclease activity, albeit with a more degenerate sequence preference in the scissile strand (5'-(A/T)(G/C)(A/T)T↓-3'), favoring thymine cleavage. Therefore, Top1 enzymatic activity exhibits a sequence preference that dictates cleavage primarily at sites containing rUMP within a defined sequence context. As a result, most rNMPs embedded in the genome are unlikely to be targeted by Top1 ribonuclease activity, limiting its mutagenic impact to specific genomic regions.

The mechanism underlying the signature 2-5 bp deletions catalyzed by Top1 involves a second incision event (Kim *et al.*, 2011). The 2',3'-cyclic phosphate nick left after Top1 cleavage remains a substrate for further Top1 activity. If a second Top1 consensus sequence is located nearby, Top1 can cleave upstream, typically 2 nucleotides away, but up to 5 nucleotides away, as demonstrated in biochemical studies (Sparks and Burgers, 2015). This sequential cleavage,

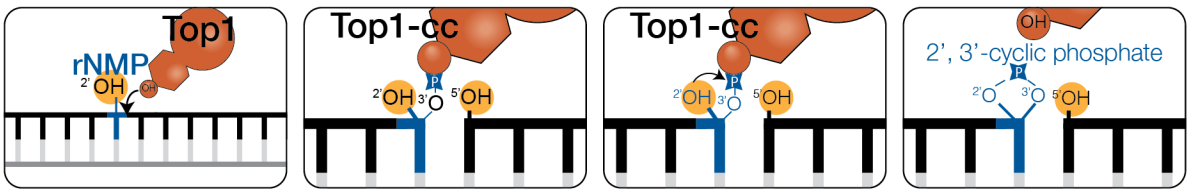

Figure 5 Mutagenic processing of ribonucleotides by DNA topoisomerase I (Top1)

Top1 can initiate mutagenic ribonucleotide excision in the absence of RNase H2 by recognizing and cleaving at rNMPs embedded in DNA.
(Left to right):
Panel 1: Top1 binds at a genomic rNMP and cleaves the DNA backbone 3′ to the rNMP, generating a covalent Top1 cleavage complex (Top1-cc) with the 3′ phosphate and a 5′ hydroxyl.
Panel 2: The presence of the 2′ hydroxyl on the ribose enables a nucleophilic attack on the 3′ phosphate, forming a 2′,3′-cyclic phosphate and releasing Top1.
Panel 3: In some cases, a second Top1 cleavage may occur upstream of the original site.
Panel 4: This second cleavage may generate a 2′,3′-cyclic phosphate end, leaving a nick with incompatible termini that can promote mutagenic repair.

coupled with inefficient religation, results in the excision of an oligonucleotide containing the rNMP, leading to the formation of a short region of ssDNA. The Top1-DNA cleavage complex (Top1-cc) can, in some cases, then transiently reposition and base-pair with the single-stranded DNA region generated by loss of the rNMP-containing oligo (Figure 6). However, if the displaced ssDNA region lacks sufficient complementarity to the upstream cleavage site, realignment may not occur, and the Top1-cc remains irreversibly stalled. In this context, the cleavage complex is converted into a Top1-DPC, which requires alternative pathways for removal. This slippage-based mechanism preferentially occurs at short stretches of short tandem repeats (SSTRs), where the DNA architecture facilitates realignment and mispairing, making these sequences hotspots for Top1-mediated deletions in the absence of RNase H2.

1.7.3. Ribonucleotide-Independent Mutagenesis by Top1

In addition to its mutagenic activity at rNMPs, Top1 activity can also result in frameshift mutations via a ribo-independent mechanism, which is enhanced in regions of high transcription. The link between RER deficiency and Top1-mediated mutagenesis was first established through the observation of similar mutation patterns in RER-deficient strains and in strains overexpressing a general forward mutation reporter to measure transcription-associated mutagenesis (TAM; (Kim *et al.*, 2011; Lippert *et al.*, 2011; Takahashi *et al.*, 2011). Early studies identified Top1 as the mutagenic factor, proposing that increased transcription rates led to higher levels of supercoiling, which in turn enhanced Top1 recruitment to the locus. Supporting this hypothesis, deletion of Top1 abolished the mutation signature in the overexpressed forward

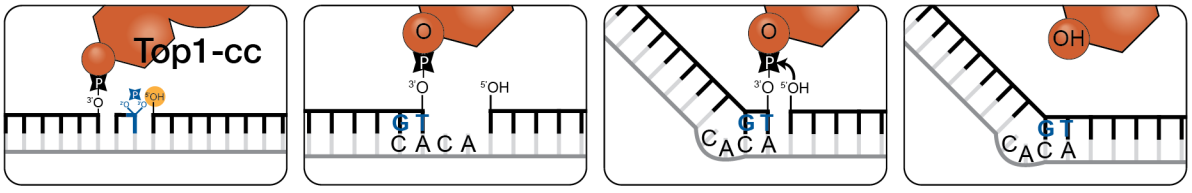

Figure 6 Top1-mediated mutagenesis at ribonucleotides within short tandem repeats.

Top1 can introduce a second cleavage upstream of a pre-existing 2′,3′-cyclic phosphate, generating a gap that promotes misalignment and mutagenic repair in repetitive sequences**.**
(Left to right):
Panel 1: A second Top1 incision occurs upstream of a previously cleaved rNMP site, leaving a gap flanked by a 2′,3′-cyclic phosphate and a 5′ hydroxyl.
Panel 2: The dinucleotide containing the original rNMP is lost, resulting in a ssDNA gap.
Panel 3: The DNA strand realigns via slippage of the tandem repeat, bringing the flanking bases into register.
Panel 4: Top1 reseals the backbone, resulting in a deletion mutation that removes one repeat, a hallmark of Top1 activity in short tandem repeats.

mutation screen, indicating that its enzymatic activity was necessary for mutation formation (Kim *et al.*, 2011; Takahashi *et al.*, 2011). Unlike most mutagenic processes, which are suppressed in transcribed regions, Top1-induced mutations are more likely to occur in regions of high transcription. This makes Top1-mediated mutagenesis particularly problematic for genomic integrity and cell viability as the mutations are more frequent in active genomic regions.

Once the connection between RER deficiency and TAM was established, researchers could then examine the contribution of rNMPs under high transcription conditions (Cho *et al.*, 2013). Although rNMP incorporation does increase mutation rates within the gene, they do not account for all Top1-mediated mutation events, indicating that Top1 can also be mutagenic on DNA alone. Certain sequences lead to ribo-dependent mutations, while others appear to be ribo-independent mutation hotspots. Surprisingly, ribo-independent mutation events are significantly increased in strains harboring the Top1-T722A allele, which has reduced religation efficiency. In contrast, mutations at sequences where Top1 causes ribo-dependent mutagenesis were decreased in this background. This finding further supports the idea that Top1 drives two distinct classes of mutations at SSTR: one dependent on rNMP incorporation and another independent of it.

1.7.4. Top1 Mutagenesis is Leading-Strand Specific

The orientation of the reporter gene used to measure SSTR mutations influences the sequences at which mutations occur, suggesting a strand bias in Top1-mediated mutagenesis (Nick McElhinny, Kumar, *et al.*, 2010). This bias indicates a difference in rNMP processing between the nascent leading and lagging strands.

Genetic studies using DNA polymerase steric gate mutants—which increase rNMP incorporation rates—further support the existence of strand-specific Top1-mediated processing. High rNMP content in the leading strand results in constitutive S-phase checkpoint activation, replicative stress, and genome instability, all indicative of increased DNA damage (Williams *et al.*, 2013). These phenotypes are dependent on Top1 expression implying that Top1 activity at rNMPs in these strains generates nucleic acid intermediates that are difficult to replicate and repair.

In contrast, these phenotypes are not observed when increased rNMPs are incorporated into the lagging strand via the steric gate mutant DNA polymerase δ (Williams *et al.*, 2015). One possible explanation is that rNMPs incorporated during lagging strand synthesis are removed

during Okazaki fragment maturation. Alternatively, an as-yet undescribed pathway may facilitate rNMP removal specifically from the lagging strand.

Beyond the replication stress phenotypes associated with persistent rNMPs, studies have carefully examined the strand bias of mutations in various reporter sequences (Cho, Kim and Jinks-Robertson, 2015). These studies confirm that mutations caused by Top1 are primarily due to rNMP incorporation by the leading strand DNA polymerase ε. This reinforces the idea that Top1-mediated mutagenesis is both sequence-dependent and shaped by replication dynamics, with a strong bias toward mutations occurring on the leading strand, where Pol ε is the primary replicative polymerase.

1.8. Aging in Baker's Yeast *Saccharomyces cerevisiae*

Because of its genetic tractability and the availability of powerful molecular tools, *Saccharomyces cerevisiae* has long served as a model organism for understanding fundamental aspects of eukaryotic biology (Burgess, Powers and Mell, 2017). The ease of genetic manipulation, short doubling time, and highly conserved DNA metabolism make yeast particularly well suited for investigating genome stability. Importantly, unlike in higher eukaryotes, RER and Top1 are non-essential in yeast, enabling precise dissection of their contributions to genome maintenance under physiological and stress conditions (Kellner and Luke, 2020). Moreover, the development of sensitive assays to quantify mutation frequency and spectra—combined with the availability of strains harboring specific polymerase or repair pathway mutations—makes yeast an ideal system for studying rNMP incorporation and processing (Lang, 2017). Beyond its utility for understanding genome maintenance, *S. cerevisiae* is also a powerful model for studying the molecular basis of aging, as it recapitulates key conserved hallmarks of aging, including genomic instability, loss of proteostasis, deregulated nutrient sensing, and mitochondrial dysfunction (Longo *et al.*, 2012; Lippuner, Julou and Barral, 2014).

Aging in yeast can be studied in two distinct but complementary paradigms: replicative aging and chronological aging (Longo *et al.*, 2012; Lippuner, Julou and Barral, 2014). Replicative aging refers to the finite number of daughter cells a mother cell can produce before senescence, and is conceptually analogous to the aging of mitotically active stem cells in higher eukaryotes. Chronological aging, by contrast, measures the survival of non-dividing, quiescent cells in stationary phase and serves as a model for aging in post-mitotic tissues. Each paradigm is

influenced by different physiological and molecular processes but shares common regulatory pathways.

Replicative lifespan (RLS) can be extended through interventions such as caloric restriction, inhibition of the TOR (target of rapamycin) pathway, or activation of sirtuins, all of which converge on pathways that promote genome stability and stress resistance (Longo *et al.*, 2012; Lippuner, Julou and Barral, 2014). Conversely, defects in DNA repair pathways can shorten RLS, highlighting the importance of genome integrity in determining cellular longevity (Lee *et al.*, 2019). Chronological lifespan (CLS) is likewise sensitive to nutrient signaling and stress response pathways, and can also be extended through caloric restriction or genetic perturbations that enhance mitochondrial function and suppress oxidative damage (Longo *et al.*, 2012; Lippuner, Julou and Barral, 2014).

Together, these features position *S. cerevisiae* as an ideal model for dissecting the interplay between genome instability and aging. The ability to manipulate specific genetic pathways, such as those involved in rNMP processing or Top1-mediated repair, allows for mechanistic studies that are not feasible in more complex organisms. Moreover, insights gained from yeast have proven highly translatable, often illuminating conserved principles of cellular aging in higher eukaryotes (Kennedy *et al.*, 1995; Sinclair and Guarente, 1997; Sinclair, Mills and Guarente, 1997).

In this thesis, I use *Saccharomyces cerevisiae* to investigate how Top1-driven mutagenesis is regulated and how it contributes to genomic instability and cellular aging. I confirm that mutations in an SSTR-containing reporter increase when RNase H2-dependent ribonucleotide excision is defective and decrease upon deletion of Top1, demonstrating the role of Top1 in processing rNMPs. Intriguingly, mutation frequency does not decrease upon reduction of rNMP incorporation via expression of a DNA polymerase ε steric gate mutant with improved sugar selectivity, nor does overexpression of RNase H2, suggesting that Top1-mediated mutagenesis at SSTRs may be largely ribo-independent in wildtype cells. I further show that aged mother cells accumulate significantly more mutations than younger cells and that caloric restriction, a known lifespan-extending intervention, reduces mutation frequency. Finally, we demonstrate that Top1 is toxic in an RNase H2-deficient worm model, reducing lifespan in a manner that is rescued by Top1 depletion. Together, these findings reveal a mutagenic role for Top1 that is shaped by sequence context, repair pathway availability, and aging, and underscore the importance of tightly regulating Top1 activity to preserve genome integrity across the lifespan.

This thesis aims to investigate how the mutagenic activity of Top1 is regulated and how dysregulation of this process contributes to genomic instability and cellular aging, using yeast as a model system.

2. Results

2.1. Establishment of a High-Throughput Fluctuation Assay

Fluctuation assays are a cornerstone method for quantifying mutation rates in microbial populations (Luria and Delbrück, 1943). In a standard fluctuation assay, multiple parallel cultures of the same genotype are grown under non-selective conditions. After a defined growth period, cells from each culture are plated onto selective media to identify mutants that arose during growth. Because mutations occur randomly and independently, the number of mutants in each culture varies, and the resulting distribution can be analyzed using statistical models to estimate the underlying mutation rate.

When performed in the traditional test-tube format, fluctuation assays are labor-intensive and difficult to scale. Each independent culture must be inoculated, incubated, and processed individually, requiring relatively large volumes of cells. This approach increases consumable use, generates more waste, and poses logistical challenges for medium- to high-throughput studies. To overcome these limitations, we adapted the assay to a 96-well plate format (Lang, 2017). Cultures were grown in small volumes, and most liquid handling steps including seeding, spotting, and dilutions, were carried out with a multichannel pipette. Importantly, the entire culture from each well was spotted onto selective media as discrete droplets, allowing multiple replicates to be plated on the same plate. This streamlined workflow reduced hands-on time and facilitated efficient, large-scale comparisons across strains and conditions.

Beyond the above-mentioned benefits, this format also decreased the burden of colony counting. Because smaller inocula were plated, the number of mutant colonies per replicate was typically less than 10. Distributions with few colonies are particularly informative for maximum-likelihood estimation of mutation rates, since they better preserve the stochastic nature of mutagenesis. For example, a culture yielding a single mutant colony clearly represents a single mutational event, whereas a culture with 100 colonies could reflect either 100 independent events or clonal expansion of an early-arising mutation (“jackpot”). Cultures with 0–1 colony therefore provide more reliable data than jackpot cultures, which can mask the underlying mutation rate distribution (Lang, 2017).

To validate the performance of the adapted assay, mutation rates were measured using the well-characterized *CAN1* forward mutation reporter (Figure 7). In wildtype cells, mutation

rates ranged from 5.3 × 10^{-8} to 8.1 × 10^{-8} mutations per cell division, consistent with values reported in the literature (Kim *et al.*, 2011). Cells lacking functional RNase H2 (*rnh201*[*]) have an increased rate of mutagenesis due Top1 mutagenic activity. In this background, mutation rate increases ranged from 23.9 × 10^{-8} to 59.8 × 10^{-8} mutations per cell division, representing a 4- to 10-fold increase in mutation frequency. These values also align well with published reports (wildtype: 10 x 10^{-8}; *rnh201*: 26 x 10^{-8}[†]) and confirm the sensitivity of the assay to known mutator phenotypes. These results demonstrate that the adapted fluctuation assay provides reproducible estimates of mutation rate and offers a flexible, robust platform for high-throughput mutation analysis.

2.2. Validation of the HygR-SSTR(STOP):P2A:KanR Reporter

2.2.1. Rationale for Reporter Choice

Understanding the factors that regulate Top1-mediated mutagenesis requires a reporter system that is both sensitive to Top1 activity and capable of detecting its characteristic mutation signature. To this end, the HygR-SSTR(STOP):P2A:KanR reporter system was utilized (hereafter referred to as the HygR-SSTR reporter; see Materials and Methods 4.2.3, Figure 22; Reijns *et al.*, 2022). The key feature of this reporter is the Hygromycin resistance gene (HygR), which has been engineered to contain a high density of short-short tandem repeat (SSTRs), the optimal sequence context for Top1 induced mutations (Figure 6). When Top1 catalyzes a 2bp deletion within these repeats, the stop codon at the end of the HygR gene is shifted out of frame, allowing translation of the downstream P2A peptide and the Kanamycin resistance gene (KanR). Thus, Top1-dependent 2bp deletion events result in expression of KanR, conferring resistance to Kanamycin and its derivatives (e.g., G418).

This reporter offers a key advantage over traditional reporters such as *CAN1*. Most conventional reporter systems are not specific to frameshift mutations, which are largely caused by Top1 activity; instead, they detect a broader range of mutations, especially nonsense

[*] In accordance with *Saccharomyces cerevisiae* nomenclature, gene names are written in all capital letters and italicized (e.g., *TOP1*, *RNH201*). Mutant alleles in which a gene is deleted are denoted in lowercase italics (e.g., *top1*, *rnh201*). Protein products are indicated in roman type with only the first letter capitalized (e.g., Top1, Rnh201).

[†] For clarity and ease of comparison across genotypes, all mutation rates in this thesis are reported with the same power of ten (× 10^{-8} mutations per cell division), regardless of their absolute value

mutations, which are driven by other processes. As a result, general mutation reporters often show only subtle changes in mutation frequency in response to perturbations in Top1 or RNase H2 activity(Figure 7; Kim *et al.*, 2011). In contrast, the *HygR-SSTR* reporter displays a broad dynamic range: deletion of *TOP1* results in a marked decrease in mutation frequency, while deletion of *RNH201* leads to a strong increase in mutation frequency (Reijns *et al.*, 2022). This robust and bidirectional response made the SSTR-based reporter an ideal tool for dissecting the mutagenic contributions of Top1, RNase H2, and related genomic stability pathways.

2.2.2. Comparison of Mutation Frequency in Wildtype, *top1*, and *rnh201* Strains

The mutation frequencies for the *HygR-SSTR* reporter was measured for a panel of strains including wildtype, cells lacking Top1 (*top1,* Figure 8), or individual RNase H2 subunits (*rnh201, rnh202, rnh203,* Figure 8). As expected, deletion of *TOP1* led to a strong reduction in mutation frequency relative to wildtype (Figure 8; 1.3 × 10^{-8} vs 16.9 x 10^{-8} mutations per cell division respectively), indicating that Top1 is the primary driver of mutagenesis at this reporter in wildtype cells. Conversely, deletion of any subunit of RNase H2 (*rnh201, rnh202, rnh203*) caused a dramatic increase in mutation frequency, with rates exceeding 1000 × 10^{-8} mutations per cell

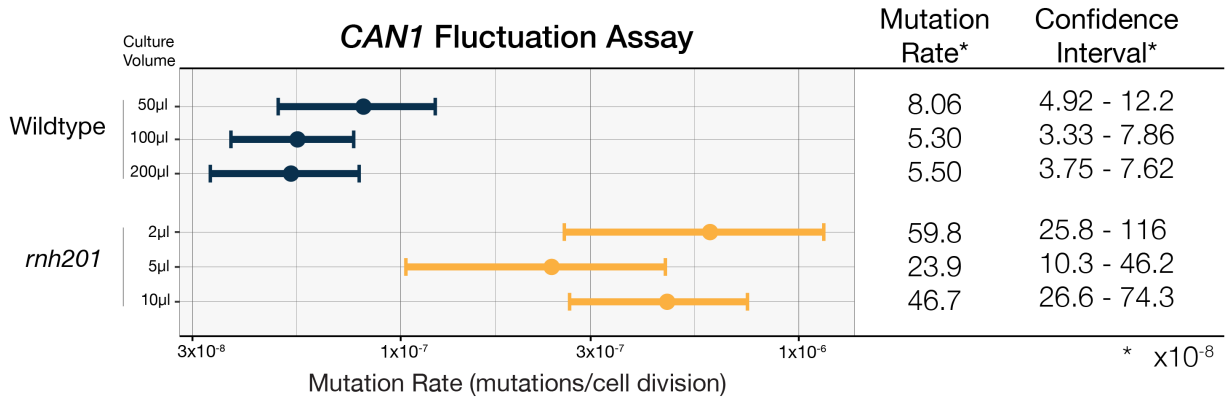

Figure 7 Validation of High-Throughput Fluctuation Assay Using a CAN1 Forward Mutation Reporter.

Mutation rates were measured in wildtype and *rnh201* strains using the CAN1 forward-mutation reporter across a range of culture volumes in a 96-well plate–based fluctuation assay. The X-axis is plotted on a log scale (base 10). Circles represent maximum likelihood estimates of mutation rates, and horizontal bars indicate 95% confidence intervals calculated using the rSalvador package. Mutation rates (×10^{-8} per cell division) are also tabulated on the right for clarity.

division. Notably, the RED (Ribonucleotide Excision Defective) allele of *RNH201*, which selectively impairs rNMP removal while preserving other functions, phenocopied the full *rnh201* deletion, confirming that rNMP excision is the critical activity required to suppress mutation events. Finally, data collected by Sophia Sergi measured mutation frequency in the *rnh201-RED top1* double mutant. The mutation rate in the double mutant was substantially reduced compared to *rnh201-RED* alone but remained modestly higher than in *top1* single mutants. These findings validate the reporter's responsiveness to both loss and gain of mutagenic pressure and establish it as a sensitive readout for Top1-dependent mutagenesis modulated by RNase H2 activity. The mutation rates determined for each of the strains are in line with published results (Reijns *et al.*, 2022).*

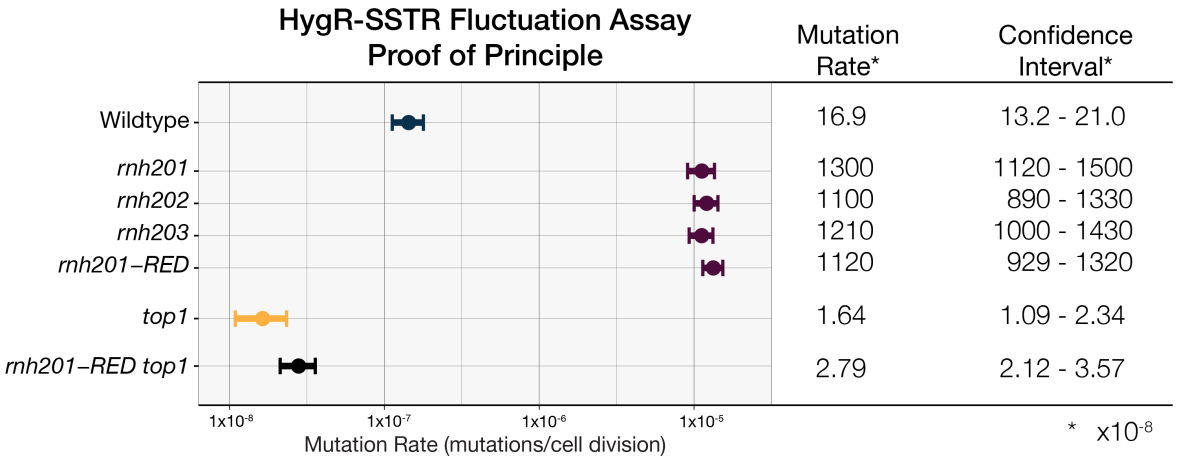

Figure 8 The HygR-SSTR reporter detects Top1-dependent mutagenesis and its regulation by RNase H2

Mutation rates were measured using the HygR-SSTR reporter in wildtype and mutants lacking components of the RNase H2 complex (*rnh201*, *rnh202*, *rnh203*), carrying the ribonucleotide excision–defective allele (*rnh201–RED*), or lacking Top1 (*top1*). Data for the *rnh201-RED top1* strain was generated by S. Sergi.
Circles represent maximum likelihood estimates of mutation rates, and horizontal bars indicate 95% confidence intervalscalculated as in Figure 7.

* The original publication (Reijns et al., 2022) presented fluctuation rates as mutations per cell division per base pair rather than mutations per cell division. The HygR gene is approximately 1kb in length; the mutation rates shown in this thesis could be converted to this unit by dividing by 1000bp.

2.2.3. Effect of Reporter Orientation and rNMP Incorporation Rate on Mutation Frequency

Top1 has been shown to induce mutations preferentially on the leading strand, where rNMP incorporation by DNA polymerase ε is more frequent (Nick McElhinny, Kumar, *et al.*, 2010). To test whether this bias also affects mutagenesis at the *HygR-SSTR* reporter, strains with an inverted version of the reporter were generated to alter its orientation relative to replication and transcription (Figure 9A). Both versions contain the same sequence elements but differ in which strand is transcribed, resulting in either co-directionality between transcription and replication or a head-on configuration where the transcription and replication machinery move in opposite directions. The original publication used the *HygR-SSTR* reporter in the head-on orientation (Reijns *et al.*, 2022), which we reproduced in Figure 8. In the head-on orientation, the transcribed strand is replicated by the lagging strand polymerase, whereas in the co-directional orientation, it is replicated by the leading strand polymerase.

Figure 9A illustrates the two reporter orientations and is drawn to scale with respect to ARS306 (cyan), a strong early replication origin. The reporter was inserted at the *AGP1* locus; the *AGP1* promoter (pAGP1), terminator, and coding sequence remain in the genome (Figure 9A; *AGP1* promoter: *pAGP1* and in medium grey, Agp*1* coding region also shown). The reporter is transcribed from the *pTEF* promoter and terminates at the *tTEF* sequence, conferring moderate to high transcriptional activity.

Mutation rates were measured by fluctuation assay for three biological replicates of each orientation in a wildtype genetic background. A slight, but reproducible increase in mutation frequency was observed with the reporter in the co-directional orientation compared to the head-on orientation (Figure 9B; compare “Wildtype Head-On” with “Wildtype Co-directional”). This result is consistent with prior findings in the literature (Nick McElhinny, Kumar, *et al.*, 2010; Williams *et al.*, 2013, 2015). However, because the reporter contains numerous Top1 mutational hotspots on both the transcribed and non-transcribed strands, this orientation-dependent difference is relatively subtle.

To better understand the interaction between orientation, strand context, and rNMP incorporation, we examined mutation frequencies in strains expressing DNA polymerase ε or δ steric gate mutants, which specifically alter rNMP incorporation on either the leading or lagging strand, respectively. Three different DNA polymerase steric gate mutants were utilized: *pol2-M644G* (referred to as “Leading ↑”): increases rNMP incorporation during leading strand

synthesis; *pol2-M644L* (“Leading ↓”): reduced rNMP incorporation on the leading strand; and *pol3-L612M* (“Lagging ↑”) increases rNMP incorporation during lagging strand synthesis. In the head-on orientation, where the transcribed strand corresponds to the lagging strand template, mutation frequency was elevated in the *pol2-M644G* context (Figure 9B Head-on leading ↑;

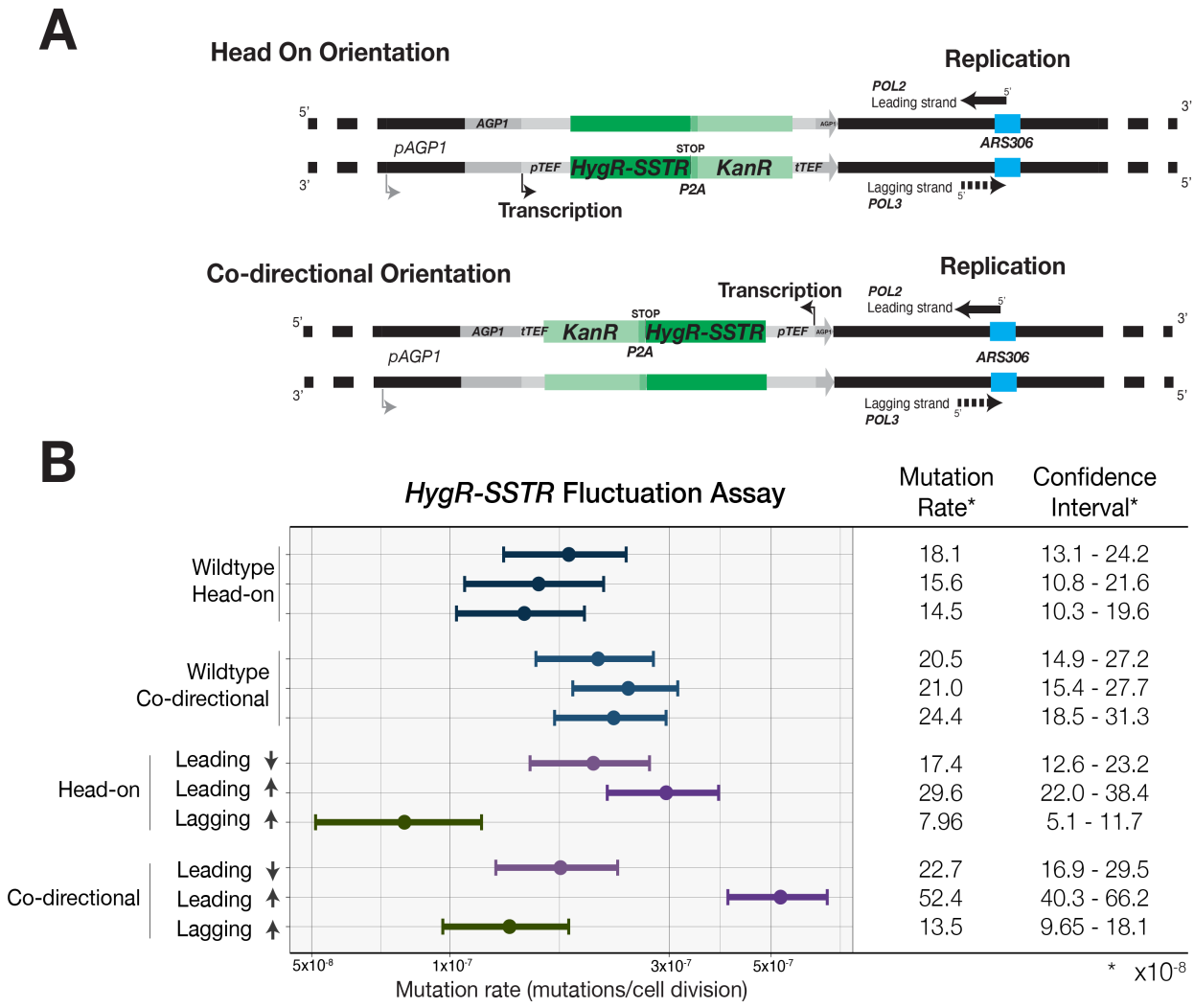

Figure 9 Reporter orientation and strand context influence mutation frequency at the HygR-SSTR reporter.

(A) Schematic of the HygR–SSTR reporter (green) in head-on (top) and co-directional (bottom) orientations relative to replication and transcription. Replication direction is inferred from proximity to ARS306 (cyan), with Pol2 synthesizing the leading strand and Pol3 synthesizing the lagging strand. The replication fork progresses left to right through the reporter integrated at the AGP1 locus.
(B) Mutation rates measured by fluctuation assay in wildtype cells and DNA polymerase steric gate mutants. Three biological replicates were assayed in both orientations. Leading ↓: *pol2-M644L* reduced rNMP incorporation on the leading strand; Leading ↑: *pol2-M644G* increased rNMP incorporation on the leading strand; Lagging ↑: *pol3-L612M* increased rNMP incorporation on the lagging strand.
Circles represent maximum likelihood estimates of mutation rates, and horizontal bars indicate 95% confidence intervals, calculated as in Figure 7.

mutation rate: 29.6 x 10^{-8} mutations/cell division). Surprisingly, *pol3-L612M* decreased mutation frequency relative to wildtype despite increased rNMP incorporation rates (Figure 9B Head-on lagging ↑; mutation rate: 7.9 x 10^{-8} mutations/cell division). When the reporter was expressed in the co-directional orientation, the *pol2-M644G* allele resulted in a greater increase in mutation frequency than when the reporter was in the head-on orientation (Figure 9B co-directional Leading ↑; mutation rate: 52.4 x 10^{-8} mutations per cell division). However, the allele of the leading strand polymerase with improved sugar selectivity, *pol2-M644L*, had little to no effect on the mutation frequency in either orientation (Figure 9B Leading ↓; mutation rates head on: 17.4 x 10^{-8} mutations/cell division; co-directional: 22.7 x 10^{-8} mutations/cell division).

Three key observations emerge from this set of experiments. First, the orientation of the reporter does not have a large effect on Top1-mediated mutation frequency in wildtype cells. Second, decreasing rNMP incorporation on the leading strand does not affect mutation frequency regardless of orientation. Third, increasing rNMP levels in the leading strand increases Top1-mediated mutation rates in either orientation, but most profoundly when the leading strand replication template serves as the template for transcription (co-directional), in line with published results. These observations suggest that in wildtype cells, Top1-mediated mutations at the *HygR-SSTR* reporter occur largely independently of rNMP incorporation. However, especially when the reporter is in the co-directional orientation, increased rNMP incorporation drives increased mutation rates. This implies that the balance between RNase H2 mediated removal and Top1-dependent mutations is very delicate, and perturbations to rNMP processing are not efficiently buffered by the cell, resulting in elevated mutagenesis. Unless otherwise noted, all further experiments in this thesis are conducted with the reporter in the head-on orientation.

2.3. Mechanistic Dissection of Reporter Mutagenesis

2.3.1. Effect of Top1 Overexpression on Mutation Frequency

Having established that the *HygR-SSTR* reporter accurately recapitulates known dependencies on Top1 activity, I next investigated the effect of Top1 overexpression on mutation frequency. This question was motivated by findings from the leading strand steric gate mutants, in which decreased rNMP incorporation did not affect mutation rates—raising the possibility that Top1-mediated mutations in this context are independent of ribonucleotide incorporation (Figure 9B). We therefore hypothesized that mutation frequency is dictated, at least in part, by Top1 abundance.

To test this hypothesis, I used a plasmid-based overexpression system expressing an epitope-tagged version of Top1 (Top1-3HA, Figure 10A). Overexpression of Top1-3HA from the strong constitutive GPD promoter led to increased mutation frequencies across all tested backgrounds, including wildtype, *top1*, and *rnh201*. In parallel, I also modified Top1 expression by replacing the endogenous *TOP1* promoter with the *GPD* promoter, driving stable overexpression of untagged Top1 from the genomic locus. This strategy led to an approximately 20-fold increase in mutation frequency (366 x 10^{-8} mutations/cell division). For comparison, *rnh201* mutation data from previous experiments are included in the figure (data from Figure 8). Notably, the *GPD-TOP1* strain exhibits a mutation frequency only ~3-fold lower than that of the

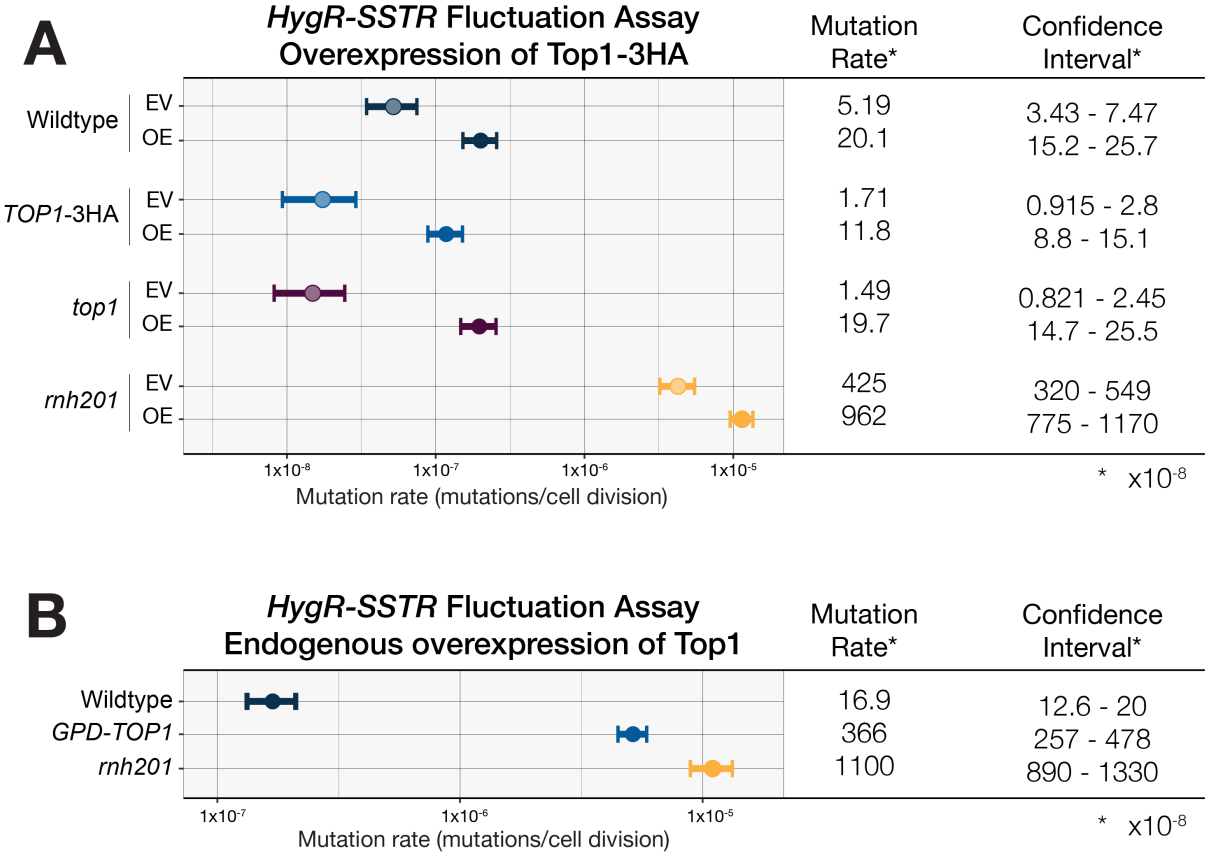

Figure 10 Overexpression of Top1 increases mutation frequency in the HygR-SSTR reporter.

(A) Mutation rates measured by fluctuation assay upon overexpression (OE) of Top1-3HA from a plasmid compared with the empty vector (EV) control.
(B) Mutation rates measured in strains where the endogenous *TOP1* promoter was replaced with the constitutive GPD promoter, driving stable overexpression of untagged Top1.
Circles represent maximum likelihood estimates of mutation rates, and horizontal bars indicate 95% confidence intervals, calculated as in Figure 7.

rnh201 strain (366 vs 1,100 x 10^{-8} mutations/cell division respectively). These results indicate that Top1 protein levels must be tightly regulated in wildtype cells to balance its important role in DNA replication, repair, and transcription against its potential to introduce harmful frameshift mutations in the genome. Preliminary titration experiments with promoters of graded strength suggest a positive correlation between Top1 levels and mutation frequency (S. Sergi, Data not shown).

2.3.1.1. Epitope Tagging of Top1 Reduces Mutagenic Activity

To quantify the degree of Top1–3HA overexpression in empty vector (EV) versus overexpression (OE) conditions, a strain expressing Top1–3HA from the endogenous *TOP1* locus was included (Figure 10A; *TOP1–3HA*). Notably, *TOP1–3HA* + EV strains exhibited mutation rates comparable to *top1* (*TOP1–3HA* + EV: 1.71 × 10^{-8} mutations/cell division; *top1* + EV: 1.49 × 10^{-8} mutations/cell division). This result suggests that C-terminal tagging of Top1 with 3HA markedly diminishes Top1-mediated mutagenic activity.

To determine whether this effect is specific to the 3HA tag or generalizable to other C-terminal epitope tags, we analyzed a *TOP1-TAP* allele. Similar to 3HA, the C-terminal TAP tag also reduced Top1-mediated frameshift mutation rates (Figure 11A). In the *rnh201-RED* background, mutation frequency in *TOP1–TAP* remained elevated relative to wildtype (*rnh201-RED TOP1-TAP*: 57.8 × 10^{-8} vs. wildtype: 22.6 × 10^{-8} mutations/cell division), indicating partial retention of Top1 activity.

Top1-mediated relief of torsional stress is critical for R-loop metabolism. In the absence of both RNase H1 and RNase H2, Top1 becomes essential to resolve toxic R-loops, particularly at the ribosomal DNA (rDNA) locus. To assess whether *TOP1-TAP* retains catalytic activity, we generated a heterozygous diploid strain carrying *TOP1-TAP*, *rnh1*, and *rnh201*. While *rnh1 rnh201 top1* spores are inviable after sporulation, *rnh1 rnh201 TOP1-TAP* spores formed colonies of normal size, suggesting that *TOP1-TAP* retains sufficient nicking activity to relieve torsional stress and prevent R-loop–associated lethality at the rDNA locus (Figure 11B).

To further characterize *TOP1-TAP*, we tested its behavior in conditions where Top1 cleavage complex (Top1-cc) trapping by camptothecin (CPT) is toxic. *RTT101* is required for resolving Top1-cc–induced damage, and *rtt101* strains are hypersensitive to CPT. The *TOP1-TAP* allele partially alleviated CPT sensitivity in *rtt101* strains, though not to the same extent as

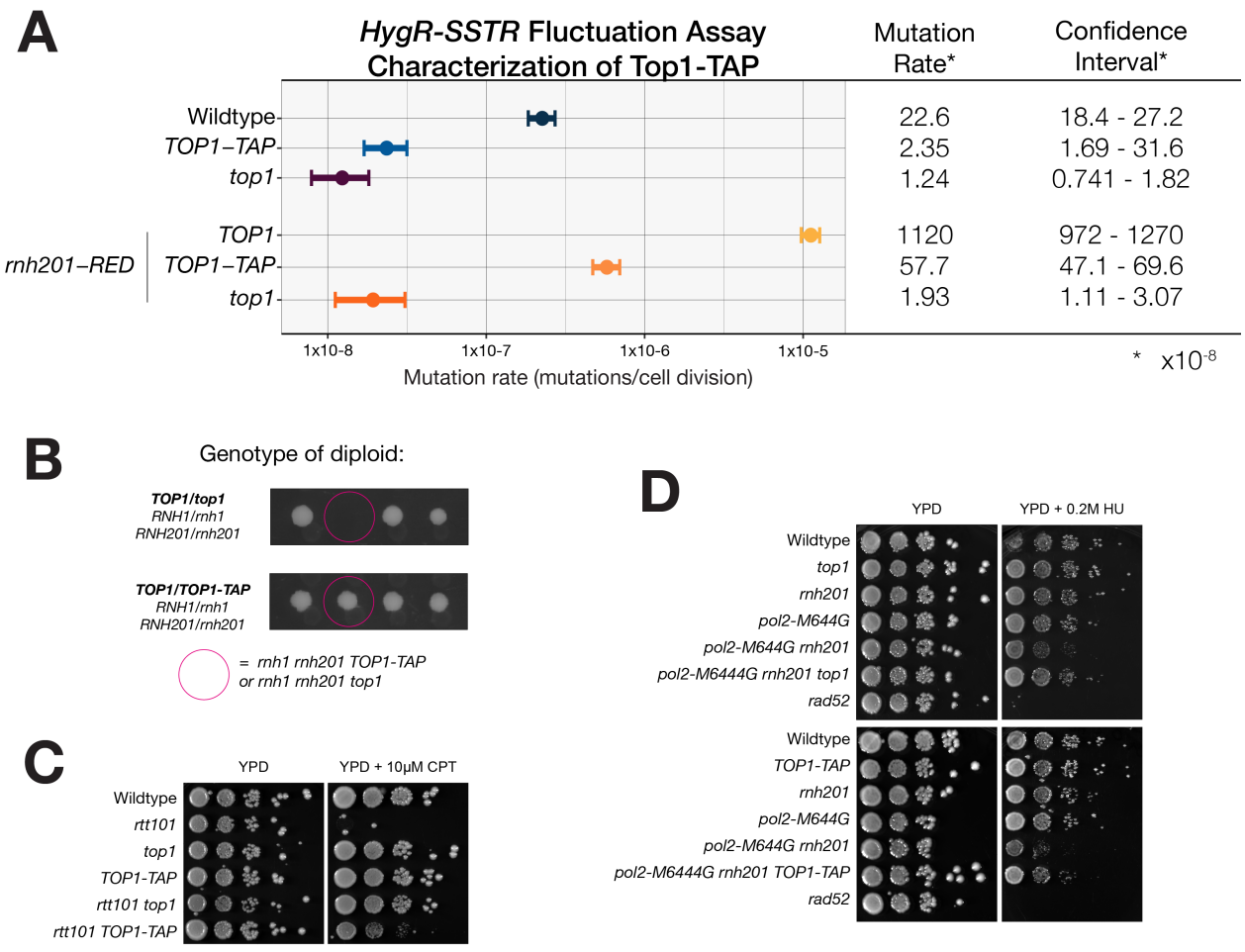

Figure 11 Functional characterization of the TAP-tagged Topoisomerase I allele (TOP1-TAP).

(A) Mutation rates measured using the HygR-SSTR fluctuation assay show that *TOP1-TAP* exhibits reduced mutagenic activity compared to untagged *TOP1*. In the *rnh201-RED* background, mutation rates for *TOP1-TAP* were intermediate between *TOP1* and *top1*. Circles represent maximum likelihood estimates of mutations rates, and horizontal bars indicate 95% confidence intervals, calculated as in Figure 7.
(B) Tetrad analysis showing that *TOP1-TAP* supports viability of haploid progeny carrying *rnh1 rnh201*, whereas *top1* does not. Colonies with the *rnh1 rnh201* genotype containing either *TOP1-TAP* or *top1 are indicated*.
(C) Serial dilution assays in the presence of 10 μM camptothecin (CPT) demonstrate that *TOP1-TAP* partially rescues CPT sensitivity of *rtt101* strains, indicating retained catalytic function but reduced Top1-cc toxicity.
(D) Growth assays under replication stress (0.2 M hydroxyurea, HU) show that *TOP1-TAP* alleviates HU sensitivity in *pol2-M644G rnh201*, similar to *top1*.
Experiments performed by Aurelia Weber.

top1, indicating that *TOP1-TAP* retains catalytic activity but generates fewer toxic Top1-ccs (Figure 11C).

Finally, we examined *TOP1-TAP* sensitivity to hydroxyurea (HU), a replication stressor that inhibits dNTP synthesis and increases rNMP incorporation. In *pol2–M644G rnh201* backgrounds,

which exhibit high genomic rNMP content, HU toxicity is Top1-dependent. Both *top1* and *TOP1–TAP* reduced HU sensitivity, consistent with diminished Top1 nicking activity (Figure 11D).

Together, these data support the conclusion that *TOP1-TAP* is a hypomorphic allele. It retains sufficient catalytic function to prevent rDNA replication stress but exhibits reduced mutagenic activity and decreased toxicity from Top1 trapping and rNMP processing. These experiments were performed by A. Weber (B. Sc. Project), and are included here to provide context for subsequent sections of this thesis.

2.3.1.2. Development of an Anti-Top1 Antibody

To overcome the limitations of using epitope-tagged alleles for protein detection, we generated a set of polyclonal antibodies targeting two distinct regions of endogenous yeast Top1: the flexible linker (amino acids 561–715) and the upper clamp (amino acids 143–360). Peptides corresponding to these regions were used to immunize rabbits, resulting in four antibodies with unique identifiers (Table 8). Cloning and recombinant protein recovery were completed by M. Möckel and colleagues in the Protein Production Core Facility at the Institute of Molecular Biology, Mainz.

To evaluate the performance of each antibody, I performed immunoblot analysis on whole-cell extracts from strains expressing untagged Top1, a *top1* deletion strain, or a Top1-AID*-tagged allele which increases the size of the protein and produces a shifted Top1-specific band. As shown in Figure 12, all four of the antibodies recognized a distinct band corresponding to the expected molecular weight of native Top1 (~110 kDa), which was absent in the *top1* strain and shifted in the Top1-AID*-tagged version (~135 kDa). The band corresponding to Top1 was strongest with antibody #146, raised against the upper clamp domain (Rabbit 3055), which also showed minimal background signal and clearly distinguished between untagged and AID*-tagged Top1. Antibodies #143 and #145 showed moderate signal strength with some non-specific bands, while #144 produced high background at a lower molecular weight. Based on these results, antibody #146 was selected for subsequent experiments to assess Top1 protein levels. This antibody enabled accurate monitoring of Top1 abundance without reliance on epitope tags, which we showed significantly impair Top1 mutagenic activity in the HygR-SSTR reporter (Figure 11A).

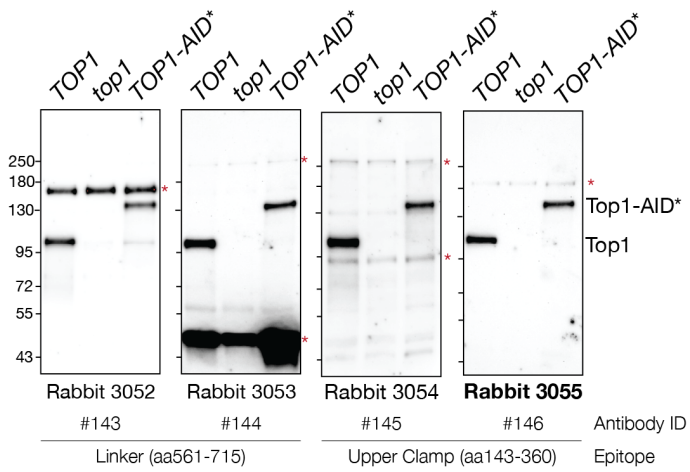

Figure 12 Validation of polyclonal antibodies targeting yeast Top1.

Immunoblot analysis of whole-cell lysates from strains expressing untagged Top1 (*TOP1*), Top1 deletion (*top1*), or a Top1-AID* allele using polyclonal antibodies raised against two Top1 epitopes: the flexible linker (aa561–715, antibodies #143 and #144) and the upper clamp (aa143–360, antibodies #145 and #146). All antibodies detect a specific band at ~110 kDa corresponding to native Top1, which was absent in the *top1* strain and shifted upward (~135 kDa) in the Top1-AID* strain. Red asterisks denote nonspecific background signals.

2.3.2. Effect of RNase H2 Overexpression on Mutation Frequency

Since the absence of RNase H2 results in a dramatic increase in mutation frequency in the *HygR-SSTR reporter*, I next tested whether increasing RNase H2 levels would have the opposite effect. To do this, I overexpressed all three subunits of RNase H2 (Rnh201, Rnh202, and Rnh203) by promoter replacement with the constitutive GPD promoter at their endogenous loci to ensure stoichiometric expression. As shown in Figure 13, RNase H2 overexpression did not significantly alter mutation frequency compared to wildtype (17.6×10^{-8} vs. 17.9×10^{-8} mutations per cell division, respectively). These findings suggest that RNase H2 is not limiting under normal conditions, and that endogenous levels of the enzyme are already sufficient to maintain rNMP repair capacity.

This set of experiments examined how mutation frequency responds to altered rNMP incorporation, Top1 protein levels, and RNase H2 expression. Collectively, the results indicate that RNase H2 is present at sufficient levels in wildtype cells to suppress Top1-mediated mutagenesis at rNMPs. This conclusion is supported by the observation that neither reducing rNMP incorporation (*pol2-M644L*, Figure 9B) nor increasing RNase H2 levels (Figure 13) alters Top1-dependent mutation frequency. In contrast, overexpression of Top1 (Figure 10A and B)

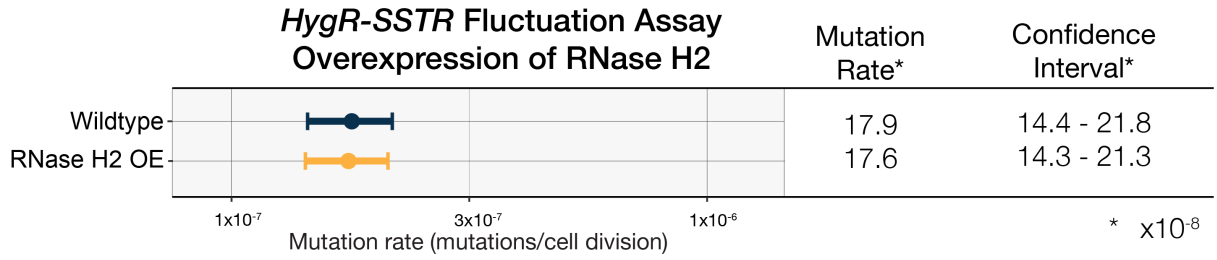

Figure 13 Overexpression of RNase H2 does not reduce mutation frequency in the HygR-SSTR reporter.

Mutation rates were measured using the HygR-SSTR fluctuation assay in wildtype cells and in strains overexpressing all three subunits of RNase H2 (Rnh201, Rnh202, and Rnh203) under the GPD promoter at their endogenous loci. Circles represent maximum likelihood estimates of mutation rates, and horizontal bars indicate 95% confidence intervals, calculated as in Figure 7.

leads to increased mutation frequency across all strain backgrounds tested, suggesting that Top1 activity can be mutagenic regardless of the sugar at the cleavage site.

Having established how Top1-mediated mutagenesis is influenced by rNMP incorporation, Top1 levels, and RNase H2 activity, I next asked whether this pathway contributes to genome instability in a physiologically relevant context: replicative aging.

2.4. Mutation Frequency in Aged Yeast Cells

Having confirmed that Top1 activity contributes to mutagenesis in our reporter system—and that this mutagenic activity can be modulated by factors such as polymerase steric gate mutants, reporter orientation, and levels of Top1, I next tested whether this pathway also contributes to genome instability in a physiologically relevant context. Since Top1 has been implicated in genome maintenance and cell viability, and because aging is associated with an accumulation of DNA damage and replication stress, I hypothesized that Top1-mediated mutagenesis might increase with replicative age. To test this, I used the replicative aging paradigm in budding yeast, which allows mother cells to be aged through successive asymmetric divisions (Jin, Cao and Liu, 2021).

When a mother yeast cell produces a daughter cell, only newly synthesized proteins are deposited on the daughter's surface. Therefore, biotinylation of surface proteins in a starting population enables selective separation of aged mother cells, which retain the biotinylated proteins, from their daughters, which contain only new, non-biotinylated proteins. Magnetic

beads coated with streptavidin or anti-biotin antibodies can be used to isolate biotinylated mother cells (see Materials and Methods section **Error! Reference source not found.**, Figure 14A). I applied this magnetic sorting protocol to isolate yeast cells of defined replicative age and used the sorted populations for fluctuation assays. Importantly, all cells were aged in the presence of hygromycin to prevent the accumulation of mutations in the *HygR-SSTR* reporter gene during the aging process. Using this method, we obtained four distinct populations: young mothers (median of 7 bud scars) and their daughters (median 0 bud scars), and old mothers (median of 14–16 bud scars) and their daughters (Figure 14B).

Fluctuation assays revealed that mutation rates increased with replicative age (Figure 14C). Young mothers exhibited a modest, non-significant increase in mutation frequency compared to the daughters they produced (6.96 vs. 4.93 × 10^{-8} mutations per cell division; $p = 0.066$). In contrast, a significant increase in mutation frequency was observed when comparing old mothers to their daughters (18.2 vs 11.3 × 10^{-8} mutations per cell division; $p = 2.44 \times 10^{-4}$). Similarly, mutation frequency was significantly higher in old mothers compared to young mothers, showing approximately 2.6 fold increase (18.2 vs 6.96 × 10^{-8} mutations per cell division; $p = 5.2 \times 10^{-11}$). These data demonstrate that mutation frequency increases with replicative age in budding yeast and support a model in which Top1-dependent mutagenesis contributes to the age-associated accumulation of genomic instability.

2.5. Effect of Lifespan-Modulating Conditions on Mutation Frequency

Having established that Top1-mediated mutagenesis increases with replicative age, I next examined whether factors known to modulate lifespan, either environmentally or genetically, also influence mutation frequency in the HygR-SSTR reporter. If Top1-dependent genome instability contributes to the aging, then lifespan-extending conditions should suppress mutation accumulation, whereas lifespan-shortening conditions might increase it. To test this, I analyzed both physiological interventions known to alter yeast lifespan, including caloric restriction and growth temperature, as well as genetic perturbations with defined effects on longevity. These experiments assessed whether the mutagenic potential of Top1 is sensitive to lifespan-modulating cues.

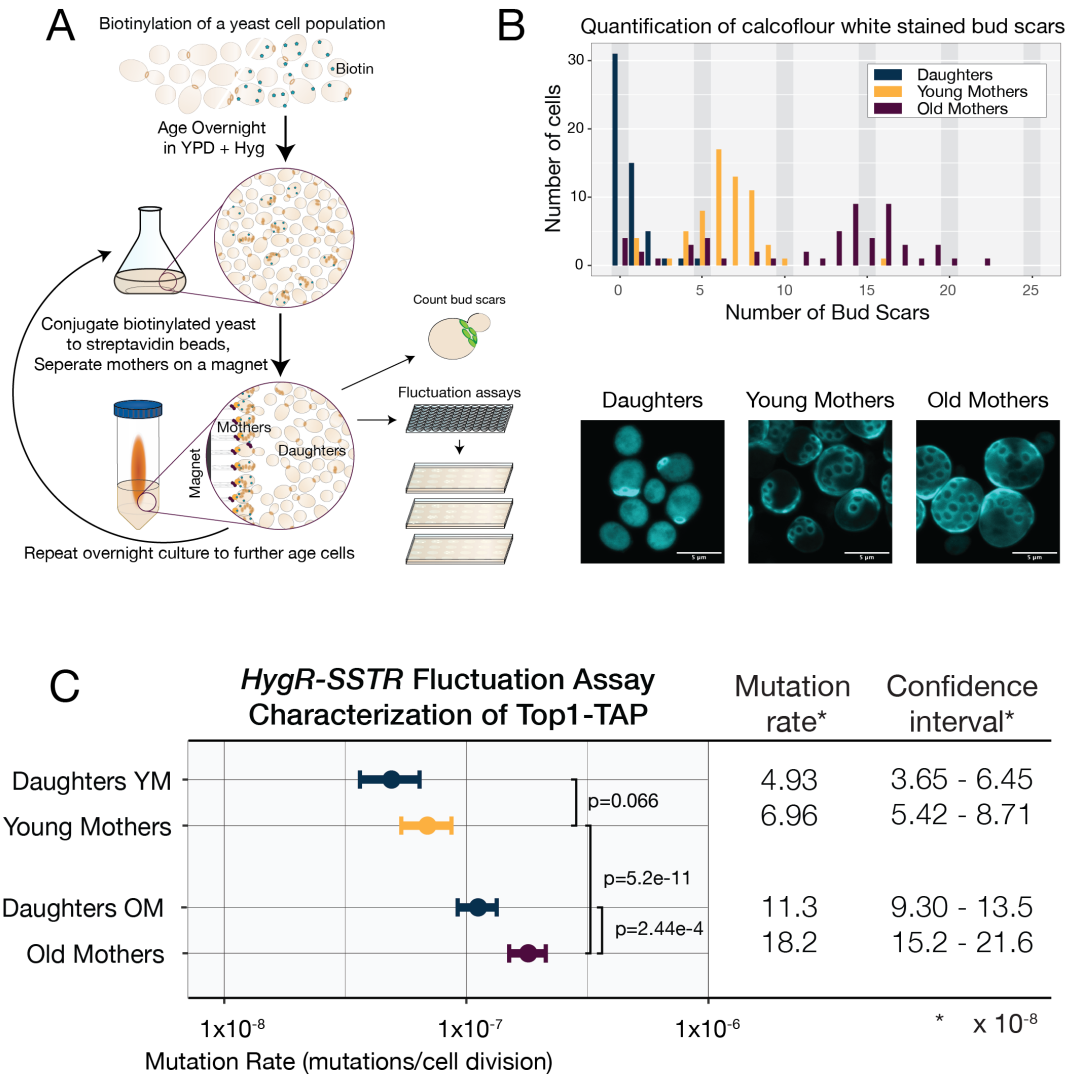

Figure 14 Top1-mediated mutagenesis increases with replicative age in budding yeast.

(A) Schematic of the magnetic sorting protocol used to isolate aged yeast mother cells. Surface proteins of a starting population were biotinylated, and cells were aged in the presence of hygromycin to prevent accumulation of mutations in the HygR-SSTR reporter. Biotinylated mother cells were isolated using streptavidin-coated magnetic beads. This process was repeated to enrich for older mother cells, and daughters from each aging cycle were collected as distinct populations.
(B) Bud scar counts for each sorted population, assessed by calcofluor white staining. Young mothers (YM) had a median of 7 bud scars, while old mothers (OM) exhibited a median of 14-16 scars. Daughters had few to no bud scars, confirming effective age stratification.
(C) Mutation frequencies measured by fluctuation assay using the *HygR-SSTR* reporter. A significant age-dependent increase in mutation frequency was observed, with old mothers exhibiting a ~1.6-fold increase compared to daughters from the same aging cycle ($p = 2.4 \times 10^{-4}$, likelihood ratio test statistic calculated with the rSalvador package).
Circles represent maximum likelihood estimates of mutation rates, and horizontal bars indicate 95% confidence intervals, calculated as in Figure 7.

2.5.1. Metabolic and Environmental Regulators of Lifespan

2.5.1.1. Caloric Restriction

To assess whether environmental conditions that alter replicative lifespan also modulate Top1-dependent mutagenesis, I measured mutation frequency under caloric restriction (CR), an intervention known to extend lifespan of budding yeast. CR was implemented by reducing glucose concentration in the growth medium from 2% to 0.5%. In wildtype cells, CR caused a marked decrease in mutation frequency, from 17.6 x 10^{-8} mutations per cell division to 7.2 × 10^{-8} mutations per cell division, an approximate 2.4 fold reduction in mutation frequency (Figure 15A). Yeast strains lacking Top1 exhibit very low mutation rates under both control and CR conditions (1.98 and 2.07 × 10^{-8} mutations per cell division, respectively), indicating that the mutation events that occur in the absence of Top1 are not affected by metabolic state. In the *rnh201* background, CR slightly increased mutation frequency, though this may not be biologically relevant considering the overlapping CIs. The reduction in mutation frequency in wildtype cells grown under CR mirrors its known effect on lifespan, suggesting that the life-extending benefits of caloric restriction may, in part, stem from reduced genome instability, including the mutations catalyzed by Top1.

2.5.1.2. Temperature

The effect of heat shock on yeast replicative lifespan is nuanced: while prolonged heat shock does not alter lifespan (Molon and Zadrag-Tecza, 2016), brief exposure to high temperatures early in life has been shown to extend it (Shama *et al.*, 1998). To evaluate the impact of growth temperature on mutation frequency, I cultured wildtype and *rnh201* cells at constant temperatures of 25°C, 30°C, or 37°C (Fig. 2.5B) and then estimated the rate of mutation accumulation at these different temperatures. In wildtype cells, mutation frequency remained relatively stable across all temperatures tested, ranging from 9.78 to 9.96 × 10^{-8} mutations per cell division. In contrast, *rnh201* cells exhibited an apparent temperature-dependent change in mutation frequency. The mutation rates between 25˚C and 30˚C were very similar (274 vs 303.x 10^{-8} mutations/cell division respectively), but at 37˚C the mutation frequency dropped significantly (130 x 10^{-8} mutations per cell division). The mutation frequency calculated for this experiment is lower than in earlier assays (e.g., compare *rnh201* in Figure 8 to *rnh201* at 30˚C in Figure 15: ~1,300 x 10^{-8} vs 303 x 10^{-8} mutations per cell division, respectively), likely reflecting technical differences in assay execution. This observation is interesting in light of how stress conditions, such as acute heat shock, can extend lifespan, and perhaps also alleviate genomic

instability by the same pathway. Together, these findings indicate that environmental conditions associated with increased lifespan, such as caloric restriction and heat stress, are also associated with reduced Top1-dependent mutagenesis.

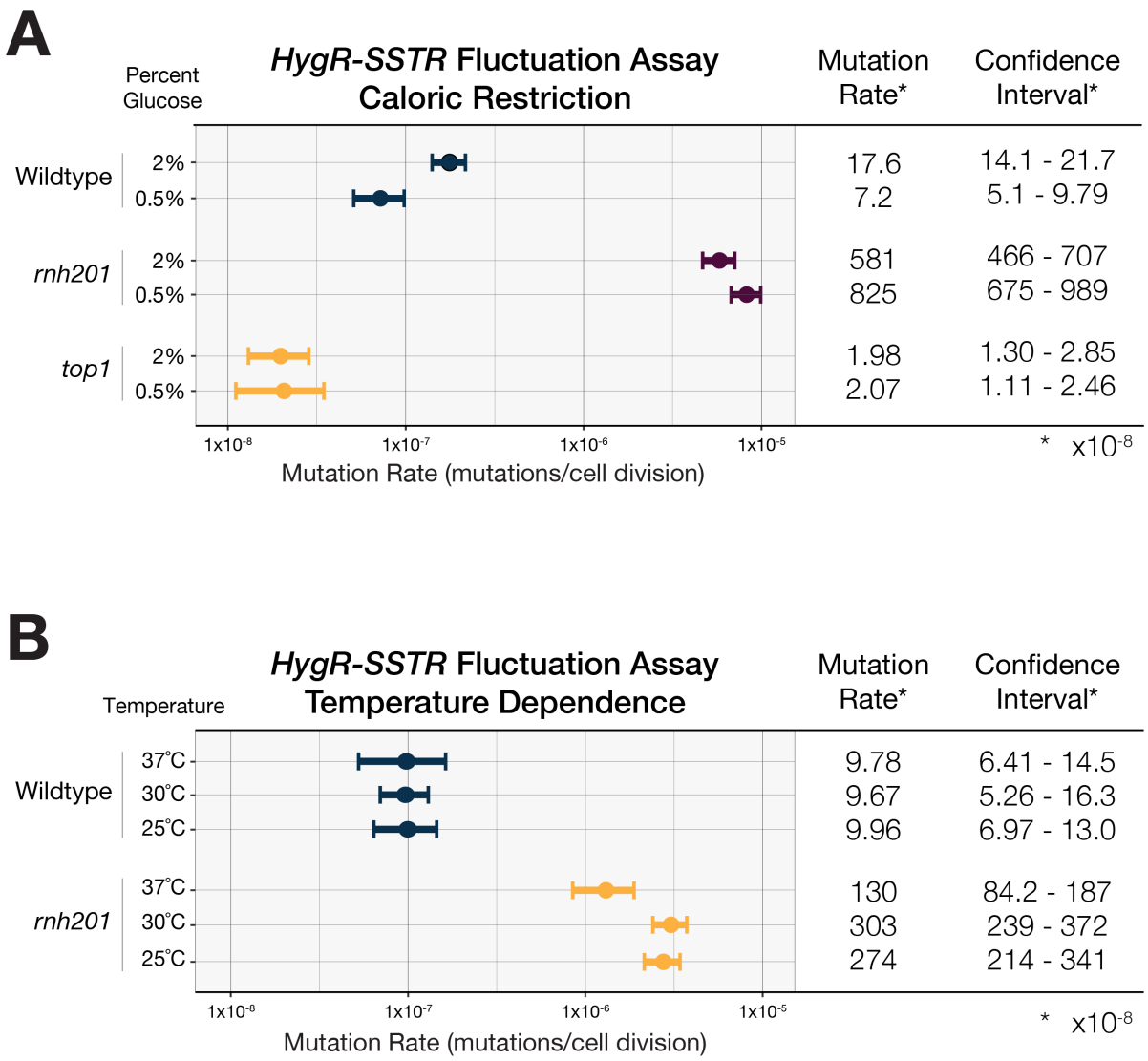

Figure 15 Lifespan-modulating growth conditions can alter Top1-dependent mutation frequency.

(A) Mutation frequency measured by fluctuation assay under standard (2% glucose) and calorically restricted (0.5% glucose) conditions in wildtype, *rnh201*, and *top1* strains using the HygR-SSTR reporter. Caloric restriction significantly reduced mutation frequency in wildtype cells, while *rnh201* and *top1* backgrounds showed no change.
(B) Mutation frequency in wildtype and *rnh201* cells grown at 25°C, 30°C, or 37°C. While wildtype mutation rates remained stable across temperatures, *rnh201* cells exhibited a temperature-dependent decrease in mutation frequency at 37°C.
Circles represent maximum likelihood estimates of mutation rates, and horizontal bars indicate 95% confidence intervals, calculated as in Figure 7.

2.5.2. Genetic Modulators of Lifespan

In addition to environmental interventions, several genetic factors are known to modulate replicative lifespan in *S. cerevisiae* through, for example, effects on chromatin structure, genome stability, or silencing of repetitive elements. To determine whether these genes also impact the frequency of Top1-dependent mutations, I measured mutation frequency in deletion strains or overexpression constructs of genes previously implicated in lifespan extension or reduction. These include *SIR2*, a well-characterized longevity gene involved in chromatin silencing; components of the HIR/Asf1 chromatin assembly pathway, which maintain genome integrity during DNA replication and repair; and rDNA copy number variants, which impact nucleolar stability. Together, these experiments were used to test the interplay between chromatin-based lifespan regulation and Top1-mediated mutagenesis.

2.5.2.1. SIR2 Overexpression

Sir2, a conserved histone deacetylase, promotes transcriptional silencing at the rDNA locus, telomeres, and silent mating-type loci, and is one of the best-characterized longevity factors in yeast (Kaeberlein, McVey and Guarente, 1999). Overexpression of *SIR2* extends replicative lifespan, whereas its deletion shortens it. The lifespan-modulating effects of Sir2 are largely attributed to its ability to prevent the accumulation of extrachromosomal rDNA circles (ERCs), which are byproducts of recombination within the rDNA array and a major driver of aging in yeast.

At the rDNA locus, Sir2-mediated deacetylation promotes chromatin compaction and transcriptional silencing, which reduces transcription and the associated topological stress. In wildtype cells, Top1 is recruited to the rDNA to relieve torsional stress, however, Top1 activity at the rDNA can also promote homologous recombination and excision of rDNA repeats, fueling ERC formation. Thus, by suppressing transcription and limiting Top1 activity at the rDNA, Sir2 indirectly reduces the generation of Top1-dependent DNA lesions that would otherwise promote genome instability, although these are a different class of lesions than the frameshift mutations catalyzed in the context of rNMPs.

To examine whether Sir2 levels influence Top1-dependent frameshift mutation rates more broadly, I measured mutation frequency in a wildtype strain carrying an extra copy of *SIR2* (Figure 16A; Sir2-OE). Overexpression of *SIR2* produced modest but significantly significant decrease in mutation frequency ($p = 0.021$). Because the confidence intervals overlap and the change is small, the biological relevance of this effect remains uncertain. If confirmed, this finding

would suggest that the chromatin-silencing function of Sir2 helps protect against mutagenic events, consistent with its known role in preserving genome stability and extending lifespan through suppression of Top1-mediated recombination at repetitive loci.

2.5.2.2. rDNA copy number

In *S. cerevisiae*, the rDNA locus consists of tandemly repeated units encoding the RNA components of the ribosome. These repeats are present in high copy number (~100–200 copies per cell) to support the massive transcriptional output required for ribosome biogenesis and cellular growth. While this amplification ensures sufficient rRNA production, the repetitive nature of the locus also makes it vulnerable to recombination, replication stress, and transcription-induced topological strain, processes that require tight regulation to maintain genome stability. Together, these factors suggest that the rDNA locus may act as a major sink for Top1 activity in the genome. Therefore, cells containing fewer rDNA repeats may have a reduced need for Top1 at this locus, potentially leading to redistribution of Top1 activity to other genomic regions, where it could contribute to increased mutagenesis and genome instability.

To assess whether rDNA copy number influences Top1-dependent mutagenesis, I measured mutation frequency in a and *fob1* background, which stabilizes the rDNA array by eliminating replication fork stalling and reducing recombination within the rDNA locus. In this system, strains harboring either 190 rDNA repeats (wildtype copy number) or 25 repeats were compared (Figure 16B). Contrary to expectation, mutation frequency was significantly higher in the 190-copy strain relative to the 25-copy strain (46.2×10^{-8} vs. 27.8×10^{-8} mutations per cell division; B). These assays were performed in the W303 genetic background, distinct from the primary BY4741-based system used elsewhere in this thesis, and the effect of *fob1* was not tested in this background. Nonetheless, the data raise the possibility that structural features of the rDNA locus itself modulate genome-wide susceptibility to mutation, though the mechanism remains unclear.

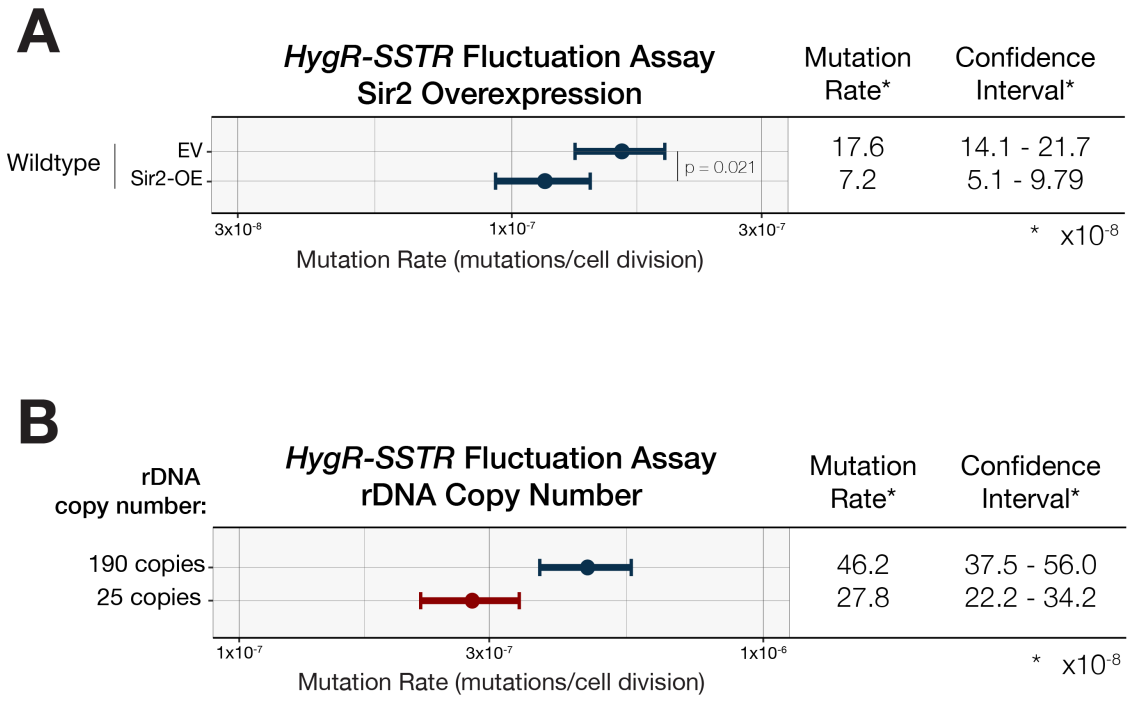

Figure 16 rDNA dynamics shape Top1-mediated mutation frequency.

(A) Mutation frequency in wildtype cells carrying either an empty vector (EV) or a SIR2-overexpression plasmid (Sir2-OE). Overexpression of *SIR2* slightly reduced mutation frequency relative to EV control (p= 0.021, likelihood ratio test). **(B)** Mutation frequencies measured in *fob1* strains carrying either 190 or 25 rDNA repeats. Mutation frequency was higher in the 190-copy strain relative to the 25-copy strain (46.2 x 10^{-8} vs. 27.8 x 10^{-8} mutations per cell division).

Circles represent maximum likelihood estimates of mutation rates, and horizontal bars indicate 95% confidence intervals, calculated as in Figure 7.

2.5.2.3. Chromatin compaction and assembly

Chromatin structure is dynamically regulated during DNA replication and repair, and disruption of histone chaperone function can impair proper nucleosome assembly, leading to increased DNA accessibility and potential genome instability. To investigate whether altered chromatin assembly influences the frequency of Top1-dependent mutations, I measured mutation rates in strains with defects in histone deposition(Feser *et al.*, 2010). The HIR complex (composed of Hir1, Hir2, and Hir3), in coordination with Asf1, mediates replication-independent chromatin assembly, particularly during transcription and repair, while Rtt109 acetylates newly synthesized histones to promote replication-coupled nucleosome assembly. Deletion of *ASF1*

or *RTT109* results in lower histone protein levels in chromatin, either through impaired histone delivery (*asf1*) or reduced acetylation-dependent deposition (*rtt109*). Furthermore, deletion of *ASF1* or *RTT109* results in a marked decrease in replicative lifespan, consistent with impaired chromatin maintenance and increased genomic instability. In contrast, deletion of *HIR1*, *HIR2*, or *HIR3* extends lifespan, an effect attributed to increased histone gene expression. However, it remains unclear whether histone overexpression in these mutants leads to increased nucleosome density, or whether chromatin becomes more compacted overall in non-aged cells.

Based on the lifespan phenotypes, I initially hypothesized that *asf1* and *rtt109* mutants would exhibit increased mutation frequencies, whereas deletion of the *HIR* genes might decrease mutation rates by improving chromatin integrity. Contrary to this expectation, all mutants displayed increased mutation frequencies relative to wildtype (Figure 17: 12.4×10^{-8} mutations per cell division). The highest rate was observed in *hir3* (32.3×10^{-8}), followed by *rtt109* (25.7×10^{-8}), and *asf1* (20.8×10^{-8}). The effect of *asf1* was somewhat variable, with one replicate closer to wildtype levels (16.1×10^{-8}). These results suggest that altered chromatin assembly, regardless of its association with lifespan, can increase the mutagenic activity of Top1, potentially by exposing genomic sites to cleavage or interfering with proper repair. As these

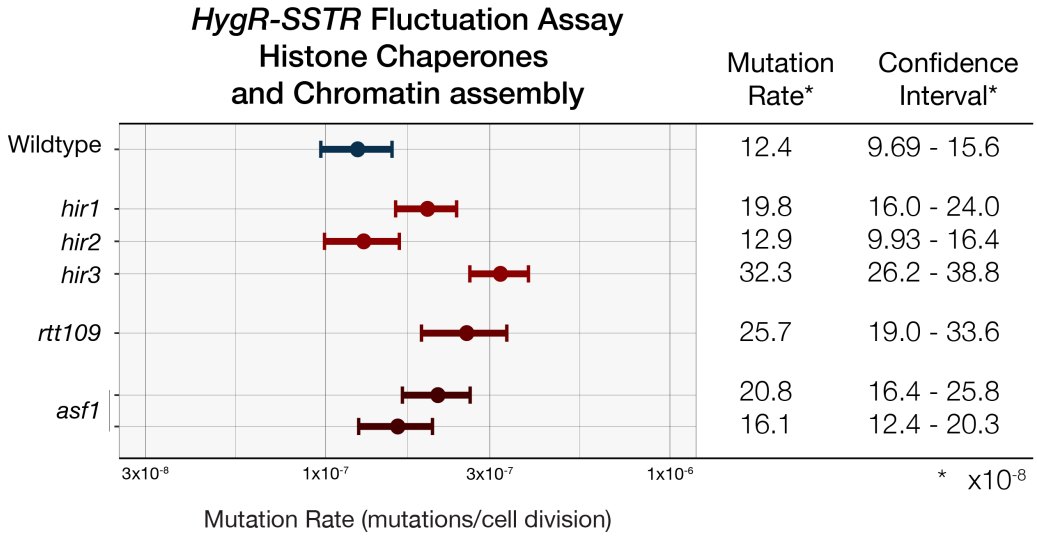

Figure 17 Histone chaperone mutants exhibit increased mutation frequency in the HygR-SSTR reporter.

Mutation rates were measured using fluctuation assays in wildtype cells and strains lacking chromatin assembly factors (*hir1, hir2, hir3, rtt109,* and *asf1*). All mutants show elevated mutation rates compared to wildtype, with the highest increase observed in *hir3*.

Circles represent maximum likelihood estimates of mutation rates, and horizontal bars indicate 95% confidence intervals, calculated as in Figure 7.

genes are not direct regulators of Top1, their effects are likely mediated through changes in nucleosome occupancy or replication dynamics that modulate DNA accessibility to Top1. Further experiments are required to elucidate the mechanism by which these pathways modulate Top1 function.

2.5.2.4. Transcription elongation speed mutants

Transcription speed has been shown to increase in aged cells, and Top1-dependent mutations are known to be enriched in regions of high transcription. To test whether transcription elongation speed rather than transcription rate also contributes to Top1-mediated mutagenesis, I measured mutation rates in strains expressing mutant forms of the largest subunit of RNA polymerase II (Rpo21) with defined transcription speeds (Geisberg, Moqtaderi and Struhl, 2020). All strains carried an FRB-tagged allele of *RPO21*, and the HygR-SSTR reporter was used to

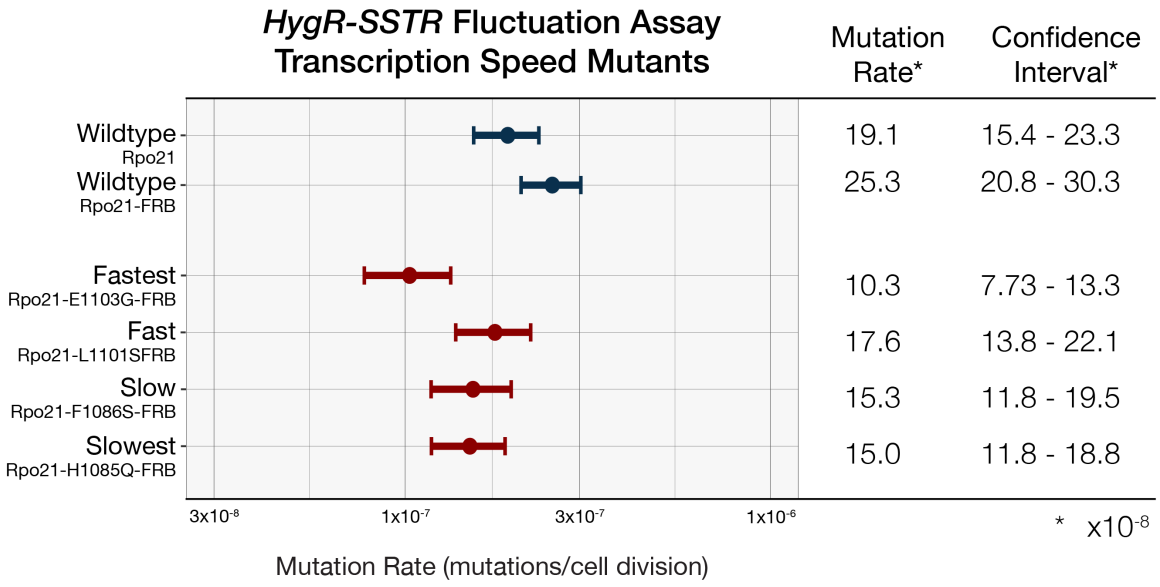

Figure 18 Transcription elongation speed does not positively correlate with Top1-dependent mutagenesis

Mutation frequencies were measured using the HygR-SSTR fluctuation assay in strains expressing FRB-tagged *RPO21* alleles with characterized transcription elongation speeds. Wildtype Rpo21 and Rpo21-FRB expressing strains served as controls. The fastest elongation mutant (Rpo21-E1103G-FRB) exhibited the lowest mutation rate (10.3×10^{-8}), while fast (Rpo21-L1101S-FRB), slow (Rpo21-F1086S-FRB), and slowest (Rpo21-H1085Q-FRB) mutants showed intermediate values ($15.0–17.6 \times 10^{-8}$). Mutation rates in all mutant strains were lower than or comparable to wildtype Rpo21-FRB (25.3×10^{-8}), suggesting that transcription elongation speed alone does not promote Top1-dependent mutagenesis at this locus.

Circles represent maximum likelihood estimates of mutation rates, and horizontal bars indicate 95% confidence intervals, calculated as in Figure 7.

quantify mutation frequency. As a baseline, wildtype Rpo21-FRB cells displayed a mutation rate of 25.3×10^{-8} mutations per cell division, slightly higher than the untagged wildtype strain (Figure 18: 19.1×10^{-8}), but within a comparable range. Among the transcription speed mutants, the fastest elongation mutant (Rpo21-E1103G) showed the lowest mutation rate (10.3×10^{-8}), while the fast (Rpo21-L1101S), slow (Rpo21-F1086S), and slowest (Rpo21-H1085Q) mutants displayed intermediate and comparable mutation rates ranging from 15.0 to 17.6×10^{-8}. These results indicate that increased transcription elongation speed does not correlate with increased Top1-dependent mutagenesis in this context, and may even be protective. Transcription rates of the reporter itself were not measured in this experiment, which limits the interpretation of the data. These data suggest that factors other than elongation speed likely play a more significant role in determining Top1 mutagenesis at this locus.

Together, these findings indicate that Top1-dependent mutagenesis is sensitive to multiple aging-related pathways. To test whether this mutagenesis impacts organismal longevity, we next examined the relationship between Top1, rNMP metabolism, and lifespan directly.

2.6. The Impact of Top1 and rNMP Pathway Alterations on Lifespan

To investigate the impact of Top1 activity and genomic rNMP load on yeast replicative lifespan, we analyzed lifespan data generated using a microfluidics-based platform (Aspert, Hentsch and Charvin, 2022). In this system, individual yeast cells are captured in a microfluidics chamber, and monitored over time, with continuous media flow to remove daughter cells. Automated microscopy records the number of divisions each mother completed before death, followed by analysis by an automated image classification pipeline to determine lifespan of individual cells. These experiments were carried out in collaboration with Aleksandr Maliavko in the Laboratory of Gilles Charvin.

2.6.1. Role of RER and Top1 in Modulating Yeast Replicative Lifespan

We hypothesized that the mutagenic activity of Top1 might contribute to a reduction in yeast replicative lifespan, such that deletion of *TOP1* (*top1*) could extend lifespan by decreasing genomic instability, particularly in aged mother cells. However, Top1 is also critical for rDNA metabolism, and loss of Top1 function has been shown to elevate DNA damage and recombination at the rDNA locus. Instability within the rDNA array could promote the

accumulation of extrachromosomal rDNA circles (ERCs), a key driver of replicative aging in yeast. To help distinguish between these opposing effects, we examined the hypomorphic or potentially separation-of-function allele, *TOP1-TAP*, which partially impairs Top1 activity without fully disrupting its role at the rDNA (Figure 11).

To test these possibilities, we measured the replicative lifespan of *top1* and *TOP1-TAP* strains using the microfluidics-based assay. Deletion of *TOP1* (*top1*) resulted in a notable reduction in replicative lifespan compared to wildtype (Figure 19A; mean of median lifespan: 18.7 vs. 23.0 divisions, respectively), consistent with a critical role for Top1 in maintaining genome stability during aging. In contrast, the *TOP1-TAP* strain exhibited a slightly reduced mean of median lifespan (20.7 divisions) compared to wildtype but showed increased heterogeneity in individual lifespans, This suggests that partial impairment of Top1 function does not extend lifespan, but individual clones with the *TOP1-TAP* allele may carry genomic variations that perturb aging trajectories. Together, these findings indicate that complete loss of Top1 activity shortens lifespan, potentially through rDNA instability, whereas partial loss of function results in increased variability between the lifespan of replicates, without extending it.

2.6.2. Changes in Top1-Mediated Mutation Frequency as a Function of Yeast Replicative Age

Given that Top1-dependent mutations accumulate in aged yeast, and the link between these mutation events and rNMP incorporation, we hypothesized that manipulating genomic rNMP incorporation or removal might impact replicative lifespan. Specifically, we predicted that *pol2-M644L*, which decreased rNMP incorporation during replication, would extend lifespan due to decreased mutational burden, while *rnh201-RED* would decrease replicative lifespan due to increased mutagenesis caused in part through faulty processing via Top1 activity. If the extension of lifespan in *pol2-M644L* is in fact due to rNMP induced mutagenesis, strains carrying both alleles would be expected to have a reduced lifespan relative to *pol2-M644L*. To test this, we analyzed the replicative lifespan of strains harboring these alleles individually or in combination.

In agreement with our hypothesis, expression of the *pol2-M644L* allele resulted in a modest extension of replicative lifespan compared to wildtype (Figure 19B, mean of median lifespan: 27.3 vs 23.0 divisions, respectively). However, the *rnh201-RED* allele, which impairs RNase H2-mediated rNMP removal and results in dramatic increase in mutagenic processing by Top1, had

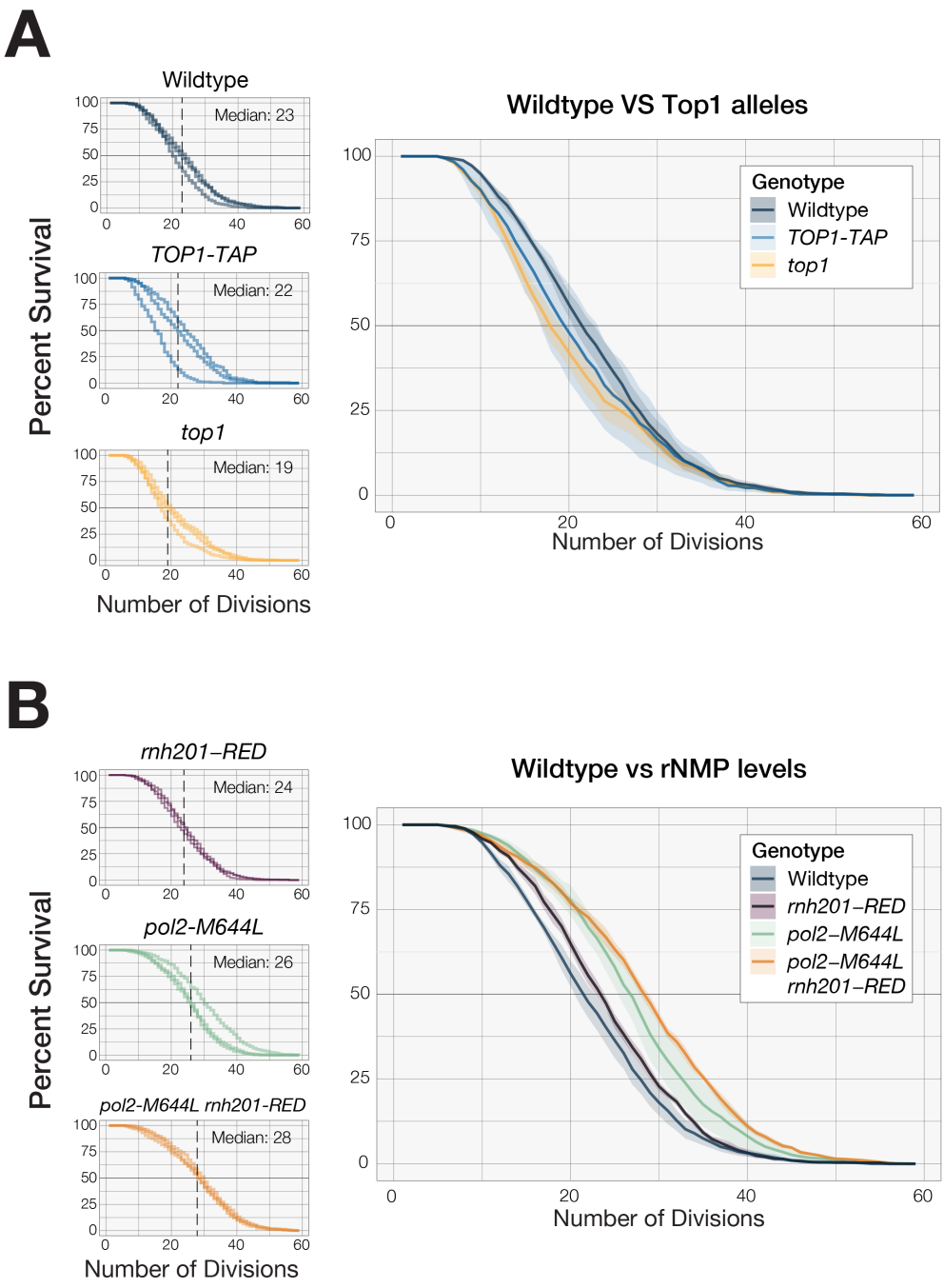

Figure 19 Replicative lifespan of yeast strains with altered Top1 activity or genomic rNMP metabolism.

(A) Replicative lifespan of wildtype, *TOP1-TAP* and *top1* strains measured using a microfluidics-based assay. Deletion of *TOP1* reduces lifespan relative to wildtype while *TOP1-TAP* showed a slightly reduced mean lifespan with increased heterogeneity among individual replicates.
(B) Replicative lifespan of wildtype, *rnh201-RED*, *pol2-M644L,* and *pol2-M644L rnh201-RED* strains. Expression of pol2-M644L extened lifespan, whole rnh201-RED had little effect. The double mutanta showed the greatest extension of lifespan among the strains tested.

Left panels: curves represent the percentage of cells alive after a given number of divisions from three biological replicates; right panels show the mean percentage across replicates with SEM indicated by shaded regions.

little effect on lifespan (mean of median lifespan: 24.0 divisions). Notably, the *pol2-M644L rnh201-RED* double mutant exhibited the greatest extension of lifespan among the strains tested (mean of median lifespan: 28.7 divisions). These results suggest that a combination of reduced rNMP incorporation with defective removal may promote replicative lifespan extension. However, the extended lifespan observed in *pol2-M644L* strains may result from changes in replication dynamics that are associated with this allele rather than being linked to rNMP metabolism.

2.6.3. Yeast Chronological Lifespan in the Absence of Top1 or RER

While replicative lifespan measures the number of times a mother cell can divide before irreversible cell cycle arrest, chronological lifespan (CLS) refers to the duration that non-dividing, quiescent cells remain viable in a stationary phase. CLS is commonly used as a model for aging in post-mitotic cells, providing a complementary perspective to studies of replicative aging. In yeast, CLS can be measured by quantifying the proportion of viable cells in stationary-phase cultures over time.

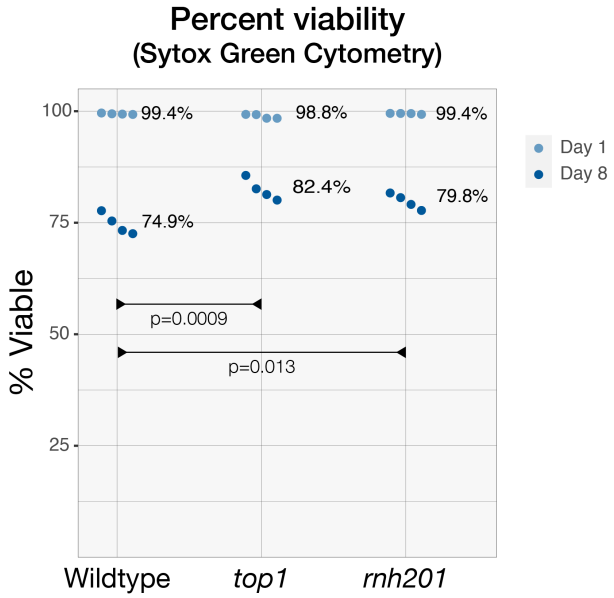

Figure 20 Loss of TOP1 or RNH201 extends chronological lifespan.

Viability of stationary-phase yeast cells was assessed using Sytox Green staining and flow cytometry on day 1 and day 8 of culture. All strains (wildtype, *top1*, and *rnh201*) displayed high viability on day 1 (>98%). By day 8, viability declined in all strains, but both *top1* and *rnh201* mutants maintained significantly higher viability than wildtype (*top1* vs. WT, p = 0.0009; *rnh201* vs. WT, p = 0.013; Tukey HSD). The difference between *top1* and *rnh201* was not statistically significant (p = 0.18). Mean values for each group are indicated.

All strains showed comparable viability on day 1 (>98%), confirming that initial survival upon entering stationary phase was unaffected. However, by day 8, wildtype viability had declined to 74.9%, while both *top1* and *rnh201* mutants exhibited significantly improved survival (82.4% and 79.8%, respectively). A one-way ANOVA followed by Tukey's post hoc test for multiple comparisons revealed that both *top1* (p = 0.0009) and *rnh201* (p = 0.013) had significantly higher viability than wild type, whereas *top1* and *rnh201* were not significantly different from one another (p = 0.18).

These findings indicate that both Top1 and RNase H2 contribute to the decline in cell viability during chronological aging. Loss of either factor extends CLS, suggesting that genome instability arising from unresolved rNMPs and/or Top1 activity contributes to reduced survival in non-dividing cells.

2.6.4. Role of RER and Top1 in Modulating Lifespan in *C. elegans*

Using a nematode model, *Caenorhabditis elegans*, we examined how Top1 activity and RER influence lifespan in multicellular organisms. To this end, a degron-tagged *top-1* allele enabled selective depletion of TOP-1 in adult worms, circumventing its essential role in development. Deletion of *rnh-2*, which encodes a key component of the ribonucleotide excision repair (RER) pathway, led to a marked reduction in lifespan compared to wildtype worms. Auxin-induced degradation of TOP-1 in otherwise wildtype adults caused a slight decrease in lifespan. In *rnh-2; top-1::degron* double mutants, mock-treated animals exhibited a shortened lifespan similar to that of the *rnh-2* single mutant as expected. However, degradation of TOP-1 in these double mutants fully rescued lifespan to wildtype levels. These findings indicate that in the absence of RER, TOP-1 activity becomes toxic in adulthood, and that removing this activity can restore normal lifespan. Thus, persistent Top1 activity appears to exacerbate the consequences of unrepaired ribonucleotides in post-mitotic cells.

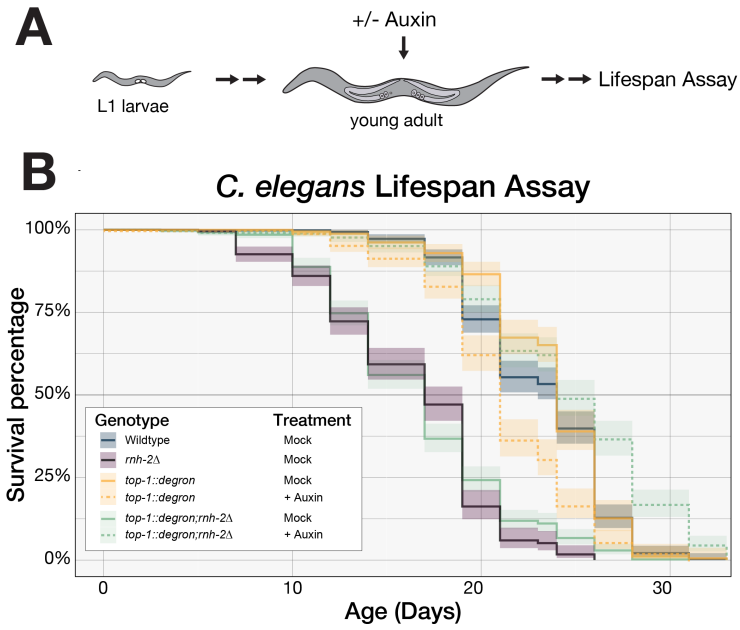

Figure 21 Degradation of Top1 in adulthood rescues the shortened lifespan of RER-deficient C. elegans.

(A) Schematic of the lifespan assay. Worms were synchronized at the L1 stage and grown to the young adult stage before treatment with auxin or mock control. Lifespan was then monitored under the indicated conditions. **(B)** Survival curves of wildtype, *rnh-2Δ*, *top-1::degron*, and *top-1::degron; rnh-2Δ* mutants with and without auxin treatment. Deletion of *rnh-2* significantly shortened lifespan compared to wildtype. Auxin-induced degradation of TOP1 in otherwise wildtype adult worms slightly reduced lifespan. In *rnh-2Δ; top-1::degron* double mutants, degradation of TOP-1 restored lifespan to wildtype levels, indicating that TOP-1 activity is detrimental in the absence of RER.

3. Discussion

3.1. Overview of Findings

This study investigated the mutagenic activity of Top1 in the context of embedded rNMPs and cellular aging, using *S. cerevisiae* as a model system. Several findings from this work advance understanding of Top1-dependent mutagenesis and provided new insights into the regulation of Top1's mutagenic activity and its connection to rNMP metabolism. Collectively, these results portray Top1 as a double-edged sword in genome maintenance: important for resolving torsional strain during replication and transcription, yet capable of introducing genomic instability in certain conditions. This project had two aims: first, to better understand the interplay between RNase H2 and Top1; and second, to determine whether and how this interplay is altered during aging.

On the topic of regulation of RNase H2 and Top1 activity, our findings provide a springboard from which further experiments can be conducted. The data suggest that Top1-mediated mutagenesis in wildtype cells is not dependent on the presence of rNMPs in the genome. Rather, Top1 activity appears to be inherently mutagenic in specific DNA sequence contexts. This conclusion is supported by two independent observations where experimental conditions that should have resulted in a decrease in rNMP-dependent Top1-mediated mutation frequency did not. First, the DNA polymerase variant *POL2-M644L*, which reduces rNMP incorporation into the genome during replication, did not lead to a decrease in mutation frequency in otherwise wildtype cells. Similarly, overexpression of RNase H2, which removes rNMPs via the RER pathway, also failed to reduce mutation rates. In contrast, Top1 overexpression led to a clear increase in mutation frequency. This result emphasizes the necessity for tight regulation of Top1 protein levels to maintain genome stability. Even in the absence of exogenous stress, elevated Top1 activity poses a risk to genome integrity, supporting the notion that precise control is essential to prevent mutagenesis.

Building on the insights we gained into Top1 activity in unaged cell populations, we next sought to determine whether the regulation of Top1 activity is altered during cellular aging, a period characterized by increased genomic instability. Given that misincorporated rNMPs are the most frequent type of genomic modification and can lead to frameshift mutations if not properly excised, they are an intriguing candidate for driving age-related genome instability. To

address this, we assessed Top1-dependent mutagenesis in aged mother cells and found a significant increase in mutation accumulation in the HygR-SSTR reporter compared to their younger counterparts. This observation raises the possibility that mutation accumulation related to rNMP metabolism and Top1 activity contribute to the mutation burden associated with aging.

Interestingly, the relationship between rNMP metabolism and cellular lifespan revealed a nuanced interplay. Yeast replicative lifespan is extended in a *pol2-M644L* genetic background, suggesting that reduced rNMP incorporation can promote longevity. However, this extension is not solely attributable to decreased rNMP levels in the genome, as deletion of RNase H2 in this background did not result in a decrease in lifespan. At the organismal level, findings from an RER-deficient worm model further emphasize the importance of rNMP processing: Top1 activity leads to a significant reduction in lifespan in these RER-deficient worms. Together, these findings suggest that aging-related decline in multicellular organisms stems not simply from the presence of rNMPs, but from their improper resolution by Top1.

3.2. Interpretation in the Context of Previous work

The findings presented here extend and refine previous work on Top1 mutagenesis and its role in genome stability during aging. In yeast, Top1 has long been known to generate short deletion mutations at tandem repeat tracts (Kim *et al.*, 2011; Lippert *et al.*, 2011; Takahashi *et al.*, 2011), and recent work extended this observation to human cells, demonstrating that Top1 is responsible for a distinctive mutational footprint at SSTRs (Reijns *et al.*, 2022). This footprint has since been recognized as the basis of the ID4 mutational signature (Reijns *et al.*, 2022). Strikingly, this same ID4 signature, though not yet attributed to Top1 at the time, was reported as a frequent insertion–deletion event in aged human neurons based on single-cell DNA sequencing (Luquette *et al.*, 2022). Among all mutation signatures analyzed, increased ID4 was most predictive of neuronal age. Notably, aged human neurons accumulate the replication-independent, clock-like ID5 and ID8 signatures, but not the replication-associated ID1 and ID2 signatures, consistent with their post-mitotic state. Complementary work from our lab indicates that Top1-dependent frameshift mutations can occur throughout the cell cycle independent of rNMP levels (L. Kindinger, unpublished data), further supporting the idea that Top1 mutagenesis is not restricted to replication. Taken together, these findings suggest that Top1-dependent indels represent a distinctive mutational signature that can accumulate even in post-mitotic cells.

In line with these observations, our work indicates that Top1-dependent mutagenesis is also relevant during aging in yeast. We observed an increase in mutagenesis of the HygR-SSTR reporter in replicatively aged cells. Preliminary data further suggest that Top1 mutagenesis may also contribute to chronological aging, the process of aging in non-dividing cells. This concept is further supported by work presented here in a multicellular organism. In worms, RNase H2-deficiency shortens lifespan, but this defect is rescued when Top1 is degraded. Because Top1 activity is essential in replicating cells of the developing worm, degradation is only induced after sexual maturity, when cell division has ceased in all somatic tissues. Together with our finding that mutation rates in wildtype yeast are only mildly affected by rNMP incorporation rates in the unaged context, these results imply that Top1 activity is mutagenic even without genomic rNMPs introduced during DNA replication. However, an alternative possibility must also be considered: DNA synthesis during repair events could incorporate rNMPs into the genomes of quiescent cells, providing a source of Top1-associated mutagenesis outside of S phase. Thus, from yeast to worms to human neurons, Top1 emerges as a mutagenic factor whose activity must be tightly regulated to preserve genomic integrity and organismal lifespan.

The mechanisms underlying the increase in Top1-dependent mutagenesis during aging remain unclear, but several possibilities can be considered, guided by the established molecular hallmarks of aging (López-Otín *et al.*, 2023). Age-associated changes in chromatin structure or nucleosome positioning may alter the accessibility of Top1 to specific genomic sites, thereby increasing the likelihood of mutagenic cleavage events. In line with this prediction, we examined genetic mutants that recapitulate these phenotypes: in the unaged context, increased mutation rates were observed in *rtt109* and *asf1* strains (Figure 17), both of which are expected to disrupt histone deposition. Alternatively, the progressive decline of DNA repair capacity in aged cells could alter the kinetics of Top1-mediated mutation events. For example, decreased activity of enzymes such as Sgs1, which has been shown to regulate Top1 mutation frequency (Niu *et al.*, 2016), and has also been linked to yeast longevity (Sinclair, Mills and Guarente, 1997) could explain the increase in mutational outcomes. Another aging-related molecular process that could influence Top1 activity is altered transcriptional regulation: global shifts in transcriptional programs during aging may enhance the exposure of highly transcribed regions to Top1 cleavage, compounding the mutagenic burden, especially in light of the well-documented transcription-associated stimulation of Top1-mediated mutation events (Lippert *et al.*, 2011). One such aging-related transcription defect is the increase in transcription elongation speed of RNA polymerase II (Debès *et al.*, 2023). In our study, we found that transcription speed did not

affect the mutation rate at the HygR-SSTR reporter in the unaged context (Figure 18); however we cannot exclude the possibility that increased transcription speed, in combination with the complex genomic changes experienced during aging, could contribute to elevated Top1-dependent mutagenesis. Our experiments represent an initial step toward dissecting the impact of aging-associated changes on Top1-mediated mutagenesis, but further work is required to deepen our understanding of how these interacting, not mutually exclusive processes contribute. These mechanisms emphasize the multiple, parallel ways in which aging-related cellular changes can influence Top1 activity and thereby shape genome stability in the later stages of life.

Taken together with our cross-species findings, these results underscore the impact of Top1 activity on genome stability and aging. While these mechanisms may underlie increased mutagenesis in aged cells, the relationship between mutagenesis and lifespan is more complex. Our data on yeast replicative lifespan revealed an unexpected result: RER deficiency did not shorten RLS as anticipated. Yet when these findings are considered alongside published results linking mutation rate to yeast RLS, the outcome is perhaps less surprising. Previous studies utilized proofreading deficient DNA polymerases in combination with mismatch repair defects to correlate mutation frequency with RLS (Lee *et al.*, 2019). These strains have an increased mutation rate in the *CAN1* forward mutation assay, and accumulate single nucleotide variations (SNVs) and indels. The mutation rate observed with the *CAN1* forward mutation reporter is inversely correlated with RLS (Lee *et al.*, 2019, Figure 1C; R^2 = 0.81). When correlating the mutation rate in the *CAN1* reporter to the RLS, the data indicate that yeast strains can tolerate a relatively high baseline mutation rate before lifespan is measurably reduced. In this study, *CAN1* mutation rates ranged from ~$5x10^{-7}$ mutations per cell division in wildtype cells to ~$1x10^{-3}$ mutations per cell division in a severe mutator strain. A statistically significant decrease in lifespan was only observed when median RLS declined from 24 to 18 generations, corresponding to a mutation rate of ~$2x10^{-5}$ mutations per cell division at the *CAN1* locus. This study also considered the rate of SNV and indel accumulation genome wide; the authors concluded that indel accumulation does correlate with lifespan, but SNV accumulation is more predictive. *CAN1* mutation rates have also been measured for RER deficient yeast strains in this work as well as others. Although the reporter is not specific, mutation frequency at the *CAN1* locus in RER deficient yeast strains (*rnh201*) rose from ~$1x10^{-7}$ in wildtype to ~3-$5x10^{-7}$ mutations per cell division, well below the threshold associated with reduced lifespan. This apparent disconnect may also reflect the dual nature of mutagenesis: while many mutations drive cellular decline and shorten lifespan, others can confer growth advantages. In this way, adaptive

mutations could mask deleterious effects of Top1-dependent events in yeast, just as mutagenesis in multicellular organisms can simultaneously contribute to aging and promote oncogenic transformation. These observations explain why RER deficiency does not measurably decrease RLS.

Quantitative mutation rates alone, however, do not tell the full story. The spectrum of mutations arising from rNMP accumulation differs from the point mutations measured in proofreading- and MMR-deficient strains. In the absence of RER, rNMPs processed by Top1 frequently give rise to small deletion mutations, causing a frameshift, especially in the most highly transcribed genes (Lippert *et al.*, 2011). Such mutations can have disproportionately deleterious consequences, as they disrupt reading frames, leading to altered protein sequence and premature truncations. Consistent with our speculation above, these qualitative differences in mutation type illustrate how aging-associated changes in transcription and repair could disproportionately exacerbate the mutagenic burden. Thus, while the overall mutation frequency in *rnh201* strains would be predicted to be insufficient to reduce lifespan, the qualitative nature of these mutations may still impose a significant burden on genome stability, especially in multicellular organisms. This distinction between quantitative thresholds and qualitative spectra of mutation provides a unified framework for interpreting the broader consequences of Top1 mutagenesis in aging and for considering future directions.

These observations not only extend our understanding of Top1 mutagenesis in the context of aging but also point toward new avenues for future research. Overall, this work reinforces the central role of genome stability in shaping lifespan. By showing how Top1 mutagenesis contributes to mutation accumulation in both dividing and non-dividing cells, these findings highlight the broader principle that multiple, overlapping sources of DNA damage must be controlled throughout life. An important challenge will be to determine how rNMP incorporation and processing intersect with the other hallmarks of aging. Yeast provides a powerful and accessible model to address these questions, offering the opportunity to test how altered rNMP levels or changes in Top1 activity influence broader features of aging such as chromatin structure, transcriptional regulation, or cellular stress responses. Conversely, aging-related changes may also influence Top1 regulation itself. Such integration will be essential to build a comprehensive view of how genome instability contributes not only to mutation burden but also to the systemic decline that characterizes aging. This broader perspective will help link molecular events to organismal outcomes.

3.3. Limitations and Future Directions

3.3.1. Methodological Constraints in Aging Fluctuation Assays

While this work provides new insights into the mutagenic activity of DNA Topoisomerase I in aging cells, several methodological considerations must be acknowledged, particularly regarding the adaptation of fluctuation assays to study replicatively aged yeast cells. First, in order to assess mutation frequency specifically in aged mother cells, it was necessary to modify standard fluctuation assay protocols in ways that violate some of the foundational assumptions outlined in the rSalvador framework (Zheng, 2017).

One key issue involves assumption 5 of the rSalvador model, which states that cell death is negligible during culture growth. This assumption does not hold when working with aged populations, which naturally exhibit increased cell death. However, this limitation is expected to result in an underestimation of mutation frequency, since dead cells cannot form colonies. Given that the observed mutation frequency in aged cells was higher than in younger populations despite this potential undercounting, it is likely that the increase reflects a genuine biological effect and that the measured values are conservative rather than exaggerated.

Another important consideration is assumption 11, which states that the number of cells used to initiate each culture should be small enough to ensure the absence of preexisting mutants. To ensure that most divisions during the assay were carried out by aged mother cells rather than their daughters, a large population of aged cells must be used to seed each culture. However, the process of aging these cells requires cell division, during which new mutations can arise. In an effort to reduce the number of preexisting frameshift mutants, aged cells were cultured in YPD containing hygromycin. This treatment was only partially effective. Specifically, some mutant cells become resistant to both Hygromycin and G418.

Although this residual background complicates the absolute quantification of mutation rates, it does not compromise the validity of comparisons between aged mothers and their daughters. There is no basis to expect an unequal distribution of these rare double-resistant mutants between mothers and daughters unless one invokes the immortal strand hypothesis (Rando, 2007). Therefore, the increased mutation frequency observed in aged cells compared to their daughters remains a valid and meaningful result. However, comparisons between aged and young cell populations, where the prevalence of preexisting mutants may differ more

substantially, should be interpreted with caution. More stringent quantification of double-resistant colony-forming units may help clarify these comparisons in future studies.

In addition to these methodological constraints, the interpretation of mutation frequency is limited by the fact that the *HygR* gene was not sequenced in the KanR colonies. Although the reporter was designed to detect -2 bp frameshift mutations within a short tandem repeat, it can also yield G418 resistance in the case of other indels within the reporter, such as +1 bp insertions, that restore the reading frame of the KanR gene. Without sequence confirmation, it is not possible to definitively conclude that all detected mutations were the expected -2 bp deletions. This uncertainty may affect the specificity of the assay and should be addressed in future work through targeted sequencing of the *HygR* locus in G418 resistant colonies.

Moreover, the role of Top1 in the observed mutagenesis during aging has not yet been fully clarified. While previous experiments demonstrate that Top1 is responsible for generating mutations in this reporter under multiple conditions, the specific contribution of Top1 to the increased mutation frequency in aged cells remains to be tested directly. Performing the same fluctuation assay in a *top1* background would help determine whether the accumulation of mutations in aged cells depends on Top1. If the elevated mutation rate in aged cells persists in the absence of Top1, this would suggest a Top1-independent mechanism. Conversely, if mutation frequency remains low in aged *top1* cells, it would provide strong evidence that the mutagenic activity of Top1 is a major driver of age-associated genome instability in this context. These follow-up experiments are essential to validate both the mechanistic specificity of the reporter system and the role of Top1 in driving mutagenesis in aged cells.

3.3.2. Interpretation of Lifespan Extension in *pol2* Mutants

This study reports an extension of replicative lifespan in the *pol2-M644L* mutant. This allele is known to reduce rNMP incorporation by DNA polymerase ε (Nick McElhinny, Kumar, *et al.*, 2010), and one possible interpretation of the lifespan extension is that decreased rNMP burden directly contributes to improved genome stability and longevity. However, this explanation may not fully capture the underlying mechanism. In vitro studies have shown that the *pol2-M644L* polymerase also exhibits reduced processivity compared to wildtype (Nick McElhinny, Kumar, *et al.*, 2010). This decrease in processivity likely results in mild replication stress, which may in turn activate protective stress response pathways or increase the fidelity of replication through compensatory mechanisms. This possibility is supported by our prior observations that a second *POL2* mutant, *pol2-M644G*, which incorporates more rNMPs than wildtype, also displayed

extended lifespan in preliminary experiments not included in this thesis. Those data were excluded from the main analysis due to confounding factors, including a slower doubling time and apparent mitochondrial instability that affected petite formation and/or viability.

These observations raise the possibility that reduced polymerase processivity, and potentially a slower replication rate rather than rNMP incorporation per se, may be a common feature underlying lifespan extension in both alleles. This model would align with broader literature suggesting that mild replication stress can promote longevity by enhancing genome surveillance and repair capacity.

3.3.3. Broader Future Directions

The implementation of the HygR-SSTR reporter allows for an unprecedented large dynamic range in mutation frequency both in the absence of Top1 or RNase H2 activity. This should allow us to implement a synthetic gene array based technology to search the yeast haploid gene deletion collection, comprised of ~5000 yeast strains, each of which has a deletion of a single, non-essential gene. Because selection for the deleted gene in this collection utilizes the KanR gene, it is not compatible with the HygR-SSTR reporter in its original form. To this end, the HygR-SSTR reporter was modified so that positive selection of mutants is possible on media conditions lacking Uracil. Pilot assays should be conducted to determine if the strategy outlined in (Novarina *et al.*, 2022) can be implemented to further investigate regulation of Top1-mediated mutation events. This approach could uncover previously unrecognized pathways that modulate Top1-activity and genome stability.

3.3.4. Conceptual outlook

Top1 cleavage generates unusual nucleic acid byproducts when the enzyme cuts twice at nearby positions. When produced from the excision of an rNMP, these short DNA fragments carry atypical end chemistries, such as a 5′-OH group paired with either a 2′,3′-cyclic phosphate or a 3′-phosphate terminus (Figure 6). Although such molecules are typically considered accidental debris of enzymatic activity, it is intriguing to consider whether they might act as regulatory signals. Recent work demonstrated that RNA:DNA hybrids excised from R-loops can be exported into the cytoplasm, where they activate innate immune pathways via cGAS-STING (Crossley *et al.*, 2023). By analogy, Top1-derived fragments could trigger cellular responses. While it is unlikely that dinucleotides of this size directly activate cGAS–STING, which generally requires longer nucleic acid fragments, their unusual chemistry raises the possibility that they

mimic other small signaling molecules. For example, cyclic GMP–AMP (cGAMP), itself a dinucleotide, functions as a central second messenger in the cGAS-STING pathway. In a similar vein, Top1-derived fragments could transform what is usually considered enzymatic debris into a molecular link between genome instability and inadvertent immune activation. This concept is particularly provocative in the context of aging: if the rate of byproduct formation increases with age, as suggested by data presented in this thesis, these molecules could act as a "self-reporting" signal of cellular decline, perhaps even contributing to a form of "altruistic aging" in which dysfunctional cells are selectively eliminated for the benefit of the organism or species (Longo, Mitteldorf and Skulachev, 2005). Taken as a whole, these directions underscore both the immediate opportunities to strengthen the present findings and the broader potential to uncover new links between genome instability, cellular signaling, and the biology of aging.

4. Materials and Methods

4.1. Materials

4.1.1. Yeast Strains

All yeast strains used in this study are listed in Table 1. With the exception of yKJ968 and yKJ974, all strains were derived from either BY4741 (*MATa his3Δ1 leu2Δ0 ura3Δ0 met15 Δ/0*) or BY4742 (*MAT α his3Δ1 leu2Δ/0 ura3Δ0 lys2Δ0*). Many strains were obtained from the Saccharomyces Genome Deletion Project collection, purchased from Dharmacon/Horizon Discovery.

Table 1: Yeast strains used in this study

Strain name	Genotype	Figures	Source
yBL1	*MATa/MATalpha his3Δ1/ his3Δ1leu2Δ0 /leu2Δ0 ura3Δ0/ura3Δ0 MET15/ met15Δ0 LYS2/lys2Δ0*		Luke Lab
yBL7	*MATa lys1 cry1*		Luke Lab
yKJ9	*MATalpha his3Δ1 leu2Δ/0 ura3Δ/0 lys2Δ/0 MET15*	7, 12, 14	This study
yBL440	*MATa his3Δ1 leu2Δ0 ura3Δ0 met15Δ0 rnh201::NatR*	7, 20	Luke Lab
ySH13	*MATa his3Δ1 leu2Δ0 ura3Δ0 LYS2 met15Δ0 agp1::HygR-SSTR:P2A:KanR HO*	8, 9B, 16A	Luke Lab
yKJ530	*MATa his3Δ1 leu2Δ/0 ura3Δ/0 rnh201::His3 agp1::HygR-SSTR:P2A:KanR HO*	8, 10B	This study
yKJ657	*MATa his3Δ1 leu2Δ0 ura3Δ0 lys2Δ0 MET15 rnh202::NatMX agp1::HygR-SSTR:P2A:KanR*	8	This study
yKJ628	*MATa his3Δ1 leu2Δ/0 ura3Δ/0 rnh203::His3 agp1::HygR-SSTR:P2A:KanR HO*	8	This study
yKJ718	*MATa his3Δ1 leu2Δ0 ura3Δ0 rnh201*-Table 1 *agp1::HygR-SSTR (STOP):P2A:KanR HO*	8, 15	This study
yKJ533	*MATa his3Δ1 leu2Δ/0 ura3Δ/0 top1::his agp1::HygR-SSTR:P2A:KanR HO*	8, 15	This study
ySGS119	*MATa his3Δ1; leu2Δ/0 ura3Δ/0 rnh201-RED-6MYC-Ura3MX top1::His agp1::Hyg-SSTR:P2A:Kan HO*	8;	This study, Sophia Giovanna Sergi
ySH13	*MATa his3Δ1 leu2Δ0 ura3Δ0 LYS2 met15Δ0 agp1::HygR-SSTR:P2A:KanR HO*	8, 9B; Wildtype Head-on	Luke Lab; Sacha Heershop
yKJ532	*MATa his3Δ1 leu2Δ/0 ura3Δ/0 agp1::HygR-SSTR:P2A:KanR HO*	9B; Wildtype Head-on	This study
yKJ872	*MATa his3Δ1 leu2Δ/0 ura3Δ/0 agp1::HygR-SSTR:P2A:KanR CD*	9B; Wildtype Co-directional	This study
yKJ873	*MATa his3Δ1 leu2Δ/0 ura3Δ/0 agp1::HygR-SSTR:P2A:KanR CD*	9B; Wildtype Co-directional	This study
yKJ891	*MATalpha his3Δ1 leu2Δ/0 ura3Δ/0 agp1::HygR-SSTR:P2A:KanR CD*	9B 18; Wildtype Co-directional	This study

Strain name	Genotype	Figures	Source
ySH12	*MATalpha his3Δ1 leu2Δ0 ura3Δ0 LYS2 met15Δ0 agp1::HygR-SSTR:P2A:KanR HO*	9B, 10B, 15, 17; Wildtype Co-directional	Luke Lab; Sacha Heershop
yKJ745	*MATalpha his3Δ1 leu2Δ0 ura3Δ0 pol2-M644L agp1::HygR-SSTR:P2A:KanR HO*	9B; Head-on Leading ↓	This study
yKJ518	*MATalpha his3Δ1 leu2Δ/0 ura3Δ/0 LYS2 MET15 pol2-M644G:NatNT2 agp1::HygR-SSTR:P2A:KanR HO*	9B; Head-on Leading ↑	This study
yKJ950	*MATalpha his3Δ1 leu2Δ/0 ura3Δ/0 pol3-L612M:NatNT2 agp1::HygR-SSTR:P2A:KanR HO*	9B; Head-on Lagging ↑	This study
yKJ988	*MATalpha his3Δ1 leu2Δ/0 ura3Δ/0 pol2-M644L agp1::HygR-SSTR:P2A:KanR CD*	9B; Co-directional Leading ↓	This study
yKJ896	*MATalpha his3Δ1 leu2Δ/0 ura3Δ/0 pol2-M644G:NatNT2 agp1::HygR-SSTR:P2A:KanR CD*	9B; Co-directional Leading ↑	This study
yKJ947	*MATalpha his3Δ1 leu2Δ/0 ura3Δ/0 POL3-L612M:NatNT2 agp1::HygR-SSTR:P2A:KanR CD*	9B; Co-directional Lagging ↑	This study
yKJ586	*MATa his3Δ1 leu2Δ0 ura3Δ0 LYS2 met15Δ0 agp1::HygR-SSTR:P2A:KanR HO + pRS416*	10A; Wildtype + EV	This study
yKJ589	*MATa his3Δ1 leu2Δ0 ura3Δ0 LYS2 met15Δ0 agp1::HygR-SSTR:P2A:KanR HO + pBL752*	10A; Wildtype + OE	This study
yKJ546	*MATalpha his3Δ1 leu2Δ/0 ura3Δ/0 TOP1-3HA:His agp1::HygR-SSTR:P2A:KanR HO + pRS416*	10A; *TOP1-3HA* + EV	This study
yKJ548	*MATalpha his3Δ1 leu2Δ/0 ura3Δ/0 TOP1-3HA:His agp1::HygR-SSTR:P2A:KanR HO + pBL752*	10A; *TOP1-3HA* + OE	This study
yKJ550	*MATalpha his3Δ1 leu2Δ/0 ura3Δ/0 top1:His agp1::HygR-SSTR:P2A:KanR HO + pRS416*	10A; *top1* + EV	This study
yKJ552	*MATalpha his3Δ1 leu2Δ/0 ura3Δ/0 top1:His agp1::HygR-SSTR:P2A:KanR HO + pBL752*	10A; *top1* + OE	This study
yKJ590	*MATa his3Δ1 leu2Δ0 ura3Δ0 LYS2 met15Δ0 rnh201::His agp1::HygR-SSTR:P2A:KanR HO + pRS416*	10A; *rnh201* + EV	This study
yKJ592	*MATa his3Δ1 leu2Δ0 ura3Δ0 LYS2 met15Δ0 rnh201::His agp1::HygR-SSTR:P2A:KanR HO + pBL752*	10A; *rnh201* + OE	This study
ySH12	*MATalpha his3Δ1 leu2Δ0 ura3Δ0 LYS2 met15Δ0 agp1::HygR-SSTR:P2A:KanR HO*	9B, 10B, 15, 17; Wildtype	This study, Sacha Heerschop
yKJ751	*MATa his3Δ1 leu2Δ0 ura3Δ0 LEU2:GPD-TOP1 agp1::HygR-SSTR:P2A:KanR*	10B; *GPD-TOP1*	This study
yKJ530	*MATa his3Δ1 leu2Δ/0 ura3Δ/0 rnh201::His3 agp1::HygR-SSTR:P2A:KanR HO*	8, 10B; *rnh201*	This study
yEG522 (parental)	*MATalpha his3Δ1 leu2Δ0 ura3Δ0 agp1::HygR-SSTR:P2A:KanR*	11A; Wildtype	(fresh spore, not frozen); This study, Eduardo Gameiro and Aurelia Weber
yEG522 (parental)	*MATa his3Δ1 leu2Δ0 ura3Δ0 TOP1-TAP:His3 agp1::HygR-SSTR:P2A:KanR*	11A; *TOP1-TAP*	(fresh spore, not frozen); This study, Eduardo Gameiro and Aurelia Weber
yEG523 (parental)	*MATalpha his3Δ1 leu2Δ0 ura3Δ0 top1::His3 agp1::HygR-SSTR:P2A:KanR*	11A; *top1*	(fresh spore, not frozen); This study, Eduardo Gameiro and Aurelia Weber
yEG522 (parental)	*MATalpha his3Δ1 leu2Δ0 ura3Δ0 TOP1-TAP:His RNH201-RED-6Myc:Ura3MX agp1::HygR-SSTR:P2A:KanR*	11A; *rnh201-RED*	(fresh spore, not frozen); This study, Eduardo Gameiro and Aurelia Weber

Strain name	Genotype	Figures	Source
yEG572	*MATalpha his3Δ1 leu2Δ0 ura3Δ0 TOP1-TAP:His RNH201-RED-6Myc:Ura3MX agp1::HygR-SSTR:P2A:KanR*	11A; *rnh201-RED TOP1-TAP*	This study, Eduardo Gameiro and Aurelia Weber
yEG574	*MATalpha his3Δ1 leu2Δ0 ura3Δ0 top1:His RNH201-RED-6Myc:Ura3MX agp1::HygR-SSTR:P2A:KanR*	11A; *rnh201-RED top1*	This study, Eduardo Gameiro and Aurelia Weber
yKJ399 (parental)	*MATa/MATalpha; his3Δ1/ his3Δ1;leu2Δ0 /leu2Δ0; ura3Δ0/ura3Δ0; met15Δ0/met15Δ0; LYS2/LYS RNH1/rnh1::KAN RNH201/rnh201::HYG TOP1/top1::HIS3*	11B	This study
yNA974 (parental)	*MATa/alpha his3Δ1/his3Δ1 leu2Δ0/leu2Δ0 ura3Δ0/ura3Δ0 RNH1/rnh1::kan RNH201/rnh201::HYG TOP1/TOP1-TAP:His3*	11B	Luke Lab, Natalie Schindler
yKJ399 (parental)	*MATalpha his3Δ1 leu2Δ0 ura3Δ0*	11C; Wildtype	(fresh spore, not frozen); This study, Eduardo Gameiro and Aurelia Weber
yVK37	*MATalpha his3Δ1 leu2Δ0 ura3Δ0 rtt101::NatR*	11C; *rtt101*	Luke Lab; Vanessa Kellner
yKJ399 (parental)	*MATa his3Δ1 leu2Δ0 ura3Δ0 top1::His3*	11C; *top1*	(fresh spore, not frozen); This study, Eduardo Gameiro and Aurelia Weber
yNA974 (parental)	*MATa his3Δ1 leu2Δ0 ura3Δ0 TOP1-TAP:His3*	11C; *TOP1-TAP*	(fresh spore, not frozen); This study, Eduardo Gameiro and Aurelia Weber
yKJ443	*MATalpha his3Δ1 leu2Δ0 ura3Δ0; met15Δ0 rtt101::HygR top1::his3*	11C; *rtt101 top1*	This study
yKJ476	*MATalpha his3Δ1 leu2Δ/0 ura3Δ/0 LYS? MET15 TOP1-TAP:His3 rtt101::HygR*	11C; *rtt101 TOP1-TAP*	This study
yNA3 x yVK833 (parental)	*MATa his3Δ1 leu2Δ0 ura3Δ0*	11D; Wildtype	(fresh spore, not frozen); This study, Eduardo Gameiro and Aurelia Weber
yNA3 x yVK833 (parental)	*MATa his3Δ1 leu2Δ0 ura3Δ0 top1::KanR*	11D; *top1*	(fresh spore, not frozen); This study, Eduardo Gameiro and Aurelia Weber
yNA3 x yVK833 (parental)	*MATa his3Δ1 leu2Δ0 ura3Δ0 rnh201::HygR*	11D; *rnh201*	(fresh spore, not frozen); This study, Eduardo Gameiro and Aurelia Weber
yNA3 x yVK833 (parental)	*MATalpha his3Δ1 leu2Δ0 ura3Δ0 pol2-M644G:NatNT2*	11D; *pol2-M644G*	(fresh spore, not frozen); This study, Eduardo Gameiro and Aurelia Weber
yNA3 x yVK833 (parental)	*MATa his3Δ1 leu2Δ0 ura3Δ0 pol2-M644G:NatNT2 rnh201::HygR*	11D; *pol2-M644G rnh201*	(fresh spore, not frozen); This study, Eduardo Gameiro and Aurelia Weber
yNA3 x yVK833 (parental)	*MATa his3Δ1 leu2Δ0 ura3Δ0 pol2-M644G:NatNT2 rnh201::HygR top1::KanR*	11D; *pol2-M644G rnh201 top1*	(fresh spore, not frozen); This study, Eduardo Gameiro and Aurelia Weber
yBL229	*MATa his3Δ1 leu2Δ0 ura3Δ0 rad52::KanR*	11D; *rad52*	Luke Lab; Brian Luke
yNA3 x yNA1080 (parental)	*MATa his3Δ1 leu2Δ0 ura3Δ0*	11D; Wildtype	(fresh spore, not frozen); This study, Eduardo Gameiro and Aurelia Weber
yNA3 x yNA1080 (parental)	*MATa his3Δ1 leu2Δ0 ura3Δ0 TOP1-TAP:His3*	11D; *TOP1-TAP*	(fresh spore, not frozen); This study, Eduardo Gameiro and Aurelia Weber
yNA3 x yNA1080 (parental)	*MATa his3Δ1 leu2Δ0 ura3Δ0 rnh201::HygR*	11D; *rnh201*	(fresh spore, not frozen); This study, Eduardo Gameiro and Aurelia Weber

Strain name	Genotype	Figures	Source
yNA3 x yNA1080 (parental)	*MATa his3Δ1 leu2Δ0 ura3Δ0 pol2-M644G:NatNT2*	11D; *pol2-M644G*	(fresh spore, not frozen); This study, Eduardo Gameiro and Aurelia Weber
yNA3 x yNA1080 (parental)	*MATa his3Δ1 leu2Δ0 ura3Δ0 pol2-M644G:NatNT2 rnh201::HygR*	11D; *pol2-M644G rnh201*	(fresh spore, not frozen); This study, Eduardo Gameiro and Aurelia Weber
yNA3 x yNA1080 (parental)	*MATa his3Δ1 leu2Δ0 ura3Δ0 pol2-M644G:NatNT2 rnh201::HygR TOP1-TAP:His3*	11D; *pol2-M644G rnh201 TOP1-TAP*	(fresh spore, not frozen); This study, Eduardo Gameiro and Aurelia Weber
yKJ9	*MATalpha his3Δ1 leu2Δ/0 ura3Δ/0 lys2Δ/0 MET15*	7, 12, 14	This study
yVK875	*MATa his3Δ1 leu2Δ0 ura3Δ0 top1::His3*	12, 20	Luke Lab; Vanessa Kellner
yKJ44	*MATalpha his3Δ1 LEU2::AFB2-LEU2 ura3Δ/0 LYS2 MET15 Top1-AID-9MYC-His3*	12	This study
yKJ951 x yKJ780 (parental)	*MAT? his3Δ1 leu2Δ0 ura3Δ0 agp1::HygR-SSTR:P2A:KanR*	13; wildtype	This study, freshly derived spore colony
yKJ989	*MATalpha his3Δ1 leu2Δ0 ura3Δ0 His3:GPD-RNH201 Ura3-GPD-RNH202-TAP-His3 Leu2:GPD-RNH203 agp1::HygR-SSTR:P2A:KanR*	13; *RNase H2 OE*	This study
yKJ9	*MATalpha his3Δ1 leu2Δ/0 ura3Δ/0 lys2Δ/0 MET15*	7, 12, 14	This study
ySH12	*MATalpha his3Δ1 leu2Δ0 ura3Δ0 LYS2 met15Δ0 agp1::HygR-SSTR:P2A:KanR HO*	9B, 10B, 15, 17; Wildtype	Luke Lab; Sacha Heershop
yKJ533	*MATa his3Δ1 leu2Δ/0 ura3Δ/0 top1::his agp1::HygR-SSTR:P2A:KanR HO*	8, 15	This study
yKJ718	*MATa his3Δ1 leu2Δ0 ura3Δ0 rnh201-RED agp1::HygR-SSTR (STOP):P2A:KanR HO*	8, 15	This study
ySH13	*MATa his3Δ1 leu2Δ0 ura3Δ0 LYS2 met15Δ0 agp1::HygR-SSTR:P2A:KanR HO + pBL290*	8, 9B, 16A	Luke Lab
ySH13	*MATa his3Δ1 leu2Δ0 ura3Δ0 LYS2 met15Δ0 agp1::HygR-SSTR:P2A:KanR HO + pBL180*	8, 9B, 16A	Luke Lab
yKJ968	*MATa ade2-1 ura3-1 trp1-1 leu2-3,112 his3-11 can1-100 fob1Δ::HIS3 agp1::HygR-SSTR:P2A:KanR HO (~190 rDNA repeats)*	16B	Jon Houseley, Cioci Mol Cell. 2003 Jul;12(1):135-45; this study
yKJ974	*MATa ade2-1 ura3-1 trp1-1 leu2-3,112 his3-11 can1-100 fob1Δ::HIS3 agp1::HygR-SSTR:P2A:KanR HO (~25 rDNA repeats)*	16B	Jon Houseley, Cioci Mol Cell. 2003 Jul;12(1):135-45; this study
ySH12	*MATalpha his3Δ1 leu2Δ0 ura3Δ0 LYS2 met15Δ0 agp1::HygR-SSTR:P2A:KanR HO*	9B, 10B, 15, 17; Wildtype	This study, Sacha Heerschop
yKJ755	*MATa his3Δ1; leu2Δ0; ura3Δ0; agp1::HygR-SSTR:P2A:KanRR; hir1::NatR*	17	This study
yKJ759	*MATa his3Δ1; leu2Δ0; ura3Δ0; agp1::HygR-SSTR:P2A:KanRR; hir2::NatR*	17	This study
yKJ763	*MATa his3Δ1; leu2Δ0; ura3Δ0; agp1::HygR-SSTR:P2A:KanRR; hir3::NatR*	17	This study
yKJ775	*MATalpha his3Δ1; leu2Δ0; ura3Δ0; agp1::HygR-SSTR:P2A:KanRR; rtt109::HisMX*	17	This study
yKJ661	*MATalpha his3Δ1 leu2Δ0 ura3Δ0 lys2Δ0 MET15 asf1::NatMX agp1::HygR-SSTR:P2A:KanR*	17	This study
yKJ662	*MATalpha his3Δ1 leu2Δ0 ura3Δ0 lys2Δ0 MET15 asf1::NatMX agp1::HygR-SSTR:P2A:KanR*	17	This study
yKJ891	*MATalpha his3Δ1 leu2Δ/0 ura3Δ/0 agp1::HygR-SSTR:P2A:KanR CD*	9B 18; Wildtype Rpo21	This study
yKJ920	*MATa his3Δ1 leu2Δ/0 ura3Δ/0 RPO21-FRB:NatMX agp1::HygR-SSTR:P2A:KanR CD*	18; Wildtype Rpo21-FRB	Kevin Struhl Lab, Harvard medical center; This study

Strain name	Genotype	Figures	Source
yKJ925	*MATa his3Δ1 leu2Δ/0 ura3Δ/0 RPO21-H1085Q-FRB:NatMX agp1::HygR-SSTR:P2A:KanR CD*	18; Slowest	Kevin Struhl Lab, Harvard medical center; This study
yKJ930	*MATa his3Δ1 leu2Δ/0 ura3Δ/0 RPO21-F1086S-FRB:NatMX agp1::HygR-SSTR:P2A:KanR CD*	18; Slow	Kevin Struhl Lab, Harvard medical center; This study
yKJ935	*MATa his3Δ1 leu2Δ/0 ura3Δ/0 RPO21-L1101S-FRB:NatMX agp1::HygR-SSTR:P2A:KanR CD*	18; Fast	Kevin Struhl Lab, Harvard medical center; This study
yKJ940	*MATa his3Δ1 leu2Δ/0 ura3Δ/0 RPO21-E1103G-FRB:NatMX agp1::HygR-SSTR:P2A:KanR CD*	18; Fastest	Kevin Struhl Lab, Harvard medical center; This study
yKJ814	*MATa his3Δ1 leu2Δ/0 ura3Δ/0 LYS2 met15Δ0*	19A	This study
yKJ815	*MATa his3Δ1 leu2Δ/0 ura3Δ/0 LYS2 met15Δ0*	19A	This study
yKJ816	*MATa his3Δ1 leu2Δ/0 ura3Δ/0 LYS2 met15Δ0*	19A	This study
yKJ817	*MATa his3Δ1 leu2Δ/0 ura3Δ/0 LYS2 met15Δ0 pol2-M644L*	19B	This study
yKJ818	*MATa his3Δ1 leu2Δ/0 ura3Δ/0 LYS2 met15Δ0 pol2-M644L*	19B	This study
yKJ819	*MATa his3Δ1 leu2Δ/0 ura3Δ/0 LYS2 met15Δ0 pol2-M644L*	19B	This study
yKJ820	*MATa his3Δ1 leu2Δ/0 ura3Δ/0 LYS2 met15Δ0 RNH201-RED*	19B	This study
yKJ821	*MATa his3Δ1 leu2Δ/0 ura3Δ/0 LYS2 met15Δ0 RNH201-RED*	19B	This study
yKJ822	*MATa his3Δ1 leu2Δ/0 ura3Δ/0 LYS2 met15Δ0 RNH201-RED*	19B	This study
yKJ823	*MATa his3Δ1 leu2Δ/0 ura3Δ/0 LYS2 met15Δ0 RNH201-RED pol2-M644L*	19B	This study
yKJ824	*MATa his3Δ1 leu2Δ/0 ura3Δ/0 LYS2 met15Δ0 RNH201-RED pol2-M644L*	19B	This study
yKJ825	*MATa his3Δ1 leu2Δ/0 ura3Δ/0 LYS2 met15Δ0 RNH201-RED pol2-M644L*	19B	This study
yKJ826	*MATa his3Δ1 leu2Δ/0 ura3Δ/0 LYS2 met15Δ0 top1::KanR*	19B	This study
yKJ827	*MATa his3Δ1 leu2Δ/0 ura3Δ/0 LYS2 met15Δ0 top1::KanR*	19B	This study
yKJ828	*MATa his3Δ1 leu2Δ/0 ura3Δ/0 LYS2 met15Δ0 top1::KanR*	19B	This study
yKJ829	*MATa his3Δ1 leu2Δ/0 ura3Δ/0 LYS2 met15Δ0 TOP1-TAP:His*	19B	This study
yKJ830	*MATa his3Δ1 leu2Δ/0 ura3Δ/0 LYS2 met15Δ0 TOP1-TAP:His*	19B	This study
yKJ831	*MATa his3Δ1 leu2Δ/0 ura3Δ/0 LYS2 met15Δ0 TOP1-TAP:His*	19B	This study
yKJ10	*MATa his3Δ1 leu2Δ/0 ura3Δ/0* met15Δ0	20	This study
yVK875	*MATa his3Δ1 leu2Δ0 ura3Δ0 top1::His3*	12, 20	Luke Lab; Vanessa Kellner
yBL440	*MATa his3Δ1 leu2Δ0 ura3Δ0 met15Δ0 rnh201::NatR*	7, 20	Luke Lab

4.1.2. Plasmids

Table 2: Plasmids used in this study.

Plasmid name	Backbone	Insert or Feature	Use	Source
Selection marker cassettes				
pBL1	Bacterial Cloning Vector	*pTEF-NatR-tTEF (NatMX)*	Selection marker switch	Matthias Peter; Luke Lab
pBL274	Bacterial Cloning Vector	*pTEF-HygB-tTEF (HygMX)*	Selection marker switch	Euroscarf; Luke Lab
pBL469	Bacterial Cloning Vector	*pTEF-Ura3-tTEF (UraMX)*	Selection marker switch	Euroscarf; Luke Lab
pBL470	Bacterial Cloning Vector	*pTEF-Leu2-tTEF (LeuMX)*	Selection marker switch	David Stillman; Luke Lab

Plasmid name	Backbone	Insert or Feature	Use	Source
Promoter integration cassettes				
pBL1139	pYM-N derived	*Ura3MX:GPD*	Promoter replacement; generation of RNase H2 overexpression strains	This study
pBL1140	pYM-N derived	*His3MX:GPD*	Promoter replacement; generation of RNase H2 overexpression strains	This study
pBL1141	pYM-N derived	*Leu2MX:GPD*	Promoter replacement; generation of RNase H2 and Top1 overexpression strains	This study
Genome engineering constructs				
pBL1132	Bacterial Cloning Vector	*pTEF-HygR-SSTR:P2A:KanR-tTEF*	Integrated into yeast genome	Andrew Jackson Lab (University of Edinburgh)
pBL1131	pRS406	*pol2-M644L*	pop-in/pop-out for integration into yeast genome	This study; Tom Kunkel (NIH)
pSLG49	pGSKU	CORE-I-SceI cassette	Delitto Perfetto method; to generate *rnh201-RED* strains	Michael Knop
pBL397	Bacterial Cloning Vector	*rnh201-RED*	Used as repair cassette for delitto Perfetto to generate *rnh201-RED* strains, e.g. Fig 8	Invitrogen
Expression vectors				
pJK14	pRS416	—	Empty vector; (Fig 10A)	Luke Lab; Robbie Loewith
pBL752	pRS416	*GPD-TOP1-3HA*	Overexpression of Top1-3HA; Fig 10A	This study
pBL58	pENTR1A	—	Entry vector for Gateway cloning;	Invitrogen; Luke Lab
pBL751	pENTR1A	*TOP1*	Entry vector for gateway cloning of *TOP1* to destination vectors	This study
pBL290	Ycp50	—	Empty vector for Sir2 overexpression experiments; Fig 16A	Luke Lab; Knop Lab
pBL180	Ycp50	*SIR2*	Single-copy Sir2 overexpression experiments; Fig 16A	Luke Lab; Jasper Rine

4.1.3. Oligonucleotides

Table 3: Oligonucleotides used in this study

Oligo	Sequence (5' to 3')	Use
oKJ1	AACCAATTCAGTCGACTGATGACTATTGCTGATGCTTCCAAAGT	Cloning of *TOP1* into Gateway system
oKJ2	GAAAGCTGGGTCTAGATATCCAAACCTCCAATTTTCATCTACCGATTCT	Cloning of *TOP1* into Gateway system
oKJ30	CCGGTACCAATTATCTAGGGTTCTCAGCCTCTTCCTTCTAACAGGCTTAG CCTGGCACGACAGGTTTC	*RNH201* Core Cassette integration
oKJ31	GTCGAAAAACCTTGAAAACAACTACTGCACACCAAATTGATACGATTAA TAGGGATAACAGGGTAATTTGGATGGACGCAAAGAAGT	*RNH201* Core Cassette integration with ISceI site
oKJ32	CCGGTACCAATTATCTAGGG	*RNH201* repair cassette
oKJ33	TGGATGATGTAAACAGGCAG	*RNH201* repair cassette

Oligo	Sequence (5' to 3')	Use
oKJ34	GTCGACCTGCAGCGTACG	S3 sequence for sequencing (*RNH201-9myc*)
oKJ35	TAATTGCGTTGCGCTCACTG	Delitto perfetto integration and sequencing oligo
oKJ47	TCTACATGATAGATCAAAGGTAGTTC	*pol2-M644L* SDM
oKJ48	TGTCGCCTCTCTGTACCCAAACA	*pol2-M644L* SDM
oKJ59	AGCTGGTGTTTTTAGGAGTG	*pol2-M644L* Sequencing
oKJ60	GTAATGCACGCTTGATCATG	*pol2-M644L* sequencing
oTW170	CAGTCGCTACGTATTACCTT	*pol2-M644L* Sequencing
oKJ71	ACTGACAATAAAAAGATTCTTG	yMT-N marker switch vector amplification F
oKJ72	GGTTGTTTATGTTCGGATG	yMT-N marker switch vector amplification R
oKJ73	CATCCGAACATAAACAACCATGTCGAAAGCTACATATAAGGAACGT	yMT-N *URA3* Marker switch F
oKJ74	CAAGAATCTTTTTATTGTCA GTACTGATTAGTTTTGCTGGCCGCATCTTC	yMT-N *URA3* Marker switch R
oKJ75	CATCCGAACATAAACAACCATGACAGAGCAGAAAGCCCTAGT	yMT-N *HIS3* Marker switch F
oKJ76	CAAGAATCTTTTTATTGTCA GTACTGACTACATAAGAACACCTTTGGTGGAG	yMT-N *HIS3* Marker switch R
oKJ77	CATCCGAACATAAACAACCATGTCTGCCCCTAAGAAGATCG	yMT-N *LEU2* Marker switch F
oKJ78	GAATCTTTTTATTGT CAGTTTAAGCAAGGATTTTCTTAACTTCTTCGG	yMT-N *LEU2* Marker switch R
oKJ79	GACTTAGTGTAAGGAGACTCCAAGGATGCTTCTACCGTGGGGGGTACCAT CATCGATGAATTCTCTGTCGTC	*HIS3:GPD-RNH201* F
oKJ80	TGTCGAAAAACCTTGAAAACAACTACTGCACACCAAATTGATACGATTAA CGTACGCTGCAGGTC	*HIS3:GPD-RNH201* R
oKJ81	TATTCTGTCGCAATAGTTGACTTTCTTTTCTGGCCTCTCGAACAAAAAGC CGTACGCTGCAGGTC	*URA3:GPD-RNH202* F
oKJ82	TCTGGTAAAATTATTAGTCGTTCTTCCCCCCCAATGTTGGAAACGGTCAT CATCGATGAATTCTCTGTCGTC	*URA3:GPD-RNH202* R
oKJ83	GGCCCGAAAATACAAGTGTGTACTAATACAGTAAGTAGGTCAAATACGCA CGTACGCTGCAGGTC	*LEU2:GPD-RNH203* F
oKJ84	GGCATGAAGCTCACGGTGTAAGCATCTAGATTCACGGCATCTTTGGTCAT CATCGATGAATTCTCTGTCGTC	*LEU2:GPD-RNH203* R
oKJ109	CACAGACGCGTTGAATTGTC	HygR-SSTR Amplification
oKJ110	GCCTCGAAACGTGAGTCTTT	HygR-SSTR Amplification
oKJ114	ATCTCTCTCAAACCTCTG	HygR-SSTR sequencing
oKJ115	GAGACTGTGTCGTCCATC	HygR-SSTR sequencing
oKJ116	ACATCAATTTGTAATGGAAAGGAAA	*HIR1*_A
oKJ117	TAATCGTTCTCAGTCCCAATAATGT	*HIR1*_D
oKJ118	CCATGATCTGCTTTTCTATCAGTTC	*HIR2*_A
oKJ119	AAGTATCCAGAAATCAATCACGAAG	*HIR2*_D
oKJ120	CATTCTACCACATATTGAACCATCA	*HIR3*_A
oKJ121	GGAGAAAAGTCCTTGGAGATTAAAG	*HIR3*_D
oKJ168	CCTGATCAACTTTCAAGGAAAACTA	*RPO21*A
oKJ169	ATCCAGTAATAGCTTACCACAGTGC	*RPO21*B
oKJ170	CCTCTCCAAACTATAGCCCTACTTC	*RPO21*C
oKJ171	TAAGCGGTAGTTCCACTCAATTTAC	*RPO21*D
oKJ172	GCAGTTACATTGTTCTGCTG	*RPO21* mutant colony PCR
oKJ173	AACGTGGATCAGGATCATAG	*RPO21* mutant colony PCR

Oligo	Sequence (5' to 3')	Use
oKJ174	CTGATCAACTTCGCTTGTTC	*RPO21* mutant sequencing
oKJ176	TGGGTTATTGGTCGGTAACGGTACCGCGTTGGTTCATGCGGGTCCAGCTG GACTACTTATCGGATCCCCGGGTTAATTAAG	*AGP1*-MXF_1 Integration of HygR-SSTR reporter at *AGP1* locus, HO
oKJ177	CTTCTTGCTTGATTAATTCTTCATCAAAGATTTGTCTATGAGAATCTAGG TCGATCTTGTGAATTCGAGCTCGTTTAAAC	*AGP1*-MXR_1 Integration of HygR-SSTR reporter at *AGP1* locus, HO
oKJ178	TGGGTTATTGGTCGGTAACGGTACCGCGTTGGTTCATGCGGGTCCAGCTG GACTACTTATGAATTCGAGCTCGTTTAAAC	*AGP1*-MXF_2 Integration of HygR-SSTR reporter at *AGP1* locus, CD
oKJ179	CTTCTTGCTTGATTAATTCTTCATCAAAGATTTGTCTATGAGAATCTAGG TCGATCTTCGGATCCCCGGGTTAATTAAG	*AGP1*-MXR_2 Integration of HygR-SSTR reporter at *AGP1* locus, CD
oAL39	GTTCTGCCCTTTGGCTGTGT	*RNH201*A
oAL40	TGCCAGCTTCATCGATACCC	*RNH201*B
oAL64	CAAGTTTGTCAAAAGCACG	*RNH202*A
oAL65	GCTCGATACGAGGTTTGG	*RNH202*B
oAL69	GAATCGCAGACCGATACC	*RNH203*A
oAL70	CTTCAGTTCCTTGCCACG	*RNH203*B
oBL29	CTGCAGCGAGGAGCCGTAAT	TEF promoter
oBL30	GAATCGCAGACCGATACC	TEF Terminator
oFB116	GACGCCTGCCAATGCTTTTG	*RNH201* promoter amplification
oFB117	CTGGATGCAGTTTACAGCAATGG	*RNH201* terminator ampflication
oNA144	GGGTAATACCTGCTGTAGTCTTCAA	*TOP1*A
oNA145	CACTGGTTCGGTCTTTATTTTCTTA	*TOP1*B
oNA146	GAGAAATTGAAAAATATCAGCGAAA	*TOP1*C
oNA147	GTATTTTTGCTTCCAAAACATCAAG	*TOP1*D

4.1.4. Buffers and Solutions

The buffers and solutions used in this study are summarized in Table 4. Standard molecular biology stock solutions (e.g. 1M Tris-HCl pH7.5, 0.5M EDTA pH 8.0, and 10N NaOH) were prepared according to established protocols and diluted to the working concentrations indicated. Only the working solutions directly used in experiments are listed below. All buffers were prepared with deionized water, pH-adjusted at room temperature, and sterilized by autoclaving or filtration as appropriate.

Table 4: Buffers and solutions prepared in this study

Buffer/Solution	Composition	Notes
1x Phosphate Buffered Saline (PBS)	137 mM NaCl 2.7 mM KCl 10 mM Na2HPO4 1.8 mM KH2PO4 adjusted to pH 7.4 with HCl, autoclaved	Diluted from 10x PBS Stock Solution; Prepared by IMB Media Lab Core Facility (MLCF)
1 x PBST	1x PBS 0.1% Tween-20	Diluted from 10x PBS Stock solution from IMB MLCF

Buffer/Solution	Composition	Notes
SDS running buffer	25mM Tris-HCl pH 7.5 glycine 0.1% SDS adjusted to pH 8.3, autoclaved	Diluted from 10x SDS Running Buffer Stock (IMB MLCF)
0.5x TBE running buffer	45mM Tris base 45mM boric acid 1mM EDTA pH 8.0	Diluted from 10x stock solution (IMB MLCF); Agarose Electrophoresis
1x TE	10mM Tris-HCl pH7.5 1mM EDTA pH 8.0	Diluted from 1M Tris-HCl pH 7.5 and 0.5M EDTA pH 8.0 (IMB MLCF)
Blocking buffer	5 % (w/v) skim milk powder in 1 x PBST	For blocking Western blots before antibody probe
Lithium Sorbitol Mix (LiSorb)	1M Sorbitol 1mM EDTA pH 8.0 10mM Tris-HCL buffer pH 8.0 100mM Lithium Acetate	Filter sterilized; used to make competent yeast cells for transformation with DNA
Lithium PEG Mix (LiPEG)	40% (w/v) PEG 3350 1mM EDTA pH8.0 10mM Tris-HCl pH 8.0 100mM Lithium Acetate	Filter sterilized; used to prepare competent yeast cells for transformation with DNA
NaOH/β-mercaptoethanol solution	1.09M β-mercaptoethanol 1.85M NaOH	Yeast Rapid Protein Extraction method solution 1
TCA solution	50% Trichloroacetic acid	Yeast Rapid Protein Extraction method solution 2
Acetone wash solution	100% Acetone	Yeast Rapid Protein Extraction method solution 3
Urea Loading Buffer	120 mM Tris-HCl pH 6.8 5 % glycerol 8 M urea 143 mM β-mercaptoethanol 8% SDS bromophenol blue	Used as a protein loading solution for Western blot analysis
DNA Loading Dye	60% glycerol in 1x TE ~ 0.025g of one of the following dyes: - Bromophenol Blue - Xylene cyanol - Orange G	Used for loading DNA for DNA electrophoresis
10% Potassium Hydroxide	10g KOH in 100ml H2O	Calcofluor White staining
0.02N NaOH	0.8g/L NaOH	Prepared by dilution of 10N NaOH stock solution

4.1.5. Media

4.1.5.1. Media Composition

The media used in this study are summarized in Table 5. Rich, defined, dropout, sporulation, and specialized induction media were prepared as indicated below. Selective dropout formulations (e.g., –Ura, –Arg) are described in Table 6, and antibiotic/counter-selection supplements are listed in Table 7. Sterilization of all media was carried out by autoclaving for 15 minutes at 121℃. After the autoclave step, an appropriate volume of sterilized 20% glucose, raffinose or galactose was added to the media.

Table 5: Media used in this study

Media	Component	Concentration
Luria Broth (LB) and Luria Agar (LA)	Bactopeptone Yeast Extract NaCl *For plates:* Agar	1% (w/v) 0.5% (w/v) 0.5% (w/v) 1.5% (w/v)
Yeast Peptone Dextrose (YPD) rich media	Yeast Extract Peptone Glucose *For plates:* Agar	1% (w/v) 2% (w/v) 2%(w/v) 2%(w/v)
Yeast Peptone Raffinose/Galactose Rich GAL induction media	Yeast Extract Peptone Raffinose Galactose	1% (w/v) 2% (w/v) 2%(w/v) 2%(w/v)
Complete synthetic media (CSM)	Yeast Nitrogen Base without Amino acids CSM Amino Acid Mixture Glucose *For plates:* Agar	6.7g/L Varies 2% (w/v) 2% (w/v)
Synthetic Defined (SD) minimal media	Yeast Nitrogen Base without Amino acids Amino acid mixture (see 1.1.5.2) Glucose *For plates:* Agar	6.7g/L Varies 2% (w/v) 2% (w/v)
Synthetic Defined (SD) minimal media with antibiotics	Yeast Nitrogen Base without Amino acids and with ammonium sulfate Amino acid mixture (see 1.1.5.2) Monosodium Glutamate Glucose *For plates:* Agar	1.7g/L Varies 1g/L 2% (w/v) 2% (w/v)

Media	Component	Concentration
Pre-sporulation (Pre-SPO) plates	Standard Nutrient broth Yeast Extract Glucose Agar	3% (w/v) 1% (w/v) 2% (w/v) 2% (w/v)
Sporulation (SPO) media	Potassium Acetate Zinc Acetate	1% (w/v) 0.0005% (w/v)
Fortified SDC medium (chronological lifespan)	Yeast Synthetic Dropout Medium Supplement without Histidine Yeast Nitrogen Base without Amino acids and with ammonium sulfate L-Methionine L-Histidine HCl L-Leucine Uracil Glucose	1.92g/L 6.7g/L 0.34g/L 0.34g/L 0.34g/L 0.34g/L 2%

4.1.5.2. Synthetic Dropout Mixture Compositions

Synthetic defined (SD) medium and Complete Supplement Mixture (CSM) was prepared using the commercially available SC mixture from MP Biomedicals. Selective dropout media were prepared using mixtures omitting one or more components of the SC mixture to allow positive selection for prototrophs.

Table 6 Components included in the Synthetic Complete mixture from MP Bio

Media	Composition	Final concentration (mg/L)
Synthetic Complete Mixture (MP Bio)	Adenine	21
	L-Alanine	86.5
	L-Arginine HCl	85.6
	L-Asparagine	85.6
	L-Aspartic Acid	85.6
	L-Cysteine HCl	85.6
	Glutamine	85.6
	L-Glutamic Acid	85.6
	Glycine	85.6
	L-Histidine HCl	85.6
	Myo-Inositol	85.6
	L-Isoleucine	85.6
	L-Leucine	85.6
	L-Lysine HCl	100
	L-Methionine	85.6
	Para-Aminobenzoic Acid	8.6
	L-Phenylalanine	85.6
	L-Proline	85.6
	L-Serine	85.6
	L-Threonine	85.6
	L-Tryptophan	85.6
	L-Tyrosine	85.6
	Uracil	85.6
	L-Valine	85.6
Complete Supplement Mixture (CSM)	Adenine	10
	L-Arginine HCl	50
	L-Aspartic Acid	80
	L-Histidine HCl	20
	L-Isoleucine	50
	L-Leucine	100
	L-Lysine HCl	50
	L-Methionine	20
	L-Phenylalanine	50
	L-Threonine	100
	L-Tryptophan	50
	Uracil	20
	L-Tyrosine	50
	L-Valine	140

4.1.5.3. Selective Agents and Antibiotics

For selection of bacterial and yeast transformants, antibiotics and counter-selection agents were added to rich or synthetic defined (SD) media at the final concentrations indicated in Table 7. Synthetic complete (SC) medium represents fully supplemented Synthetic Defined (SD) and selective dropout media (e.g., SD –Ura, SD –Leu) were prepared by omitting the relevant component(s). Antibiotics such as G418, ClonNat, and hygromycin B were used in both YPD and

SD-based media formulated for use with antibiotics (see Table 5), depending on the experimental context.

Table 7: Antibiotics added to media for positive selection of transformants

Antibiotic	**Organism**	**Media**	**Concentration in media (mg/L)**
Carbenicillin	*E. coli*	LB	100
Kanamycin	*E. coli*	LB	30
G418 disulfate	*S. cerevisiae*	YPD or SD	300 (general use) 1000 (fluctuation assays)
Nourseothricin-dihydrogen sulfate (ClonNat)	*S. cerevisiae*	YPD or SD	100
Hygromycin B	*S. cerevisiae*	YPD or SD	300
Canavanine	*S. cerevisiae*	CSM -Arg	60
5- fluoroorotic acid (5-FOA)	*S. cerevisiae*	SC low Ura	1000

4.1.6. Antibodies

Table 8: Antibodies used in this study.

Antibody	**Target**	**Host Species**	**Dilution**	**Supplier**
Primary Antibodies				
Anti-PAP	PAP (Peroxidase-Anti-Peroxidase-Soluble Complex; TAP tag)	Rabbit	1:3,000	Sigma Aldrich P1291
Anti-pGK	pGK phosphoglycerate kinase	Mouse	1:20,000	Invitrogen 459250
Anti-TOP1 #143	ScTop1 (linker, aa561-715) ID: 3052	Rabbit	1:3,000	EuroGenTec; custom antibody
Anti-TOP1 #144	ScTop1 (linker, aa561-715) ID: 3053	Rabbit	1:3,000	EuroGenTec; custom antibody
Anti-TOP1 #145	ScTop1(UC, aa143-360) ID: 3054	Rabbit	1:3,000	EuroGenTec; custom antibody
Anti-TOP1 #146	ScTop1(UC, aa143-360) ID: 3055	Rabbit	1:3,000	EuroGenTec; custom antibody
Secondary Antibodies				
Anti-Rabbit	Anti-Rabbit (GAR)-HRP Conjugate	Goat	1:3,000	BioRad 170-5046
Anti-Mouse	Goat Anti-Mouse (GAM)-HRP Conjugate	Goat	1:3,000	BioRad 170-5047

4.2. Methods

4.2.1. Bacterial Transformations

Chemically competent *Escherichia coli* DH5α cells were transformed using standard heat-shock protocols. Briefly, cells were thawed on ice and mixed with plasmid DNA, followed by incubation on ice for 15 minutes. Heat shock was performed at 42 °C for 30 s, after which cells were placed on ice for 2 minutes and then supplemented with 250 µl SOC medium. Cultures were incubated at 37°C with shaking at 250 rpm for 1 hour prior to plating 10–200 µl on pre-warmed selective LB plates.

For ampicillin resistance selection, a shortened protocol was used: competent cells were incubated with DNA on ice for 30 minutes and plated directly onto pre-warmed LB plates containing carbenicillin to reduce satellite colony growth.

Following transformation, plates were incubated at 37°C for approximately 16 hours. Positive transformants were verified by colony PCR, restriction digestion of isolated plasmid, and Sanger sequencing.

4.2.2. Yeast Cultures and Creating Yeast Strains

4.2.2.1. General Yeast Methods

All *Saccharomyces cerevisiae* strains used in this study are listed in Table 1. Cells were cultured using standard procedures. Unless otherwise stated, cells were grown in rich medium (YPD) at 30°C with shaking at 200 rpm. Selective or minimal defined media were used as appropriate, with recipes provided in Table 5-Table 7.

Diploid yeast strains were generated by mixing haploid yeast strains of opposite mating types on rich medium plates at 30˚C for 5-16 hours. Diploids were selected on double-selective plates when possible, or by picking zygotes using a Singer SporePlay micromanipulator. To obtain double mutant strains, meiosis was induced in heterozygous diploid strains in SPO media (see Table 5). Tetrads were digested with lyticase at room temperature for 15–30 minutes to weaken the ascus wall. Spores were plated on YPD and separated using a micromanipulator to isolate meiotic segregants. The resulting colonies were genotyped by replica plating onto selective media or by colony PCR, as appropriate for the expected genotypes.

For long-term storage, strains were maintained in 15% glycerol stocks at –80 °C. Fresh cultures were initiated from frozen stocks and grown on selective or non-selective plates prior to liquid culture inoculation.

4.2.2.2. Yeast Transformation

Yeast transformations were performed using a lithium acetate/PEG-based method with denatured carrier DNA. Competent cells were prepared by inoculating overnight cultures from single colonies in YPD medium and diluting to an OD_{600} of 0.15 in fresh medium. Cultures were grown at 30°C until reaching mid-log phase (OD_{600} 0.6–0.8). Cells were harvested by centrifugation, washed once in sterile water, and once in LiSorb solution (see Table 4), before resuspension in LiSorb supplemented with denatured salmon sperm DNA (Invitrogen UltraPure). Aliquots of competent cells were either used immediately or stored at –80°C.

For transformation, 50 µl of competent cells were mixed with DNA (5µl PCR product for cassette integration, 200ng digested plasmid, or 5ng circular plasmid DNA) and 300µl LiPEG solution. After a 15 minute incubation at room temperature, DMSO was added to 1%, and samples were incubated for 10 minutes at 42°C in a water bath. Following heat shock, cells were pelleted by centrifugation, resuspended in PBS. To recover transformants, cells were either plated on YPD medium for overnight outgrowth followed by replica plating (for antibiotic resistance selection), or plated directly on minimal defined medium lacking the appropriate nutrient (for auxotrophic selection).

4.2.2.3. Yeast Colony PCR

Yeast colony PCR was performed using a simple alkaline lysis method. A small amount of yeast cells from an isolated colony was resuspended in 20µl 0.02N sodium hydroxide. The cells were incubated at 100˚C for 10 minutes in a thermal cycler. The lysate was cooled on ice, diluted with 180µL sterile double distilled water and centrifuged briefly in a tabletop microcentrifuge to pellet cell debris. One microliter of the resultant supernatant was used as template in a 20-50µl PCR reaction with the Q5 DNA polymerase (New England Biolabs). If amplification was unsuccessful, the lysate was further diluted 1:10 and the PCR repeated. This method allows for rapid genotyping of yeast colonies.

4.2.2.4. Delitto Perfetto

Delitto Perfetto protocol was performed as described in (Storici *et al.*, 2019). The CORE cassette was amplified from the pSLG49 plasmid using oligos with 50 nucleotide overlap at the desired insertion location. The cassette was inserted so that the *KlURA3* gene was transcribed

in the opposite direction from the gene into which the cassette was inserted. The I-SceI site was inserted via PCR. The forward primer design was 5'-(50nt homology N-terminus of desired gene)- TTCGTACGCTGCAGGTCGAC-3'. The reverse primer was 5'-(50nt homology C-terminus of desired gene)- TAGGGATAACAGGGTAAT- CCGCGCGTTGGCCGATTCAT-3' where the sequence in blue denotes the I-SceI cut site. Standard procedure was used for yeast transformation with recovery on YPD agar plates for 16-24 hours before replica plating to YPD + Hygromycin B plates to select for positive transformants. Correct integration of the CORE cassette was confirmed by growth on media lacking uracil, and colony PCR confirmed integration at the desired locus.

The CORE cassette was then replaced using a repair cassette with the desired mutations. To this end, transformed yeast with the CORE cassette were grown for four hours in SC media containing 2% raffinose and 1% galactose to induce expression of the I-SceI nuclease, which catalyzed a DNA double-strand break at the inserted I-SceI cut site next to the cassette. Transformants were then selected on SC media containing 1g/L 5- fluoroороticacid (5-FOA) to select for yeast cells that have lost the *KlURA3* gene. Colonies that were not able to grow in the presence of Hygromycin B or in the absence of uracil in the media were subjected to yeast colony PCR followed by Sanger sequencing to ensure correct integration of the repair sequence.

4.2.3. Molecular and Biochemical Methods

4.2.3.1. Yeast Rapid Protein Extraction and Immunoblotting

Whole-cell yeast extracts were prepared using a rapid protein extraction protocol involving alkaline lysis, trichloroacetic acid precipitation, acetone wash, and solubilization in urea loading buffer. Equal amounts of protein were separated on pre-cast gradient SDS–PAGE gels (Bio-Rad) and transferred to nitrocellulose membranes using the Bio-Rad Trans-Blot Turbo transfer system according to the manufacturer's instructions. Membranes were blocked in 5% (w/v) milk in PBS containing 0.1% Tween-20 for 1 h at room temperature and incubated overnight at 4°C with primary antibodies diluted in blocking buffer. After four washes in PBST, membranes were incubated with HRP-conjugated secondary antibodies for 1 h at room temperature. Blots were developed using enhanced chemiluminescence (SuperSignal West Pico, Thermo Fisher) and imaged with a Bio-Rad ChemiDoc system. The antibodies used are listed in Table 8.

4.2.3.2. Custom Polyclonal Anti-Top1 Antibodies

Polyclonal antibodies against *S. cerevisiae* Top1 were generated in collaboration with Eurogentec (Liège, Belgium). Two purified, tag-free protein fragments corresponding to the upper clamp (UC, amino acids 143–360) and the linker region (amino acids 561–715) of Top1 were used as antigens. The cloning, recombinant protein production, and purification of these fragments were carried out by Martin Möckel at the Protein Production Core Facility (PPCF), Institute of Molecular Biology (IMB), Mainz. Two rabbits per antigen were immunized using Eurogentec's "Speedy 28-Day" polyclonal protocol with antigen supplied in solution (PBS + 5% glycerol, –80 °C storage). Sera was collected at multiple timepoints through the immunization process, but only the sera from the terminal bleed was tested in further experiments.

Antigen-specific IgG was purified by affinity chromatography using SulfoLink resin coupled to the respective antigen fragments, following the manufacturer's instructions. For each serum, 10 ml was applied to antigen-coupled columns, washed extensively, and eluted under acidic conditions before neutralization. Eluted antibodies were rebuffered into PBS with 10% glycerol and stored in aliquots at –80 °C. The final yields ranged from ~1–6 mg per rabbit, with working stocks maintained at 4 °C to avoid freeze–thaw cycles. These custom antibodies are listed in Table 8 as Anti-Top1 #143 to #146.

4.2.3.3. Drug Sensitivity and Spotting Assays

Growth sensitivity assays were performed using five-fold serial dilution spotting. Yeast strains were streaked to single colonies and grown overnight in liquid YPD at 30 °C with shaking. Over-night cultures were resuspended at 0.5 OD units in 200µl final volume using sterile water. Serial five-fold dilutions were prepared in sterile water in 96-well plates, and approximately 3–5 µl of each dilution was transferred to YPD control plates or YPD plates supplemented with camptothecin (CPT), hydroxyurea (HU), or other indicated drugs using a 48-pin replicator. Plates were air-dried before incubation at 30 °C for 2–3 days. Growth differences were assessed relative to the YPD control plate. Each assay was performed with at least two independent biological replicates, and representative plates are shown in the figures.

4.2.4. The 96-well format Fluctuation assays

4.2.4.1. Principle of Fluctuation Assays

Fluctuation assays measure mutation rates by exploiting the stochastic occurrence of rare mutational events across independent cultures. Because mutations arise randomly in timing and

frequency, multiple cultures are required to obtain accurate estimates and to account for "jackpot" events caused by early-arising mutations. This method was validated in this study by comparing mutation frequencies of wild-type and RNase H2-deficient cells using the well-characterized CAN1 reporter assay.

4.2.4.2. Reporter Selection

Mutation rates were measured using selectable reporter systems. The primary reporter was the HygR–SSTR(STOP):P2A:KanR construct integrated at the *AGP1* locus (Figure 22; Reijns *et al.*, 2022). Mutants were identified by growth on YPD plates containing G418. For proof-of-principle experiments, the CAN1 forward-mutation reporter was also used, with mutants selected on synthetic medium lacking arginine and supplemented with canavanine (60 µg/mL) (Takahashi *et al.*, 2011).

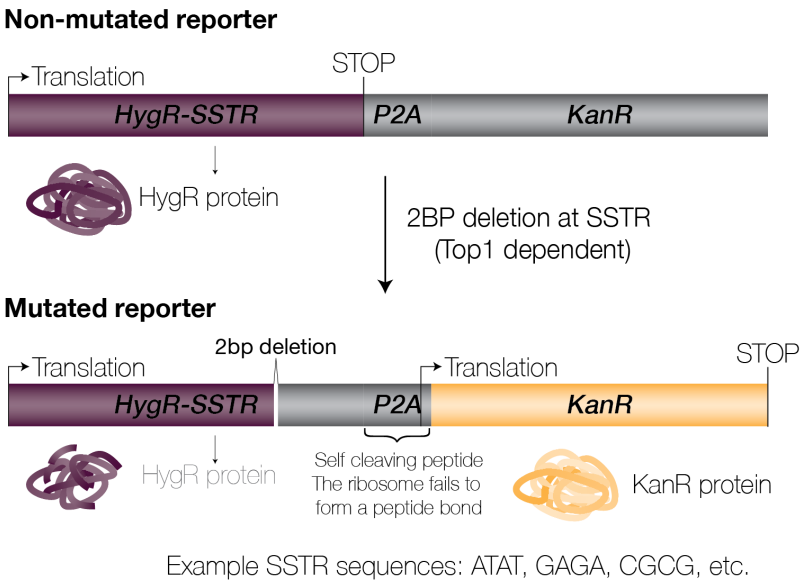

Figure 22 Schematic of the HygR-SSTR:P2A:KanR reporter system.

In the non-mutated reporter, translation begins at the HygR-SSTR open reading frame, terminating at the in-frame stop codon before the P2A peptide, resulting in the production of HygR protein. Upon a 2 bp deletion (typically caused by Top1 at an SSTR sequence), the reading frame shifts, leading to translation through the P2A self-cleaving peptide and into the downstream KanR sequence. This frameshift bypasses the upstream stop codon, allowing for KanR protein production. The Hygromycin resistance gene was modified to contain the maximum number of Top1 target sequences, SSTRs, which include for example ATAT, GAGA, and CGCG.

4.2.4.3. Experimental Design and Culture Conditions

During experimental design steps, one should consult the list of assumptions made by the mathematical model used to analyze the data and decide if the experiment violates any of those assumptions (Zheng, 2017). Due to the stochastic nature of mutation events, a large number of independent cultures (technical replicates) are required for each strain to obtain an accurate estimation of mutation rates (Figure 23). Each culture represents an independent population in which mutations can arise at different times and in different numbers, making it essential to analyze multiple replicates to account for natural variability.

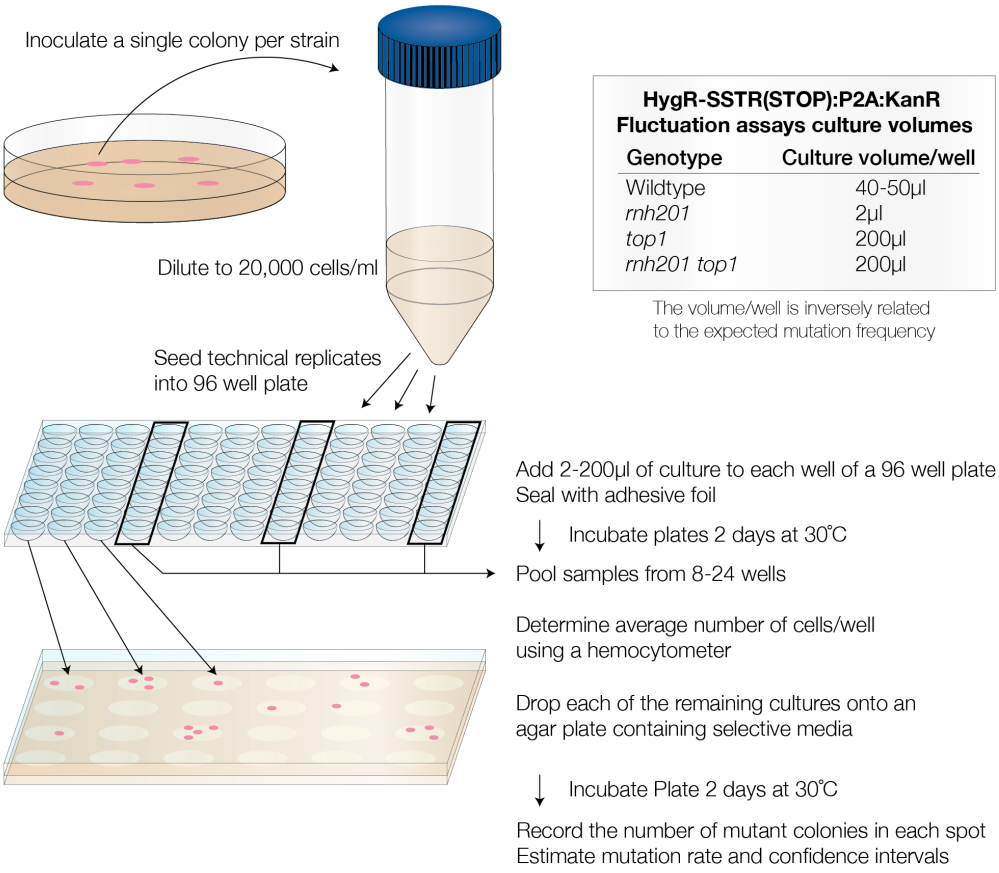

Figure 23: Workflow of 96-well plate fluctuation assay.

Independent cultures were established by diluting a single colony to 2 × 10^4 cells/mL and seeding 2–200 µl into wells of a 96-well plate, with culture volume adjusted according to strain genotype (e.g., wildtype, 40-50 µl; *rnh201*, 2 µl; *top1*, 200 µl; *rnh201 top1*, 200 µl). Plates were sealed with adhesive film and incubated at 30 °C for 2 days. To estimate the number of cell divisions, 8-24 wells were pooled and counted using a hemocytometer. The remaining wells were plated onto selective medium (YPD + G418 or SC –Arg + canavanine), and plates were incubated at 30 °C for 2 days before colonies were counted. Mutant counts were compiled for each replicate, and mutation rates with 95% confidence intervals were calculated using the Lea–Coulson maximum likelihood method implemented in rSalvador.

The culture volume was adjusted for different genetic backgrounds to ensure that the number of mutant colonies remained within a countable range. Ideally, culture conditions yielded zero mutant colonies in 20–80% of replicates (Lang, 2017). To determine suitable inoculum sizes and volumes, pilot assays were performed to estimate mutation frequency, and simulations were conducted using the `simu.cultures` function in the R package rSalvador. For wildtype and all mutants with mutation frequency similar to wildtype, 40-50µl cultures were used. For RNase H2 deficient cultures, 2µl cultures were used, and for *top1*, 200µl culture volume was used.

4.2.4.4. Plating and Estimating Number of Cell Divisions

To estimate the number of cell divisions, cultures were pooled (typically 24 wells per strain), diluted (50 µl into 950 µl sterile water, twice), and counted with a hemocytometer. For conditions with small culture volumes (e.g., RNase H2 deficient strains), sterile water was added to each well to achieve a 1:20 dilution, and the samples were pooled into two tubes for counting. The remaining wells were resuspended and plated onto selective medium. For the HygR–SSTR reporter, cultures were plated onto YPD containing G418 at 1 g/L; for the *CAN1* reporter, cultures were plated onto synthetic medium lacking arginine and supplemented with canavanine (60 µg/mL). Plates were incubated at 30 °C for 2 days before colonies were counted. Entire cultures were plated in droplets such that multiple replicates were on a single plate.

4.2.4.5. Data analysis

Mutant colony counts from individual cultures were compiled and analyzed in R using the package rSalvador (Zheng, 2017). Further details of statistical methods are provided in 4.2.8.

4.2.5. Replicative Aging Assays

Replicative lifespan (RLS) assays measure the number of daughter cells produced by an individual mother cell until cessation of division. Two complementary approaches were used: biotinylation-based purification of aged mother cells and microfluidics-based continuous monitoring of single mother cells.

4.2.5.1. Biotinylation Base Purification Assays

4.2.5.1.1. Experimental design considerations

The method for isolation of aged yeast cells was adapted from published protocols (Jin, Cao and Liu, 2021; Mojumdar *et al.*, 2022). Experimental design accounted for the number of aged cells required for downstream assays and the target age distribution (e.g., 5, 10, 15, and

20 bud scars). Because viability decreases with replicative age, initial culture sizes were chosen to exceed the desired final yield by ~50%. Pilot experiments were performed to optimize inoculation densities and ages obtained. For example, inoculation at 6.25×10^6 cells/ml limited growth to approximately five generations before reaching stationary phase at ~2×10^8 cells/ml. Cell density was determined by hemocytometer counts. Two purification methods were used depending on the number of aged cells required: tube magnet (small scale, Figure 24) or SuperMACS column (large scale).

4.2.5.1.2. Biotinylation of an unaged starting population

Log-phase cells were harvested from YPD cultures, washed three times with PBS (pH 7.4), and resuspended at 1×10^9 cells/ml in PBS + 5mg/ml EZ-Link™ Sulfo-NHS-LC biotin (Thermo Fisher, 21335). Cells were labeled for 30 min at room temperature with rotation. Cells were washed three times with PBS supplemented with 0.1 M glycine to quench unreacted biotin. Biotinylated cells were inoculated into fresh YPD and grown overnight at 25°C to allow aging to the desired bud scar distributio*n*

4.2.5.1.3. Small Scale Aged Yeast Purification (Tube Magnet)

Isolating of aged yeast population was adapted from (Jin, Cao and Liu, 2021). Briefly, biotinylated cultures were harvested, washed twice in ice-cold PBS (pH 7.4), and resuspended in 9 mL ice cold PBS. MagnaBind Streptavidin Beads (Thermo Fisher) were prepared at 0.1 mL per 5×10^8 mother cells, washed, and incubated with cells for 30 min at 4°C with gentle rotation. Bead-cell conjugates were collected using a tube magnet. Supernatants containing unbound daughter cells were removed, and bead-bound mother cells were washed four times with ice-cold PBS. Mother cells were retained for downstream applications, and daughters were collected separately.

Experimental planning example:
Number of cells/age: $1x10^8$ cells
Ages harvested: 5, 10, 15, 20bud scars
Total number of cells = $4x10^8$ cells + $4x10^8$ * 0.5 = **6 x 10^8 cells total**

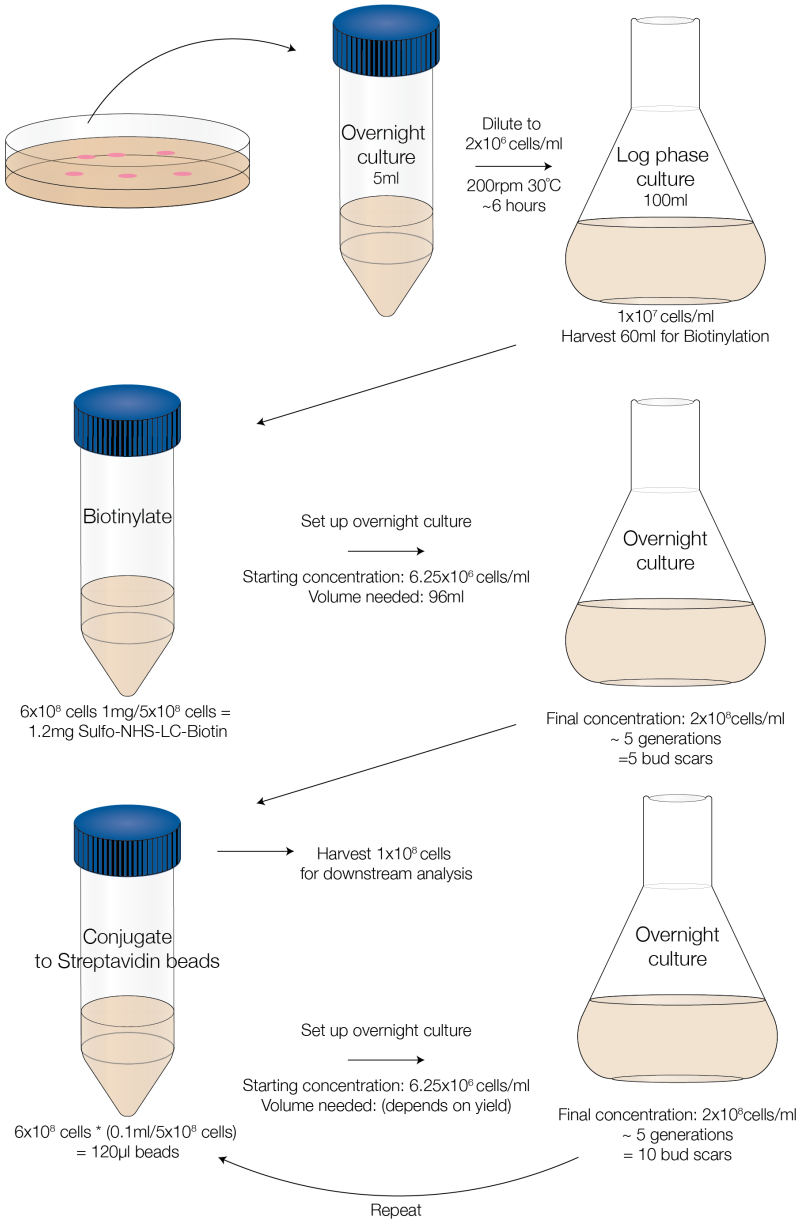

Figure 24: Example of experimental planning scheme for small scale aged yeast isolation.

4.2.5.1.4. Large-Scale Aged Yeast Purification with the SuperMACS II column

When >1 × 10^9 aged cells were required, purification was performed with a SuperMACS II system (Miltenyi Biotec) using anti-biotin microbeads (Miltenyi 130-041-202). Biotinylated cultures were harvested, washed in PBS, and incubated with anti-biotin microbeads (1 mL beads per 2.5 × 10^8 aged cells) for 30 min at 4 °C. The conjugated culture was loaded onto a pre-equilibrated XS column placed in a SuperMACS II magnet. Flow-through fractions containing daughter cells were collected, and bead-bound mother cells were retained in the column. After washing, mother cells were eluted in PBS and counted with a hemocytometer before use in downstream assays. Protocol adapted from (Mojumdar *et al.*, 2022).

4.2.5.1.5. Performing Fluctuation Assays using Aged Cells

To measure mutation rates in aged populations, 5 × 10^6 aged cells were seeded per well in 100 µl YPD (5 × 10^7 cells/mL). To suppress accumulation of reporter mutants during aging, cells were maintained in YPD containing 300 µg/mL Hygromycin until harvesting. Fluctuation assay plates were incubated at 30˚C for 24 hours, 8 cultures were pooled to estimate the number of cell divisions in each well. Entire cultures were plated onto YPD + 1 g/L G418 to determine mutation frequency as described in 4.2.4.

4.2.5.1.6. Determining Replicative Age With Calcofluor White Staining

Bud scar counts were determined by staining with calcofluor white. Approximately 5 × 10^7 cells were harvested, resuspended in 3 µl PBS, and mixed with 3 µl calcofluor white and 3 µl 10% KOH. Cells were mounted under a coverslip and imaged on a Zeiss LSM900 using DAPI filters. Bud scars were manually counted from at least 60 cells per sample.

4.2.5.2. Microfluidics-Based Replicative Aging (Charvin Platform)

RLS was measured using a microfluidic device that traps mother cells and continuously flushes away daughters, as described for the Charvin laboratory platform (Aspert, Hentsch and Charvin, 2022). Briefly, *S. cerevisiae* cultures were loaded into microfabricated traps connected to a constant media flow and maintained at 30 °C on an inverted microscope with automated stage control. Time-lapse images were acquired at fixed intervals to capture successive budding events throughout each mother cell's lifespan. Mothers were tracked until cessation of budding; cells lost from traps or otherwise unscorable were censored at the time of loss. Experimental handling and imaging logic followed the DetecDiv pipeline and hardware/geometry principles, which combines mother-cell retention traps with automated deep-learning analysis for division counting (Aspert, Hentsch and Charvin, 2022).

Experiments were performed in collaboration with the Charvin lab team by A. Maliavko using their established device and analysis workflow.

4.2.6. Chronological Lifespan (CLS) Assays

4.2.6.1. Yeast Culture Information

CLS was measured in fortified SDC medium (Leu/Met/His/Ura supplemented; recipe in Table 5) using batch cultures maintained in stationary phase. Overnight precultures were started from single colonies in YPD at 30 °C with shaking (200 rpm). The next day, cultures were diluted to OD_{600} = 0.1 in 5 mL fortified SDC in bioreactor tubes and incubated at 30 °C, 200 rpm. At indicated time points, viability was assayed by Sytox Green staining and flow cytometry; tube weight was monitored daily and sterile water was added as needed to compensate evaporation.

4.2.6.2. Sytox Green Staining for Cell Viability

For each sample, 0.8 OD units (~1 × 10^7 cells) were harvested by centrifugation, supernatant removed, and cells resuspended in 1 mL 50 mM Tris (pH 7.4) containing 0.5 µM Sytox Green (1:10,000 from a 5 mM DMSO stock). Samples were protected from light and analyzed immediately by flow cytometry using a NovoCyte Quanteon flow cytometer (Agilent, USA). Gating controls included unstained cells (background) and heat-killed cells (95 °C, 10 min) to define the Sytox-positive population.

Viability was reported as the percentage of Sytox-negative (live) cells at each time point. Four independent biological replicates were analyzed per strain. Statistical tests are described in the Statistical Analysis section.

4.2.7. *C. elegans* Lifespan Assays

C. elegans strains were obtained from the Caenorhabditis Genetics Center (funded by NIH Office of Research Infrastructure Programs, P40 OD010440) and maintained on OP50 bacteria at 20°C under standard conditions. The Bristol strain N2 was used as wild type. The following strains were used for lifespan analysis: rnh-2 (rnh-2(iow18) II), top-1::degron (top-1(ers56[top-1::degron::GFP]) I; ieSi57 II [eft-3p::TIR1::mRuby::unc-54 3′UTR + Cbr-unc-119(+)] II), and top-1::degron;rnh-2 (top-1(ers56[top-1::degron::GFP]) I; ieSi57 [eft-3p::TIR1::mRuby::unc-54 3′UTR + Cbr-unc-119(+)] II; rnh-2(iow18) II). The rnh-2 mutant was generated by crossing strain SSM422 (rnh-2(iow18); rnh-1.0(iow66)II/mIn1[mIs14 dpy-10(e128)] II) with N2, and the top-1::degron;rnh-2 double mutant was generated by crossing ERC84 (top-1::degron) with rnh-2.

Synchronized populations were obtained by bleaching gravid adults, and embryos were hatched overnight in M9 buffer at 20°C to arrest at the L1 stage. L1 larvae were transferred to NGM plates seeded with OP50 for 36–42 h until the young adult stage (day 0 of lifespan analysis). For each strain and condition, 9–15 young adults were transferred into each well of a 12-well plate containing 1mL NGM supplemented with 5-fluoro-2′-deoxyuridine (FUdR) at a final concentration of 50μM to prevent progeny production. Treatment plates additionally contained 50μM indole-3-acetic acid (IAA, auxin) dissolved in ethanol; control plates contained an equivalent volume of ethanol (final concentration 1.8%). Both auxin and control plates were seeded with OP50 grown overnight in LB.

Lifespan was monitored every 2–3 days by scoring movement under a stereomicroscope. Worms that failed to respond to gentle prodding were scored as dead; animals that crawled off the plate were censored from the analysis. Survival curves were generated using the Kaplan–Meier method, and statistical comparisons were performed with log-rank tests (see Statistical Analysis section).

4.2.8. Statistical Analysis

4.2.8.1. Fluctuation Rate, Confidence Interval and Significance Evaluation

Statistical analyses were performed using R. Mutation rates from fluctuation assays were estimated using the Lea–Coulson maximum likelihood method (Lea and Coulson, 1949), implemented in the R package rSalvador (Zheng, 2017). This method models the distribution of mutant counts across independent cultures according to the Luria-Delbrück distribution (Luria and Delbrück, 1943), which accounts for the fact that mutations can occur at different times during culture growth, producing a highly skewed distribution of mutant numbers. Estimates were obtained using the functions `newton.LD` or `newton.LD.plating`, depending on the plating strategy (Zheng, 2017). These functions apply Newton-Raphson iteration to numerically identify the mutation rate that maximizes the likelihood of the observed data. The mutation rate estimates were normalized to the estimated number of cell divisions in each sample. Ninety-five percent confidence intervals were calculated using the likelihood ratio method using the functions `confint.LD` or `confint.LD.plating` in rSalvador and were also normalized to the estimated number of cell divisions per sample. Pairwise comparisons of mutation rates between strains or conditions were performed using the likelihood ratio test (LRT.LD) in rSalvador. Most assays were carried out under conditions in which the starting cell number (N_0) was far less than

the final cell number (N_t), however, in cases where cultures were inoculated with a relatively high number of cells, the parameter $\phi = 1 - N_0 / N_t$ was used to account for the finite starting population size.

4.2.8.2. Other statistical methods

For chronological lifespan experiments, survival data (percentage of Sytox-negative cells) were compared using one-way ANOVA with Tukey's post hoc test for multiple comparisons. Replicative lifespan assays in yeast (microfluidics) and *C. elegans* lifespan assays were analyzed using Kaplan-Meier survival estimation, and differences between strains or conditions were assessed with log-rank (Mantel-Cox) tests

.

5. References

1) Aditi *et al.* (2021) “Genome instability independent of type I interferon signaling drives neuropathology caused by impaired ribonucleotide excision repair,” *Neuron*, 109(24), pp. 3962-3979.e6. Available at: https://doi.org/10.1016/j.neuron.2021.09.040.

2) Agapov, A., Olina, A. and Kulbachinskiy, A. (2022) “RNA polymerase pausing, stalling and bypass during transcription of damaged DNA: from molecular basis to functional consequences,” *Nucleic Acids Research*, 50(6), pp. 3018–3041. Available at: https://doi.org/10.1093/nar/gkac174.

3) Aicardi, J. and Goutières, F. (1984) “A Progressive familial encephalopathy in infancy with calcifications of the basal ganglia and chronic cerebrospinal fluid lymphocytosis,” *Annals of Neurology*, 15(1), pp. 49–54. Available at: https://doi.org/10.1002/ana.410150109.

4) Alberts, B. *et al.* (2007) *Molecular biology of the Cell*. 5th Edition. New York, NY: Garland Science.

5) Armstrong, G.T. *et al.* (2014) “Aging and Risk of Severe, Disabling, Life-Threatening, and Fatal Events in the Childhood Cancer Survivor Study,” *Journal of Clinical Oncology*, 32(12), pp. 1218–1227. Available at: https://doi.org/10.1200/JCO.2013.51.1055.

6) Arudchandran, A. *et al.* (2000) “The absence of ribonuclease H1 or H2 alters the sensitivity of Saccharomyces cerevisiae to hydroxyurea, caffeine and ethyl methanesulphonate: implications for roles of RNases H in DNA replication and repair,” *Genes to Cells*, 5(10), pp. 789–802. Available at: https://doi.org/10.1046/j.1365-2443.2000.00373.x.

7) Aspert, T., Hentsch, D. and Charvin, G. (2022) “DetecDiv, a generalist deep-learning platform for automated cell division tracking and survival analysis,” *eLife*, 11, p. e79519. Available at: https://doi.org/10.7554/eLife.79519.

8) Barbari, S.R. and Shcherbakova, P.V. (2017) “Replicative DNA polymerase defects in human cancers: Consequences, mechanisms, and implications for therapy,” *DNA Repair*, 56, pp. 16–25. Available at: https://doi.org/10.1016/j.dnarep.2017.06.003.

9) Berben, L. *et al.* (2021) “Cancer and Aging: Two Tightly Interconnected Biological Processes,” *Cancers*, 13(6), p. 1400. Available at: https://doi.org/10.3390/cancers13061400.

10) Bernhard, D. *et al.* (2007) “Cigarette smoke – an aging accelerator?,” *Experimental Gerontology*, 42(3), pp. 160–165. Available at: https://doi.org/10.1016/j.exger.2006.09.016.

11) Brown, J.A. and Suo, Z. (2011) “Unlocking the Sugar ‘Steric Gate’ of DNA Polymerases,” *Biochemistry*, 50(7), pp. 1135–1142. Available at: https://doi.org/10.1021/bi101915z.

12) Burgess, S.M., Powers, T. and Mell, J.C. (2017) “Budding Yeast *S accharomyces Cerevisiae* as a Model Genetic Organism,” in Wiley, *Encyclopedia of Life Sciences*. 1st ed. Wiley, pp. 1–12. Available at: https://doi.org/10.1002/9780470015902.a0000821.pub2.

13) Cagan, A. *et al.* (2022) “Somatic mutation rates scale with lifespan across mammals,” *Nature*, 604(7906), pp. 517–524. Available at: https://doi.org/10.1038/s41586-022-04618-z.

14) Cerritelli, S.M. and Crouch, R.J. (2019) “RNase H2-RED carpets the path to eukaryotic RNase H2 functions,” *DNA Repair*, 84, p. 102736. Available at: https://doi.org/10.1016/j.dnarep.2019.102736.

15) Cerritelli, S.M. and El Hage, A. (2020) “RNases H1 and H2: guardians of the stability of the nuclear genome when supply of dNTPs is limiting for DNA synthesis,” *Current Genetics*, 66(6), pp. 1073–1084. Available at: https://doi.org/10.1007/s00294-020-01086-8.

16) Champoux, J.J. (2001) “DNA Topoisomerases: Structure, Function, and Mechanism,” *Annual Review of Biochemistry*, 70(1), pp. 369–413. Available at: https://doi.org/10.1146/annurev.biochem.70.1.369.

17) Chatsirisupachai, K. and De Magalhães, J.P. (2024) “Somatic mutations in human ageing: New insights from DNA sequencing and inherited mutations,” *Ageing Research Reviews*, 96, p. 102268. Available at: https://doi.org/10.1016/j.arr.2024.102268.

18) Cho, J.-E. *et al.* (2013) “Two distinct mechanisms of Topoisomerase 1-dependent mutagenesis in yeast,” *DNA Repair*, 12(3), pp. 205–211. Available at: https://doi.org/10.1016/j.dnarep.2012.12.004.

19) Cho, J.-E., Kim, N. and Jinks-Robertson, S. (2015) “Topoisomerase 1-dependent deletions initiated by incision at ribonucleotides are biased to the non-transcribed strand of a highly activated reporter,” *Nucleic Acids Research*, 43(19), pp. 9306–9313. Available at: https://doi.org/10.1093/nar/gkv824.

20) Clausen, A.R. *et al.* (2013) “Ribonucleotide incorporation, proofreading and bypass by human DNA polymerase δ,” *DNA Repair*, 12(2), pp. 121–127. Available at: https://doi.org/10.1016/j.dnarep.2012.11.006.

21) Crossley, M.P. *et al.* (2023) “R-loop-derived cytoplasmic RNA–DNA hybrids activate an immune response,” *Nature*, 613(7942), pp. 187–194. Available at: https://doi.org/10.1038/s41586-022-05545-9.

22) Crow, Y.J., Leitch, A., *et al.* (2006) “Mutations in genes encoding ribonuclease H2 subunits cause Aicardi-Goutières syndrome and mimic congenital viral brain infection,” *Nature Genetics*, 38(8), pp. 910–916. Available at: https://doi.org/10.1038/ng1842.

23) Crow, Y.J., Hayward, B.E., *et al.* (2006) “Mutations in the gene encoding the 3′-5′ DNA exonuclease TREX1 cause Aicardi-Goutières syndrome at the AGS1 locus,” *Nature Genetics*, 38(8), pp. 917–920. Available at: https://doi.org/10.1038/ng1845.

24) Crow, Y.J. and Stetson, D.B. (2022) “The type I interferonopathies: 10 years on,” *Nature Reviews Immunology*, 22(8), pp. 471–483. Available at: https://doi.org/10.1038/s41577-021-00633-9.

25) Debès, C. *et al.* (2023) “Ageing-associated changes in transcriptional elongation influence longevity,” *Nature*, 616(7958), pp. 814–821. Available at: https://doi.org/10.1038/s41586-023-05922-y.

26) DeGregori, J. *et al.* (1997) “Distinct roles for E2F proteins in cell growth control and apoptosis,” *Proceedings of the National Academy of Sciences*, 94(14), pp. 7245–7250. Available at: https://doi.org/10.1073/pnas.94.14.7245.

27) DeRose, E.F. *et al.* (2012) “Solution Structure of the Dickerson DNA Dodecamer Containing a Single Ribonucleotide,” *Biochemistry*, 51(12), pp. 2407–2416. Available at: https://doi.org/10.1021/bi201710q.

28) Dunn, K. and Griffith, J.D. (1980) “The presence of RNA in a double helix inhibits its interaction with histone protein,” *Nucleic Acids Research*, 8(3), pp. 555–566. Available at: https://doi.org/10.1093/nar/8.3.555.

29) Egli, M., Usman, N. and Rich, A. (1993) “Conformational influence of the ribose 2’-hydroxyl group: Crystal structures of DNA-RNA chimeric duplexes,” *Biochemistry*, 32(13), pp. 3221–3237.

30) Evdokimov, A. *et al.* (2018) “Naked mole rat cells display more efficient excision repair than mouse cells,” *Aging*, 10(6), pp. 1454–1473. Available at: https://doi.org/10.18632/aging.101482.

31) Feser, J. *et al.* (2010) “Elevated Histone Expression Promotes Life Span Extension,” *Molecular Cell*, 39(5), pp. 724–735. Available at: https://doi.org/10.1016/j.molcel.2010.08.015.

32) Frick, D.N. and Richardson, C.C. (2001) “DNA Primases,” *Annual Review of Biochemistry*, 70(1), pp. 39–80. Available at: https://doi.org/10.1146/annurev.biochem.70.1.39.

33) Geisberg, J.V., Moqtaderi, Z. and Struhl, K. (2020) “The transcriptional elongation rate regulates alternative polyadenylation in yeast,” *eLife*, 9, p. e59810. Available at: https://doi.org/10.7554/eLife.59810.

34) Göksenin, A.Y. *et al.* (2012) “Human DNA Polymerase ϵ Is Able to Efficiently Extend from Multiple Consecutive Ribonucleotides,” *Journal of Biological Chemistry*, 287(51), pp. 42675–42684. Available at: https://doi.org/10.1074/jbc.M112.422733.

35) Gonzaga, E.R. (2009) “Role of UV Light in Photodamage, Skin Aging, and Skin Cancer: Importance of Photoprotection,” *American Journal of Clinical Dermatology*, 10(Supplement 1), pp. 19–24. Available at: https://doi.org/10.2165/0128071-200910001-00004.

36) Goutières, F. (2005) “Aicardi–Goutières syndrome,” *Brain and Development*, 27(3), pp. 201–206. Available at: https://doi.org/10.1016/j.braindev.2003.12.011.

37) Günther, C. *et al.* (2015) “Defective removal of ribonucleotides from DNA promotes systemic autoimmunity,” *Journal of Clinical Investigation*, 125(1), pp. 413–424. Available at: https://doi.org/10.1172/JCI78001.

38) Hendler, A. *et al.* (2018) “The evolution of a G1/S transcriptional network in yeasts,” *Current Genetics*, 64(1), pp. 81–86. Available at: https://doi.org/10.1007/s00294-017-0726-3.

39) Hiller, B. *et al.* (2018) “Ribonucleotide Excision Repair Is Essential to Prevent Squamous Cell Carcinoma of the Skin,” *Cancer Research*, 78(20), pp. 5917–5926. Available at: https://doi.org/10.1158/0008-5472.CAN-18-1099.

40) Hovatter, K.R. and Martinson, H.G. (1987) “Ribonucleotide-induced helical alteration in DNA prevents nucleosome formation.,” *Proceedings of the National Academy of Sciences*, 84(5), pp. 1162–1166. Available at: https://doi.org/10.1073/pnas.84.5.1162.

41) Jin, X., Cao, X. and Liu, B. (2021) “Isolation of Aged Yeast Cells Using Biotin-Streptavidin Affinity Purification,” *Methods in Molecular Biology*, 2196, pp. 223–228. Available at: https://doi.org/10.1007/978-1-0716-0868-5_17.

42) Kaeberlein, M., McVey, M. and Guarente, L. (1999) “The SIR2/3/4 complex and SIR2 alone promote longevity in Saccharomyces cerevisiae by two different mechanisms,” *Genes & Development*, 13(19), pp. 2570–2580. Available at: https://doi.org/10.1101/gad.13.19.2570.

43) Kellner, V. and Luke, B. (2020) “Molecular and physiological consequences of faulty eukaryotic ribonucleotide excision repair,” *The EMBO Journal*, 39(3), p. e102309. Available at: https://doi.org/10.15252/embj.2019102309.

44) Kennedy, B.K. *et al.* (1995) “Mutation in the Silencing Gene SIR4 Can Delay Aging in S. cerevisiae.”

45) Kim, N. *et al.* (2011) “Mutagenic Processing of Ribonucleotides in DNA by Yeast Topoisomerase I,” *Science*, 332(6037), pp. 1561–1564. Available at: https://doi.org/10.1126/science.1205016.

46) Kipps, T.J. *et al.* (2017) “Chronic lymphocytic leukaemia,” *Nature Reviews Disease Primers*, 3(1), p. 16096. Available at: https://doi.org/10.1038/nrdp.2016.96.

47) Kunkel, T.A. and Bebenek, K. (2000) “DNA REPLICATION FIDELITY.”

48) Lang, G.I. (2017) “Measuring Mutation Rates Using the Luria-Delbrück Fluctuation Assay,” *Methods in Molecular Biology*, 1672, pp. 21–31. Available at: https://doi.org/10.1007/978-1-4939-7306-4_3.

49) Lea, D.E. and Coulson, C.A. (1949) “The distribution of the numbers of mutants in bacterial populations,” *Journal of Genetics*, 49(3), p. 264. Available at: https://doi.org/10.1007/bf02986080.

50) Lee, M.B. *et al.* (2019) “Defining the impact of mutation accumulation on replicative lifespan in yeast using cancer-associated mutator phenotypes,” *Proceedings of the National*

Academy of Sciences, 116(8), pp. 3062–3071. Available at: https://doi.org/10.1073/pnas.1815966116.

51) Lessel, D. *et al.* (2014) "Mutations in SPRTN cause early onset hepatocellular carcinoma, genomic instability and progeroid features," *Nature Genetics*, 46(11), pp. 1239–1244. Available at: https://doi.org/10.1038/ng.3103.

52) Li, X. *et al.* (2023) "Inflammation and aging: signaling pathways and intervention therapies," *Signal Transduction and Targeted Therapy*, 8(1), p. 239. Available at: https://doi.org/10.1038/s41392-023-01502-8.

53) Li, Y. and Breaker, R.R. (1999) "Kinetics of RNA Degradation by Specific Base Catalysis of Transesterification Involving the 2'-Hydroxyl Group," *Journal of the American Chemical Society*, 121(23), pp. 5364–5372. Available at: https://doi.org/10.1021/ja990592p.

54) Lippert, M.J. *et al.* (2011) "Role for topoisomerase 1 in transcription-associated mutagenesis in yeast," *Proceedings of the National Academy of Sciences*, 108(2), pp. 698–703. Available at: https://doi.org/10.1073/pnas.1012363108.

55) Lippuner, A.D., Julou, T. and Barral, Y. (2014) "Budding yeast as a model organism to study the effects of age," *FEMS Microbiology Reviews*, 38(2), pp. 300–325. Available at: https://doi.org/10.1111/1574-6976.12060.

56) Lockhart, A. *et al.* (2019) "RNase H1 and H2 Are Differentially Regulated to Process RNA-DNA Hybrids," *Cell Reports*, 29(9), pp. 2890-2900.e5. Available at: https://doi.org/10.1016/j.celrep.2019.10.108.

57) Longo, V.D. *et al.* (2012) "Replicative and Chronological Aging in Saccharomyces cerevisiae," *Cell Metabolism*, 16(1), pp. 18–31. Available at: https://doi.org/10.1016/j.cmet.2012.06.002.

58) Longo, V.D., Mitteldorf, J. and Skulachev, V.P. (2005) "Programmed and altruistic ageing," *Nature Reviews Genetics*, 6(11), pp. 866–872. Available at: https://doi.org/10.1038/nrg1706.

59) López-Otín, C. *et al.* (2013) "The Hallmarks of Aging," *Cell*, 153(6), pp. 1194–1217. Available at: https://doi.org/10.1016/j.cell.2013.05.039.

60) López-Otín, C. *et al.* (2023) "Hallmarks of aging: An expanding universe," *Cell*, 186(2), pp. 243–278. Available at: https://doi.org/10.1016/j.cell.2022.11.001.

61) Lubberts, S. *et al.* (2020) "Early ageing after cytotoxic treatment for testicular cancer and cellular senescence: Time to act," *Critical Reviews in Oncology/Hematology*, 151, p. 102963. Available at: https://doi.org/10.1016/j.critrevonc.2020.102963.

62) Lujan, S.A., Williams, J.S. and Kunkel, T.A. (2016) "DNA Polymerases Divide the Labor of Genome Replication," *Trends in Cell Biology*, 26(9), pp. 640–654. Available at: https://doi.org/10.1016/j.tcb.2016.04.012.

63) Luke, A.M. *et al.* (2010) “Accumulation of true single strand breaks and AP sites in base excision repair deficient cells,” *Mutation Research/Fundamental and Molecular Mechanisms of Mutagenesis*, 694(1–2), pp. 65–71. Available at: https://doi.org/10.1016/j.mrfmmm.2010.08.008.

64) Luquette, L.J. *et al.* (2022) “Single-cell genome sequencing of human neurons identifies somatic point mutation and indel enrichment in regulatory elements,” *Nature Genetics*, 54(10), pp. 1564–1571. Available at: https://doi.org/10.1038/s41588-022-01180-2.

65) Luria, S.E. and Delbrück, M. (1943) “MUTATIONS OF BACTERIA FROM VIRUS SENSITIVITY TO VIRUS RESISTANCE,” *Genetics*, 28(6), pp. 491–511. Available at: https://doi.org/10.1093/genetics/28.6.491.

66) Mangerich, A. *et al.* (2010) “Inflammatory and age-related pathologies in mice with ectopic expression of human PARP-1,” *Mechanisms of Ageing and Development*, 131(6), pp. 389–404. Available at: https://doi.org/10.1016/j.mad.2010.05.005.

67) Mojumdar, A. *et al.* (2022) “Changes in DNA double-strand break repair during aging correlate with an increase in genomic mutations,” *Journal of Molecular Biology*, 434(20), p. 167798. Available at: https://doi.org/10.1016/j.jmb.2022.167798.

68) Molon, M. and Zadrag-Tecza, R. (2016) “Effect of temperature on replicative aging of the budding yeast Saccharomyces cerevisiae,” *Biogerontology*, 17(2), pp. 347–357. Available at: https://doi.org/10.1007/s10522-015-9619-3.

69) Nick McElhinny, S.A., Watts, B.E., *et al.* (2010) “Abundant ribonucleotide incorporation into DNA by yeast replicative polymerases,” *Proceedings of the National Academy of Sciences*, 107(11), pp. 4949–4954. Available at: https://doi.org/10.1073/pnas.0914857107.

70) Nick McElhinny, S.A., Kumar, D., *et al.* (2010) “Genome instability due to ribonucleotide incorporation into DNA,” *Nature Chemical Biology*, 6(10), pp. 774–781. Available at: https://doi.org/10.1038/nchembio.424.

71) Niedernhofer, L.J. *et al.* (2018) “Nuclear Genomic Instability and Aging,” *Annual Review of Biochemistry*, 87(1), pp. 295–322. Available at: https://doi.org/10.1146/annurev-biochem-062917-012239.

72) Niu, H. *et al.* (2016) “Roles of DNA helicases and Exo1 in the avoidance of mutations induced by Top1-mediated cleavage at ribonucleotides in DNA,” *Cell Cycle*, 15(3), pp. 331–336. Available at: https://doi.org/10.1080/15384101.2015.1128594.

73) Novarina, D. *et al.* (2022) “High-throughput replica-pinning approach to screen for yeast genes controlling low-frequency events,” *STAR Protocols*, 3(1), p. 101082. Available at: https://doi.org/10.1016/j.xpro.2021.101082.

74) Parkash, V. *et al.* (2023) “A sensor complements the steric gate when DNA polymerase ϵ discriminates ribonucleotides,” *Nucleic Acids Research*, 51(20), pp. 11225–11238. Available at: https://doi.org/10.1093/nar/gkad817.

75) Pascual-Torner, M. *et al.* (2022) “Comparative genomics of mortal and immortal cnidarians unveils novel keys behind rejuvenation,” *Proceedings of the National Academy of Sciences*, 119(36), p. e2118763119. Available at: https://doi.org/10.1073/pnas.2118763119.

76) Pavlov, Y.I., Shcherbakova, P.V. and Kunkel, T.A. (2001) “In Vivo Consequences of Putative Active Site Mutations in Yeast DNA Polymerases alpha, epsilon, delta and zeta,” *Genetics*, 159(1), pp. 47–64. Available at: https://doi.org/10.1093/genetics/159.1.47.

77) Petermann, E., Lan, L. and Zou, L. (2022) “Sources, resolution and physiological relevance of R-loops and RNA–DNA hybrids,” *Nature Reviews Molecular Cell Biology*, 23(8), pp. 521–540. Available at: https://doi.org/10.1038/s41580-022-00474-x.

78) Pommier, Y. *et al.* (2016) “Roles of eukaryotic topoisomerases in transcription, replication and genomic stability,” *Nature Reviews Molecular Cell Biology*, 17(11), pp. 703–721. Available at: https://doi.org/10.1038/nrm.2016.111.

79) Pommier, Y. *et al.* (2022) “Human topoisomerases and their roles in genome stability and organization,” *Nature Reviews Molecular Cell Biology*, 23(6), pp. 407–427. Available at: https://doi.org/10.1038/s41580-022-00452-3.

80) Rando, T.A. (2007) “The Immortal Strand Hypothesis: Segregation and Reconstruction,” *Cell*, 129(7), pp. 1239–1243. Available at: https://doi.org/10.1016/j.cell.2007.06.019.

81) Reijns, M.A.M. *et al.* (2012) “Enzymatic Removal of Ribonucleotides from DNA Is Essential for Mammalian Genome Integrity and Development,” *Cell*, 149(5), pp. 1008–1022. Available at: https://doi.org/10.1016/j.cell.2012.04.011.

82) Reijns, M.A.M. *et al.* (2022) “Signatures of TOP1 transcription-associated mutagenesis in cancer and germline,” *Nature*, 602(7898), pp. 623–631. Available at: https://doi.org/10.1038/s41586-022-04403-y.

83) Richardson, R.B. (2009) “Ionizing radiation and aging: rejuvenating an old idea,” *Aging*, 1(11), pp. 887–902. Available at: https://doi.org/10.18632/aging.100081.

84) Robinson, P.S. *et al.* (2021) “Increased somatic mutation burdens in normal human cells due to defective DNA polymerases,” *Nature Genetics*, 53(10), pp. 1434–1442. Available at: https://doi.org/10.1038/s41588-021-00930-y.

85) Rychlik, M.P. *et al.* (2010) “Crystal Structures of RNase H2 in Complex with Nucleic Acid Reveal the Mechanism of RNA-DNA Junction Recognition and Cleavage,” *Molecular Cell*, 40(4), pp. 658–670. Available at: https://doi.org/10.1016/j.molcel.2010.11.001.

86) Schindler, N. *et al.* (2023) “Genetic requirements for repair of lesions caused by single genomic ribonucleotides in S phase,” *Nature Communications*, 14(1), p. 1227. Available at: https://doi.org/10.1038/s41467-023-36866-6.

87) Schumacher, B. *et al.* (2021) “The central role of DNA damage in the ageing process,” *Nature*, 592(7856), pp. 695–703. Available at: https://doi.org/10.1038/s41586-021-03307-7.

88) Sekiguchi, J. and Shuman, S. (1997) “Site-Specific Ribonuclease Activity of Eukaryotic DNA Topoisomerase I,” *Molecular Cell*, 1(1), pp. 89–97. Available at: https://doi.org/10.1016/S1097-2765(00)80010-6.

89) Shama, S. *et al.* (1998) “Heat Stress-Induced Life Span Extension in Yeast,” *Experimental Cell Research*, 245(2), pp. 379–388. Available at: https://doi.org/10.1006/excr.1998.4279.

90) Shaposhnikov, M. *et al.* (2015) “Lifespan and Stress Resistance in Drosophila with Overexpressed DNA Repair Genes,” *Scientific Reports*, 5(1), p. 15299. Available at: https://doi.org/10.1038/srep15299.

91) Shuman, S. and Prescott, J. (1990) “Specific DNA cleavage and binding by vaccinia virus DNA topoisomerase I.,” *Journal of Biological Chemistry*, 265(29), pp. 17826–17836. Available at: https://doi.org/10.1016/S0021-9258(18)38238-3.

92) Sinclair, D.A. and Guarente, L. (1997) “Extrachromosomal rDNA Circles— A Cause of Aging in Yeast,” *Cell*, 91(7), pp. 1033–1042. Available at: https://doi.org/10.1016/S0092-8674(00)80493-6.

93) Sinclair, D.A., Mills, K. and Guarente, L. (1997) “Accelerated Aging and Nucleolar Fragmentation in Yeast *sgs1* Mutants,” *Science*, 277(5330), pp. 1313–1316. Available at: https://doi.org/10.1126/science.277.5330.1313.

94) Singh, M. *et al.* (2022) “Ribonucleotides embedded in template DNA impair mitochondrial RNA polymerase progression,” *Nucleic Acids Research*, 50(2), pp. 989–999. Available at: https://doi.org/10.1093/nar/gkab1251.

95) Smith, J.M. (1962) “Review Lectures on Senescence. I. The Causes of Ageing,” *Proceedings of the Royal Society of London*, 157(966), pp. 115–127.

96) Smolka, J.A. *et al.* (2021) “Recognition of RNA by the S9.6 antibody creates pervasive artifacts when imaging RNA:DNA hybrids,” *Journal of Cell Biology*, 220(6), p. e202004079. Available at: https://doi.org/10.1083/jcb.202004079.

97) Soto-Palma, C. *et al.* (2022) “Epigenetics, DNA damage, and aging,” *Journal of Clinical Investigation*, 132(16), p. e158446. Available at: https://doi.org/10.1172/JCI158446.

98) Sparks, J.L. and Burgers, P.M. (2015) “Error-free and mutagenic processing of topoisomerase 1-provoked damage at genomic ribonucleotides,” *The EMBO Journal*, 34(9), pp. 1259–1269. Available at: https://doi.org/10.15252/embj.201490868.

99) Stingele, J. *et al.* (2014) “A DNA-Dependent Protease Involved in DNA-Protein Crosslink Repair,” *Cell*, 158(2), pp. 327–338. Available at: https://doi.org/10.1016/j.cell.2014.04.053.

100) Stingele, J. *et al.* (2016) “Mechanism and Regulation of DNA-Protein Crosslink Repair by the DNA-Dependent Metalloprotease SPRTN,” *Molecular Cell*, 64(4), pp. 688–703. Available at: https://doi.org/10.1016/j.molcel.2016.09.031.

101) Storici, F. *et al.* (2019) “Genomic stability, anti-inflammatory phenotype, and up-regulation of the RNAseH2 in cells from centenarians,” *Cell Death & Differentiation*, 26(9), pp. 1845–1858. Available at: https://doi.org/10.1038/s41418-018-0255-8.

102) Sugawara, S. *et al.* (2022) “RNaseH2A downregulation drives inflammatory gene expression via genomic DNA fragmentation in senescent and cancer cells,” *Communications Biology*, 5(1), p. 1420. Available at: https://doi.org/10.1038/s42003-022-04369-7.

103) Sun, H. *et al.* (2023) “Okazaki fragment maturation: DNA flap dynamics for cell proliferation and survival,” *Trends in Cell Biology*, 33(3), pp. 221–234. Available at: https://doi.org/10.1016/j.tcb.2022.06.014.

104) Szilard, L. (1959) “On the nature of the aging process,” *Proceedings of the National Academy of Sciences*, 45(1), pp. 30–45. Available at: https://doi.org/10.1073/pnas.45.1.30.

105) Takahashi, T. *et al.* (2011) “Topoisomerase 1 provokes the formation of short deletions in repeated sequences upon high transcription in Saccharomyces cerevisiae,” *Proceedings of the National Academy of Sciences*, 108(2), pp. 692–697. Available at: https://doi.org/10.1073/pnas.1012582108.

106) Wanrooij, P.H. and Chabes, A. (2019) “Ribonucleotides in mitochondrial DNA,” *FEBS Letters*, 593(13), pp. 1554–1565. Available at: https://doi.org/10.1002/1873-3468.13440.

107) Watt, D.L. *et al.* (2011) “Replication of ribonucleotide-containing DNA templates by yeast replicative polymerases,” *DNA Repair*, 10(8), pp. 897–902. Available at: https://doi.org/10.1016/j.dnarep.2011.05.009.

108) Williams, J.S. *et al.* (2012) “Proofreading of ribonucleotides inserted into DNA by yeast DNA polymerase ε,” *DNA Repair*, 11(8), pp. 649–656. Available at: https://doi.org/10.1016/j.dnarep.2012.05.004.

109) Williams, J.S. *et al.* (2013) “Topoisomerase 1-Mediated Removal of Ribonucleotides from Nascent Leading-Strand DNA,” *Molecular Cell*, 49(5), pp. 1010–1015. Available at: https://doi.org/10.1016/j.molcel.2012.12.021.

110) Williams, J.S. *et al.* (2015) “Evidence that processing of ribonucleotides in DNA by topoisomerase 1 is leading-strand specific,” *Nature Structural & Molecular Biology*, 22(4), pp. 291–297. Available at: https://doi.org/10.1038/nsmb.2989.

111) Williams, J.S. and Kunkel, T.A. (2014) “Ribonucleotides in DNA: Origins, repair and consequences,” *DNA Repair*, 19, pp. 27–37. Available at: https://doi.org/10.1016/j.dnarep.2014.03.029.

112) Williams, J.S., Lujan, S.A. and Kunkel, T.A. (2016) “Processing ribonucleotides incorporated during eukaryotic DNA replication,” *Nature Reviews Molecular Cell Biology*, 17(6), pp. 350–363. Available at: https://doi.org/10.1038/nrm.2016.37.

113) Wojtaszek, J.L. and Williams, R.S. (2024) “From the TOP: Formation, recognition and resolution of topoisomerase DNA protein crosslinks,” *DNA Repair*, 142, p. 103751. Available at: https://doi.org/10.1016/j.dnarep.2024.103751.

114) Yang, J.-H. *et al.* (2023) “Loss of epigenetic information as a cause of mammalian aging,” *Cell*, 186(2), pp. 305-326.e27. Available at: https://doi.org/10.1016/j.cell.2022.12.027.

115) Zheng, Q. (2017) “rSalvador: An R Package for the Fluctuation Experiment,” *G3: Genes, Genomes, Genetics*, 7(12), pp. 3849–3856. Available at: https://doi.org/10.1534/g3.117.300120.

116) Zimmermann, M. *et al.* (2018) “CRISPR screens identify genomic ribonucleotides as a source of PARP-trapping lesions,” *Nature*, 559(7713), pp. 285–289. Available at: https://doi.org/10.1038/s41586-018-0291-z.

6. Acknowledgements